LA-13742-MS

Approved for public release;
distribution is unlimited.

Characterization Well R-9 Completion Report

Los Alamos
NATIONAL LABORATORY

Los Alamos National Laboratory is operated by the University of California for the United States Department of Energy under contract W-7405-ENG-36.

Produced by the Environmental Restoration Project,
Groundwater Investigations Focus Area

Cover photo shows a modified Foremost Dual Rotary (DR-24) drill rig. The DR-24 is one of several drill-rig types being used for drilling, well installation, and well development in support of the Los Alamos National Laboratory Hydrogeologic Workplan. The Hydrogeologic Workplan is jointly funded by the Environmental Restoration Project and Defense Programs to characterize groundwater flow beneath the 43-square-mile area of the Laboratory and to assess the impact of Laboratory activities on groundwater quality. The centerpiece of the Hydrogeologic Workplan is the installation of up to 32 deep wells in the regional aquifer.

An Affirmative Action/Equal Opportunity Employer

LA-13742-MS
Issued: May 2001

Characterization Well R-9 Completion Report

David Broxton
Robert Gilkeson
Patrick Longmire
Jon Marin
Rick Warren
David Vaniman
Andy Crowder
Brent Newman
Bill Lowry
David Rogers
William Stone
Steve McLin
Giday WoldeGabriel
Deba Daymon
David Wycoff

Los Alamos
NATIONAL LABORATORY
Los Alamos, New Mexico 87545

TABLE OF CONTENTS

1.0 INTRODUCTION 1

2.0 SUMMARY OF DRILLING ACTIVITIES 3

2.1 Equipment 3
2.2 Schedule 3
2.3 Production 4
2.3.1 Open-Borehole Drilling 4
2.3.2 Core Drilling 4
2.3.3 Casing Advancement 6
2.3.4 Other Drilling Activities 6

3.0 STRATIGRAPHY/LITHOLOGY 6

3.1 Alluvium 6
3.2 Cerros del Rio Basalt 6
3.2.1 Upper Tholeiite (10- to 118.5-ft depth) 15
3.2.2 Lower Tholeiite (118.5- to 180-ft depth) 15
3.2.3 Upper Alkalic Basalt (180- to 206-ft depth) 15
3.2.4 Lower Alkalic Basalt (206- to 282-ft depth) 16
3.2.5 Basaltic Tephra (282- to 289.8-ft depth) 17
3.3 Old Alluvium (289.8- to 329-ft depth) 17
3.4 Puye Formation (329- to 686.4-ft depth) 19
3.4.1 Upper Puye Formation (329- to 539-ft depth) 20
3.4.2 Lower Puye Formation (539- to 686.4-ft depth) 20
3.5 Puye Formation (Axial Faces) 22
3.6 Late Miocene Basalt (686.4- to >710-ft depth) 22
3.7 Relations Between Clay Zones and Hydrostratigraphy 23

4.0 OCCURRENCES OF GROUNDWATER 26

4.1 Perched Zones 26
4.2 Regional Aquifer 28

5.0 SAMPLING AND ANALYSIS 29

5.1 Contaminant Characterization of Core and Cuttings 29
5.1.1 Methods 29
5.1.2 Results 30
5.2 Water Quality Determinations 30
5.2.1 Methods 33
5.2.2 Results 33
5.3 Anion Profiles 46
5.3.1 Methods 46
5.3.2 Results 46
5.4 Moisture Content of Core and Cuttings 49
5.4.1 Methods 49
5.4.2 Results 49
5.5 Matric Potential 51
5.5.1 Methods 51
5.5.2 Results 52
5.6 Hydraulic Properties 52
5.6.1 Methods 52

5.6.2 Results....54
5.7 Air Permeability and Borehole Anemometry....54
5.7.1 Methods....55
5.7.2 Results....58
5.8 Borehole Geophysics....58
5.8.1 Methods....58
5.8.2 Results....60

6.0 WASTE MANAGEMENT....68

7.0 SURVEY ACTIVITIES....69
7.1 Geodetic Survey....69
7.2 Surface Radiological Survey....69

8.0 WELL DESIGN, CONSTRUCTION, AND DEVELOPMENT....70
8.1 Well Design....70
8.2 Well Construction....70
8.3 Well Development....72
8.4 Pump Installation....72
8.5 Wellhead Protection....72

9.0 SITE RESTORATION....74

10.0 MODIFICATIONS TO WORK PLANS....74

11.0 SUMMARY OF SIGNIFICANT RESULTS....80

12.0 ACKNOWLEDGMENTS....81

13.0 REFERENCES....82

Appendixes

Appendix A Lithologic Log
Appendix B Descriptions of Geologic Samples
Appendix C Moisture and Matric-Potential Results
Appendix D Results of Unsaturated Hydraulic-Property Testing

List of Figures

Figure 1.0-1 Location of R-9, existing water supply wells and test wells, and generalized water-level contours for the regional water table....2
Figure 2.3-1 Configuration of R-9 borehole as of January 30, 1998....7
Figure 3.2-1 Variations in SiO_2, K_2O/P_2O_5, Sr, and Mg# with stratigraphic depth in the sequence of Pliocene basalts sampled at R-9....12
Figure 3.2-2 Chondrite-normalized lanthanide-element profiles for R-9 samples from (a) unaltered tholeiitic and alkalic basaltic lavas and clay-altered tephra, (b) clay-altered tuffaceous ash of the Puye Formation and clay-rich top of the Miocene basalt, and (c) smectite separates from alkalic basalt at 219- to 281.8-ft depth as well as from the old alluvium at 292.7-ft depth....13

Figure 3.2-3 Variations of K + Ba, Sr, and Fe_2O_3 content in plagioclase phenocrysts from the lower alkalic basalt and from the Miocene tholeiite in drill hole R-9 14
Figure 3.4-1 Abundances of glass, smectite, tridymite, and kaolinite in representative samples from the old alluvium and the Puye Formation in R-9 21
Figure 3.7-1 U versus Th systematics at R-9 for unaltered basalts, clay-altered basalts, and clay separates from basalts, as well as from an altered ash in the Puye Formation 25
Figure 4.1-1 Setting of perched water in the basaltic rocks of the Cerros del Rio volcanic field in R-9 27
Figure 4.2-1 Water level for the regional aquifer in borehole R-9 from March 3, 1998, to March 8, 1999 29
Figure 5.2-1 Comparison of major ion and nutrient chemistry of Cerros del Rio basalt groundwater in R-9 with alluvial groundwater and intermediate-depth perched groundwater in basalt 40
Figure 5.2-2 Comparison of major ion and nutrient chemistry of Puye Formation and Santa Fe Group groundwater in R-9 with regional aquifer groundwater in nearby water supply wells PM-1 and PM-3. 43
Figure 5.3-1 Pore water anion profiles for R-9 47
Figure 5.4-1 Moisture content for core and cuttings from R-9 50
Figure 5.4-2 Gravimetric-moisture and matric-potential measurements in R-9 51
Figure 5.5-1 Gravimetric moisture and matric potential as a function of lithology in R-9 53
Figure 5.7-1 Approximation of a spherical air-flow geometry with a conventional straddle packer design for in situ soil gas permeability measurements 56
Figure 5.7-2 Downhole instrument package and packers 56
Figure 5.7-3 Air-permeability measurement system 57
Figure 5.8-1 Borehole geophysical measurements in an open borehole with nonradioactive source tools in R-9 for the depth interval of 10 to 96 ft 61
Figure 5.8-2 Borehole geophysical measurements in an open borehole with radioactive source tools in R-9 for the depth interval of 10 to 96 ft 62
Figure 5.8-3 Borehole geophysical measurements in an open borehole with nonradioactive source tools in R-9 for the depth interval of 120 to 225 ft 63
Figure 5.8-4a Borehole geophysical measurements through steel casing with radioactive source tools in R-9 for the depth interval of 5 to 100 ft 64
Figure 5.8-4b Borehole geophysical measurements in an open borehole with radioactive source tools in R-9 for the depth interval of 120 to 226 ft 65
Figure 5.8-5 Borehole geophysical measurements in an open borehole with nonradioactive source tools in R-9 for the depth interval of 224 to 278 ft 66
Figure 5.8-6 Borehole geophysical measurements in an open borehole with radioactive source tools in R-9 for the depth interval of 220 to 280 ft 67
Figure 8.1-1 Configuration of the temporary well for R-9 71
Figure 8.2-1 As-built well completion diagram of well R-9 73
Figure 8.3-1 Well R-9 pumping development 74
Figure 8.5-1 Well R-9 wellhead diagram 75

List of Tables

Table 2.3-1	Drilling Performance Statistics	5
Table 3.0-1	Chemical Analyses of Representative Lithologies, Drill Hole R-9	8
Table 3.2-1	Geochronology of Basalts in R-9	11
Table 3.2-2	Normalized Mineral Content from Detailed Petrographic Analyses of R-9 Samples	16
Table 3.3-1	Summary of Petrographic Character for Lithic Clasts in Sedimentary Units of R-9	18
Table 3.3-2	Quantitative X-Ray Diffraction Analyses of Representative Lithologies, Drill Hole R-9	19
Table 3.7-1	INAA Chemical Analyses of Clay Separates from Drill Hole R-9	24
Table 3.7-2	Electron Microprobe Analysis of Clay in Miocene Basalt, R9-690.4	25
Table 5.1-1	Radionuclide Activities in Samples of Core and Cuttings from R-9	31
Table 5.2-1	Quality of Groundwater Samples Collected at R-9	34
Table 5.2-2	Field-Measured Parameters for Groundwater Samples Collected at R-9	38
Table 5.2-3	Radionuclide Activities in Samples of Nonfiltered Groundwater from R-9	38
Table 5.2-4	Radionuclide Activities in Samples of Filtered Groundwater from R-9	39
Table 5.2-5	Stable Isotopic Data for Nonfiltered Groundwater Samples Collected from R-9	41
Table 5.2-6	Statistical Distribution of Uranium in Groundwater from the Pajarito Plateau and Surrounding Areas	45
Table 5.3-1	R-9 Pore Water Anion Concentrations	48
Table 5.6-1	Samples from R-9 Selected for Testing of Hydraulic Properties	54
Table 5.7-1	R-9 Packer Permeability Results for Cerros del Rio Basalt	58
Table 5.8-1	Borehole Measurements at R-9	59
Table 7.1-1	Geodetic Data for Well R-9	69
Table 10.0-1	Activities Planned for R-9 Compared with Work Performed	76

List of Acronyms

ASTM	American Society for Testing and Materials
BIPS	borehole digital-image processing system
CVAA	cold vapor atomic absorption
DO	dissolved oxygen
DOE	US Department of Energy
DR	dual rotation
EM	electromagnetic induction
EN	epithermal neutron
ER	environmental restoration
FIMAD	Facility for Information Management, Analysis, and Display
FSF	field support facility
GFAA	graphite furnace atomic absorption
IC	ion chromatography

ICPES	inductively coupled plasma emission spectroscopy
I.D.	inside diameter
INAA	instrumental neutron activation analysis
LSC	liquid scintillation counting
MDA	minimum detectable activity
MS	magnetic susceptibility
NGR	natural gamma radiation
NMED	New Mexico Environment Department
NOI	Notice of Intent
NTU	nephelometric turbidity unit
O.D.	outside diameter
PID	photoionization detector
PVC	polyvinyl chloride
PWZ	perched water zone
RC	reverse circulation
RCRA	Resource Conservation and Recovery Act
SEA	Science and Engineering Associates
SVOC	semivolatile organic compound
SWL	static water level
TA	technical area
TD	total depth
TDS	total dissolved solid
TIMS	thermal ionization mass spectrometry
TN	thermal neutron
UDR	underground drill rig
VOC	volatile organic compound
WCSF	waste characterization strategy form
XRD	x-ray diffraction
XRF	x-ray fluorescence

Metric to English Conversions

Multiply SI (Metric) Unit	by	To Obtain US Customary Unit
kilometers (km)	0.622	miles (mi)
kilometers (km)	3281	feet (ft)
meters (m)	3.281	feet (ft)
meters (m)	39.37	inches (in.)
centimeters (cm)	0.03281	feet (ft)
centimeters (cm)	0.394	inches (in.)
millimeters (mm)	0.0394	inches (in.)
micrometers or microns (µm)	0.0000394	inches (in.)
square kilometers (km^2)	0.3861	square miles (mi^2)
hectares (ha)	2.5	acres
square meters (m^2)	10.764	square feet (ft^2)
cubic meters (m^3)	35.31	cubic feet (ft^3)
kilograms (kg)	2.2046	pounds (lb)
grams (g)	0.0353	ounces (oz)
grams per cubic centimeter (g/cm^3)	62.422	pounds per cubic foot (lb/ft^3)
milligrams per kilogram (mg/kg)	1	parts per million (ppm)
micrograms per gram (µg/g)	1	parts per million (ppm)
liters (L)	0.26	gallons (gal.)
milligrams per liter (mg/L)	1	parts per million (ppm)
degrees Celsius (°C)	9/5 + 32	degrees Fahrenheit (°F)

CHARACTERIZATION WELL R-9 REPORT

by

David Broxton, Robert Gilkeson, Patrick Longmire, Jon Marin, Rick Warren, David Vaniman, Andy Crowder, Brent Newman, Bill Lowry, David Rogers, William Stone, Steve McLin, Giday WoldeGabriel, Deba Daymon, David Wycoff

ABSTRACT

Characterization well R-9, located in Los Alamos Canyon near the eastern boundary of Los Alamos National Laboratory ("the Laboratory"), is the first of approximately 32 wells being installed in the regional aquifer as part of the Laboratory's "Hydrogeologic Workplan" (LANL 1998, 59599). R-9 was installed by the Laboratory's Environmental Restoration (ER) Project and is primarily designed to provide water-quality and water-level data for potential intermediate-depth perched zones and for the regional aquifer downgradient of multiple mesa-top and canyon floor contaminant source areas in upper Los Alamos Canyon and Pueblo Canyon. R-9 is also designed to collect geologic, hydrologic, and geochemical data that contribute to the understanding of the vadose zone and regional aquifer in this part of the Laboratory.

R-9 was drilled to a total depth of 771 ft using air-rotary techniques. Drilling methods included downhole percussion hammers and dual-wall casing to drill open hole, a continuous coring system to core open hole, and Holte/Stratex casing advance systems that operated on dual-wall casing and downhole percussion hammers. In descending order, geologic units penetrated in R-9 include alluvium, basaltic rocks of the Cerros del Rio volcanic field, old alluvium, the Puye Formation, and basaltic rocks of the Santa Fe Group.

Four zones of saturation were encountered during the drilling of R-9. Two zones of perched groundwater were encountered in Cerros del Rio basalt. Water first appeared in the borehole at depths of 180 and 275 ft. In the upper zone water rose in the hole to 137 ft. This may indicate confined conditions or simply that water entered the borehole too slowly to be detected above 180 ft. The saturated thickness of the upper zone is at least 45 ft thick, and it may be as much as 89 ft thick. The second perched zone occurs at the base of the Cerros del Rio basalt and is at least 7 ft thick and may be as much as 18 ft thick. Saturation was also encountered in a third zone in the Puye Formation at depths of 579, 615, and 624 ft. These transmissive zones are intercalated in clay-rich tuffaceous sedimentary deposits. These three permeable zones appear to be hydraulically connected because water levels rose to a depth of 524 ft after the tops of each zone was penetrated. The deepest groundwater zone was encountered at a depth of 688 ft near the top of basalt in the Santa Fe Group. This deep groundwater is unconfined, and it is almost certainly associated with the regional aquifer.

Borehole samples of groundwater collected from the four saturated zones during drilling were chemically characterized for major ions, trace elements, dissolved organic carbon, stable isotopes, tritium, and other radionuclides. Methods recommended by both the Environmental Protection Agency (EPA) and the Laboratory were followed for analysis of groundwater (filtered and nonfiltered) and core samples. Groundwater from the uppermost perched zone (180-ft depth) is characterized by a sodium-calcium-chloride-bicarbonate ionic composition with a pH value of 8.30. This zone is characterized by 347 pCi/L tritium (analysis by low-level electrolytic enrichment), which is similar to tritium activities detected in alluvial groundwater within upper Los Alamos Canyon. The perched zone at the base of the Cerros del Rio basalt at a depth of 275 ft is characterized by a sodium-sulfate-bicarbonate ionic composition with a pH value of 8.8. This zone is characterized by 106 pCi/L tritium (low-level electrolytic enrichment) and

48 parts per billion (ppb) dissolved uranium. The lower zone in the Cerros del Rio basalt has a higher total dissolved solids (TDS) content (389 parts per million [ppm]) than the upper zone (252 ppm), possibly reflecting a longer residence time. Composition of groundwater within the Puye Formation varies from a calcium-sodium-bicarbonate to sodium-chloride-bicarbonate type. Tritium activities in groundwater of the Puye Formation range from 2.7 to 30 pCi/L. The saturated zone in Santa Fe Group basalt at a depth of 688 ft is characterized by a calcium-sodium-bicarbonate ionic composition with a TDS content of 387 ppm. This groundwater is chemically similar to that in the regional aquifer in wells PM-1 and PM-3. It has a tritium activity of 14.4 pCi/L.

1.0 INTRODUCTION

This well completion report describes the drilling, well completion, and testing activities for characterization well R-9. R-9 is located in Los Alamos Canyon at the eastern Los Alamos National Laboratory boundary (Figure 1.0-1) west of state road NM 4. This well was installed by personnel from the Canyons Focus Area of the Environmental Restoration (ER) Project. It is the first characterization well drilled to the regional aquifer as part of the "Hydrogeologic Workplan" (LANL 1998, 59599) in support of the Laboratory's "Groundwater Protection Management Program Plan" (LANL 1995, 50124).

Preliminary interpretations are presented for some of the data collected, but discussion of other data is deferred until they can be evaluated in the context of site-wide information collected from other ER Project and "Hydrogeologic Workplan" boreholes. A future report will provide a human health risk assessment for deep groundwater in Los Alamos Canyon and will include groundwater data from R-9 and other regional aquifer wells.

R-9 was identified as well LAOI-7 in the "Task/Site Work Plan for Operable Unit 1049: Los Alamos Canyon and Pueblo Canyon" ("the work plan"; LANL 1995, 50290). The original intent was to complete this well in the first intermediate-depth perched groundwater zone encountered at this location. Work on LAOI-7 began in May 1997, but drilling was suspended at a depth of 32.5 ft and surface casing was set to a depth of 10 ft after caving problems were encountered in the borehole. The purpose of LAOI-7 was reevaluated during development of the "Hydrogeologic Workplan" (LANL 1998, 59599) in the summer of 1997, and it was redesignated as a characterization well to the regional aquifer. The well was renamed R-9 to be consistent with the nomenclature used to designate regional aquifer wells in the "Hydrogeologic Workplan" and the "Core Document for Canyons Investigations" ("the core document"; LANL 1997, 55622).

Work on R-9 resumed on September 24, 1997, using LAOI-7 as a starter hole; the well was temporarily completed at a depth of 710 ft on February 3, 1998. At the time of its temporary completion, the depth to the regional aquifer in R-9 could not be identified with certainty because several discrete zones of saturation had been encountered in the lower part of the borehole. A decision was made to halt further work on R-9 until R-12, located 1 km to the south, could be drilled and the regional water table could be defined more confidently. Data collected from drilling activities at R-12 helped clarify groundwater conditions at R-9, and the final phase of drilling and installation of a permanent well at R-9 took place from September 22, 1999, through October 18, 1999.

R-9 was designed to address and satisfy a portion of the requirements in Module VIII of the Laboratory's Hazardous Waste Facility Permit. Based on the current understanding of groundwater flow directions, R-9 was sited to characterize water quality within the regional aquifer downgradient of potential contaminant source areas, including Technical Area (TA) -1, -2, -21, -45, and -53, located in the upper part of the Los Alamos Canyon and Pueblo Canyon drainage basins. The general direction of groundwater flow in the regional aquifer is eastward near R-9 (Figure 1.0-1). R-9 was also designed to characterize the occurrence, movement, and quality of intermediate-depth perched groundwater at this location. This well also provided an opportunity to collect hydrologic and geologic data that contribute to the understanding of the vadose zone and regional aquifer in this part of the Laboratory. Data collected include key parameters that will be used for numerical flow and transport models and for geochemical models. The hydrologic and geologic data collected in R-9 are being used in conjunction with data from other planned characterization boreholes as well as from other data sources to evaluate and update the sitewide conceptual hydrogeologic model.

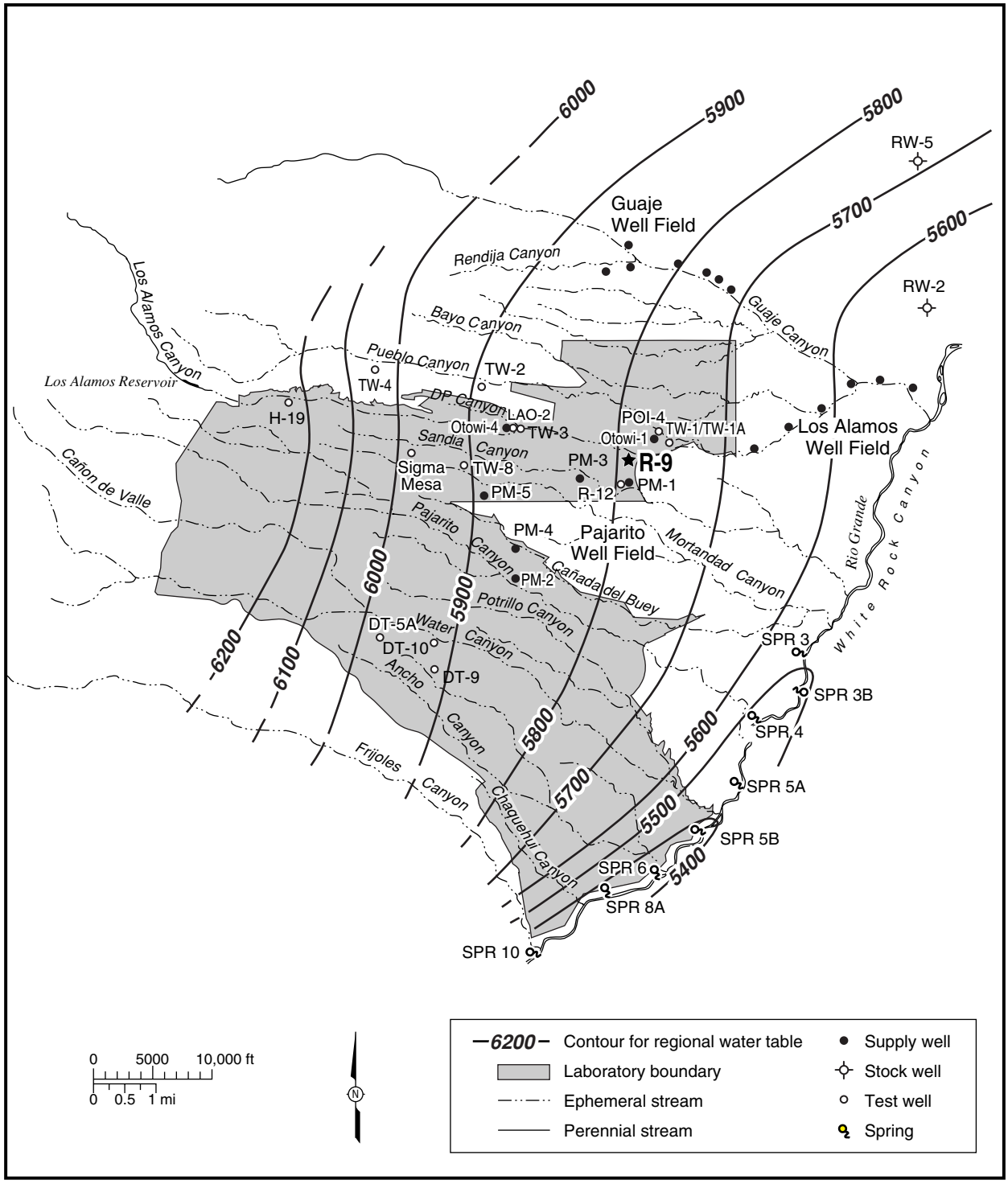

Source: Purtymun 1984, 6513.

F1.0-1 / R-9 WELL COMPLETION RPT / 050400 / PTM

Figure 1.0-1. Location of R-9, existing water supply wells and test wells, and generalized water-level contours for the regional water table

Although R-9 is primarily a characterization well, its design also meets the requirements of a monitoring well as defined in the Laboratory's Hazardous Waste Facility Permit. Incorporation of this well into a Laboratory-wide groundwater monitoring program will be evaluated at a later date when the results of this characterization activity are integrated with other groundwater investigations in the "Hydrogeologic Workplan" (LANL 1998, 59599).

2.0 SUMMARY OF DRILLING ACTIVITIES

R-9 was drilled to a depth of 771 ft and a single-screen well was installed. This section summarizes drilling and temporary completion activities.

2.1 Equipment

From September 22, 1997, to February 3, 1998, R-9 was drilled to a depth of 710 ft by Tonto Drilling Company (Tonto) using an Ingersoll-Rand T-4 drill rig with a T-5 rotating head. From September 22, 1999, through October 18, 1999, the borehole was completed to a depth of 771 ft and the permanent well was installed by Dynatec Drilling Company (formerly Tonto Drilling Company) using a Foremost dual rotation (DR)-24 drill rig. Tonto provided three-man drilling crews, crew vehicles, drilling hammers and bits, the Longyear 101-mm Geobarrel core system, dual-wall rod systems, a 1-ton flatbed truck, and a 5-ton boom truck for handling casing, drill pipe, and heavy support apparatus such as casing jacks.

The ER Project's field support facility (FSF) provided drill casings, drilling bits, a small front-end loader, the dust suppression system, field-support trailers including logging and sampling, water containment tanks, drums for cuttings management, and a diesel-powered electric generator. The Laboratory's Environmental Technology Group (E-ET) provided on-site water sample testing and filtering apparatus. The Water Quality and Hydrology Group (ESH-18) of the Environment, Safety, and Health (ESH) Division provided a Hermit data logger, depth-to-water meter, bailers, and pressure transducers. The Geology and Geochemistry Group (EES-1) of the Earth and Environmental Sciences (EES) Division and the FSF provided core logging microscopes.

The subcontractors Colog, Inc., and Science and Engineering Associates, Inc. (SEA) provided geophysical logging equipment and air permeability measuring equipment, respectively.

2.2 Schedule

The T-4 drill rig was mobilized to R-9 on September 22, 1997, and it was demobilized on February 3, 1998. The DR-24 drill rig was mobilized to the site on September 22, 1999, and it was demobilized on October 18, 1999. Drilling and well installation operations required 139 drilling shifts. The following table compares the actual number of shifts with the number of shifts projected for R-9 in planning documents.

	Conceptual Design Report	Field Implementation Plan	Actual
Number of shifts	32	51	139

The following reasons account for the difference between planned and actual duration at R-9.

- The multiple perched water zones encountered in R-9 required more time for characterization than originally planned.
- A high hydraulic head (approximately 100 ft) at the base of the first perched water zone (180 ft below the ground surface) presented problems achieving a casing seal; extra under-reaming operations using a Servco three-wing under-reamer had been unexpected.

- The thick sequence of clay-rich sedimentary rocks in the lower part of the Puye Formation was unexpected, and the clay repeatedly plugged drilling systems.
- The 14-in.-diameter drill casing and Holte 14-in.-diameter under-reamer were not delivered in time to start drilling R-9 as planned; therefore, the alternative was to start drilling R-9 using available systems inside the poorly installed LAOI-7 surface casing. This process caused numerous operational problems and reduced production efficiency.

Drilling shifts were either 10 or 12 hr each, depending on production needs. From October 22, 1997, to October 30, 1997, and from November 10, 1997, to December 18, 1997, Tonto provided two drill crews who worked two 12-hr shifts per day. To minimize rig standby costs, support contractors performed activities such as air permeability measurements and geophysical logging during nondrilling periods, such as weekends.

2.3 Production

Drilling techniques used in R-9 consisted of open-borehole drilling, air-rotary coring, air-rotary placement of a surface casing, and air-rotary under-reamer advance of five different casing strings. In addition, other drilling operations involved borehole/corehole/casing drill out, reaming, augering, milling, and cleaning. Changing drilling systems typically involved tripping-out one system, modifying the drilling head and/or circulation plumbing, and tripping-in another drilling system from the ground surface to the depth of operations. Production statistics are summarized in Table 2.3-1.

From the ground surface to 771 ft, the total footage drilled by the different drilling techniques and casing sizes was 2631 ft. The total footage drilled does not include the footage of one drill system or casing size tripped in or out of another drill system or casing size. The total trip-in footage was 27,567 ft, and the total trip-out footage was 25,121 ft.

2.3.1 Open-Borehole Drilling

Open-borehole drilling provided a suitable environment for geophysical logging and air permeability profiles of bedrock strata without the interference of drill systems or casing strings. Open-borehole drilling was also used to explore deeper sections of bedrock before coring or casing advancement. Tonto drilled 175 ft of open borehole in basaltic rocks at an average rate of 22.6 ft per hour using an RC 44 4-7/8-in.-diameter percussion hammer or a 4-1/2-in.-diameter tricone roller bit. Open-borehole drilling in sedimentary strata was not attempted because of concerns about borehole stability in loose, unconsolidated materials.

2.3.2 Core Drilling

Core was collected in R-9 to provide undisturbed samples for geological, contaminant, and hydrological characterization. In addition, core was used to identify confining layers beneath perched groundwater zones and provide information for placing casing seals. Tonto cored a total of 244.5 ft, or 31.7% of the 771-ft depth, using a Longyear 101-mm Geobarrel air-rotary coring system.

Average core recovery was 81% from all cored intervals. Of the 244.5 ft cored, 120 ft were produced from basaltic rocks at an average rate of 2.8 ft per hour and average recovery of 84%; 124.5 ft were produced from sedimentary rocks at an average rate of 4.2 ft per hour and average recovery of 78%.

Table 2.3-1
Drilling Performance Statistics

Drilling Types	Open Hole	Core	Other[a]	6-5/8-in. Casing[b]	8-5/8-in. Casing[b]	10-3/4-in. Casing[c]	12-3/4-in. Casing[c]	14-in. Casing[d]	16-in. Casing	Casing Advance System (4-1/2-in. rods)[b]	Casing Advance System (7-in. rods)[c,d]	Total (ft)[e]
Total footage drilled (ft)	175	244.5[d]	648.8	728	415	162.5	54.5	239	7.5	0	0	2674.1
Total footage rate (ft/hr)[f]	22.6	3.3	9.8	9.1	5.8	4.5	1.8	3.4	2			
Total recovery		81%										
Basalt footage (ft)[g]	175	120	489.8	275	135	0	42.5	239	7.5	0	0	1483.8
Basalt rate (ft/hr)[f,g]	22.6	2.8	9.9	5.5	5.4		1.5	3.4	2			
Puye clastics footage (ft)[h]	0	124.5	159	445	268	162.5	12	0	0	0	0	1171
Puye clastics rate (ft/hr)[f,h]		4.2	9.6	15.1	6.0	4.5	4.8					
Trip-in footage (ft)	0	3782.5	11430	4323	2855.9	677.5	959.5	6.5	0	4772	1392	30,198.9
Trip-in rate (ft/hr)[f]		322.8	236.2	225.2	175.7	46.7	37.3	26		277.4	151.3	
Trip-out footage (ft)	0	3336	11776.8	0	771	0	0	0	0	10,483.5	1684.5	28,051.8
Trip-out rate (ft/hr)[f]		307.5	338.7		0					349.1	137.5	
Pull back footage (ft)	0	0	0	1341	319	0	258.5	34.5	0	0	0	1953
Pull back rate (ft/hr)[f]				79.8	93.8		48.3	5.9				
											Total	**65,533.3**
Mill shoe (number)[i]					2		1	3				
Mill shoe (hr)					5.7			19.9				
Seal extrusion (number)					1		2	4				
Under-ream (ft)							4	7.5				
Under-ream footage (ft)							285–289	236–243.5				
Under-ream (hr)[j]							43	132				
Life-of-hole casing TD (ft)				645.5	679	420	292.5	243.8	7.5			
Water zone					3rd		2nd	1st				

Note: These performance statistics represent performance for the completed well.

[a] Other drilling includes borehole/corehole/casing drill out, reaming, augering, and cleaning with percussion hammer, tricone bit, or bentonite auger.

[b] Stratex 6-5/8-in. and 8-5/8-in. casing advance systems use 4-1/2-in. reverse circulation (RC) rods.

[c] Stratex 10-3/4-in. and 12-3/4-in. casing advance systems use 7-in. RC rods.

[d] Holte 14-in. casing advance system uses 7-in. RC rods.

[e] Total depth (TD) of borehole is 771 ft. Total cored footage (244.5 ft) is 31.7% of total borehole footage (771 ft).

[f] Rates are weighted averages over footages drilled or tripped, including breaks but excluding repairs and changeout of tools.

[g] Basalt footage and rates include Cerros del Rio basalt from 10 to 282 ft and Santa Fe Group basalt from 686 to 710 ft.

[h] Puye footage and rates include the old alluvium stratigraphic interval from 282 to 329 ft.

[i] Milling bits for 14-in., 12-3/4-in., and 10-3/4-in. casing shoes are tripped in on 7-in. RC rods.

[j] Duration encompasses activity-specific operations (i.e., operations that would not have been done if under-reaming had not been implemented).

2.3.3 Casing Advancement

After the 16-in.-diameter surface casing was installed, four casing strings were installed in a telescoped fashion to prevent perched water from communicating downhole as the borehole advanced (see Figure 2.3-1). As a casing string was used to seal off a perched water zone (e.g., 14-in.-diameter and 12-3/4-in.-diameter casings) the casing shoe was milled downhole allowing the next smaller casing size to advance past the shoe and continue borehole production. Table 2.3-1 lists the casings and casing advance systems used in R-9.

2.3.4 Other Drilling Activities

Other drilling activities included milling the casing shoes and reaming the borehole. These activities were summarized as "other drilling" in the operations chronology and are tabulated in the performance statistics (Table 2.3-1). These activities also included operations to clean bentonite out of the borehole or casings after the casing seals were emplaced and to remove clay cake from drill bits, casing, and air-circulation equipment during drilling of clay-rich Puye Formation sedimentary rocks.

3.0 STRATIGRAPHY/LITHOLOGY

The principal geologic units encountered in R-9, in descending order, consist of alluvium, basalts of the Cerros del Rio volcanic field and basaltic tephra, old alluvium, sediments of the Puye Formation, and basalt of the Santa Fe Group. A detailed stratigraphy of these units and of subunits within them is provided in the lithologic log of Appendix A. Samples of representative lithologies were collected for further analysis; a listing and description of each of these samples is given in the geologic sample descriptions of Appendix B. Appendix B includes descriptions obtained either by binocular microscope or by petrographic microscope using thin sections, as well as details of sample processing for the subset of samples analyzed by quantitative x-ray diffraction (QXRD). Four basalt samples from R-9 were dated using $^{40}Ar/^{39}Ar$ methods to provide age constraints on the volcanic units in this part of the Laboratory site. Chemical analyses of representative samples were acquired by x-ray fluorescence (XRF) and instrumental neutron activation analysis (INAA). The chemical analyses are particularly useful for understanding the lithologies present at R-9 and are summarized in Table 3.0-1. This table is referred to throughout the discussion of lithologies in R-9. In addition to the description of stratigraphic units, this section includes a discussion of the mineralogy and chemical composition of clay-mineral separates from basalts and sediments, with a summary of information from clay minerals that bears on the record of water-rock interactions at drill hole R-9.

3.1 Alluvium

Quaternary alluvium was penetrated from the surface to 10-ft depth at R-9. The alluvium at this site consists predominantly of detritus from the Bandelier Tuff along with detritus contributed from other volcanic sources (Tschicoma Formation intermediate lavas and Cerros del Rio basalts). No samples of the alluvium were collected for detailed characterization.

3.2 Cerros del Rio Basalt

Basalts of the Cerros del Rio Formation at R-9 extend from the base of the alluvium (10-ft depth) to 282-ft depth. The Cerros del Rio volcanic field is exposed principally to the east of the Laboratory, with most recognized source vents located along or east of the Rio Grande. However, the Cerros del Rio volcanic field extends westward beneath the Pajarito Plateau where it is buried by Bandelier Tuff and the upper part of the Puye Formation. Some source vents occur west of the Rio Grande, but the locations of these buried vents are poorly known. The bottom of the Cerros del Rio sequence in R-9 consists of a basaltic tephra that may have been derived from a nearby vent.

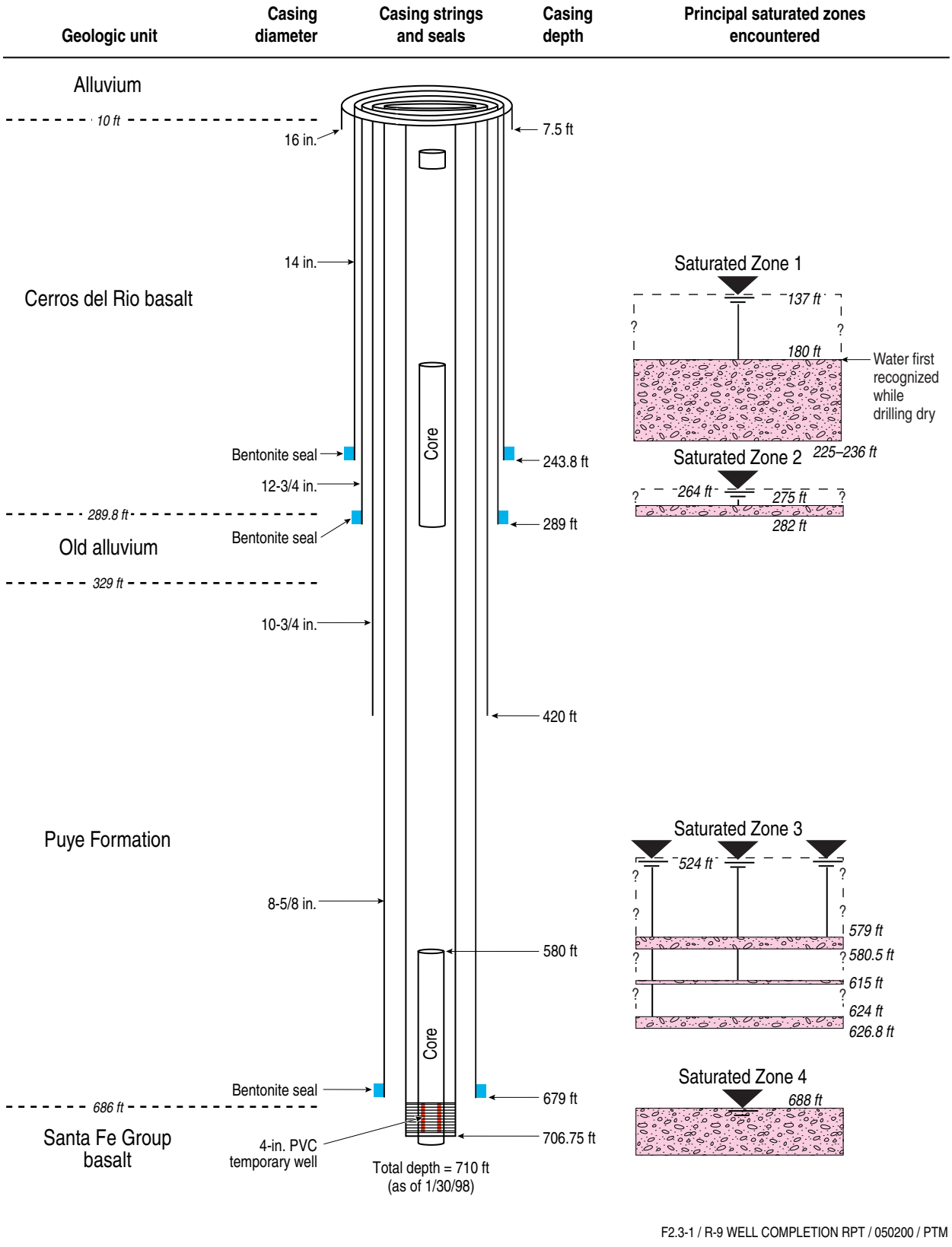

Figure 2.3-1. Configuration of R-9 borehole as of January 30, 1998

Table 3.0-1
Chemical Analyses of Representative Lithologies, Drill Hole R-9

Part 1									
Sample	R9-50.5D	R9-92D	R9-122D	R9-162D	R9-181.3	R9-201.5	R9-228	R9-273.7	R9-282.2
lithology	upper tholeiite	upper tholeiite	lower tholeiite	lower tholeiite	upper alkalic basalt	upper alkalic basalt	lower alkalic basalt	lower alkalic basalt	alkalic basalt tephra
XRF Data (major elements)									
SiO_2 %	52.4	51.6	51.2	51.2	50.0	49.9	48.6	48.6	50.3
TiO_2 %	1.49	1.50	1.45	1.45	1.61	1.62	1.77	1.79	1.69
Al_2O_3 %	16.09	16.00	15.93	16.00	16.15	16.03	15.32	15.55	15.01
Fe_2O_3 %	11.26	11.25	11.85	11.68	11.21	11.21	11.37	11.31	10.54
MnO %	0.16	0.16	0.17	0.17	0.17	0.17	0.17	0.17	0.15
MgO %	5.83	6.32	7.23	7.16	6.58	7.00	8.37	8.53	7.60
CaO %	9.01	9.03	8.94	9.25	9.08	9.09	9.07	8.96	8.70
Na_2O %	3.33	3.28	3.18	3.28	3.38	3.23	3.41	3.44	2.49
K_2O %	1.03	1.13	0.94	0.84	1.29	1.30	1.52	1.56	1.26
P_2O_5 %	0.29	0.31	0.30	0.29	0.54	0.56	0.64	0.67	0.65
LOI %	-0.04	-0.14	-0.43	-0.42	0.18	0.27	-0.32	-0.36	1.64
Total %	101.1	100.8	101.4	101.5	100.5	100.7	100.5	100.9	100.3
XRF Data (trace elements)									
V ppm	176	180	173	189	192	181	186	183	170
Cr ppm	148	187	252	254	205	215	242	241	235
Ni ppm	64	78	106	96	119	125	184	198	159
Zn ppm	108	79	106	85	110	103	107	111	99
Rb ppm	14	26	19	15	19	18	26	28	27
Sr ppm	427	451	440	413	669	676	794	827	628
Y ppm	21	25	25	29	25	32	26	38	21
Zr ppm	149	153	138	137	191	187	200	207	187
Nb ppm	16	19	15	13	26	29	27	33	28
Ba ppm	391	373	389	404	775	732	794	822	628
INAA Data									
Na_2O %	3.40					3.46		3.49	
K_2O %	1.00					1.00		0.99	
CaO %	8.94					9.65		9.47	
Fe_2O_3 %	11.85					11.81		11.58	
Sc ppm	25					27		24	
Cr ppm	149					215		230	
Co ppm	41					42		45	
Zn ppm	151					142		130	
As ppm	0.25					0.85		0.05	
Rb ppm	27					27		30	
Sr ppm	436					702		858	
Zr ppm	155					200		199	
Sb ppm	0.10					0.05		0.06	

Table 3.0-1 (continued)

Part 1 (continued)									
Sample	R9-50.5D	R9-92D	R9-122D	R9-162D	R9-181.3	R9-201.5	R9-228	R9-273.7	R9-282.2
lithology	upper tholeiite	upper tholeiite	lower tholeiite	lower tholeiite	upper alkalic basalt	upper alkalic basalt	lower alkalic basalt	lower alkalic basalt	alkalic basalt tephra
INAA Data (continued)									
Cs ppm	0.45					0.29		0.24	
Ba ppm	397					762		816	
La ppm	21					39		45	
Ce ppm	43					75		87	
Nd ppm	24					37		41	
Sm ppm	5.47					7.59		8.00	
Eu ppm	1.62					2.14		2.21	
Gd ppm	5.28					6.99		6.94	
Tb ppm	0.81					0.97		1.01	
Tm ppm	0.40					0.46		0.43	
Yb ppm	2.36					2.81		2.62	
Lu ppm	0.36					0.39		0.37	
Hf ppm	3.51					4.23		4.16	
Ta ppm	1.09					2.00		2.28	
W ppm	0.49					1.24		1.15	
Th ppm	2.67					4.55		5.45	
U ppm	0.93					1.52		1.46	

Part 2								
Sample	R9-282.6	R9-285.5	R9-292.7	R9-297B	R9-596	R9-616.5	R9-688.6	R9-690.4
lithology	alkalic basalt tephra	alkalic basalt tephra	old alluvium	alkalic basalt in alluvium	tuff ash in Puye Formation	sandstone	soil in Miocene basalt	Miocene basalt
XRF data (major elements)								
SiO_2 %		49.7	65.1	52.0	57.3	60.3		48.0
TiO_2 %		1.70	0.87	1.51	0.82	0.81		1.60
Al_2O_3 %		14.52	14.10	16.30	20.36	16.60		15.55
Fe_2O_3 %		11.03	5.50	9.68	5.26	5.64		10.40
MnO %		0.19	0.09	0.15	0.09	0.08		0.14
MgO %		8.01	2.64	5.44	4.53	2.51		5.44
CaO %		7.69	3.70	7.88	4.10	5.03		12.34
Na_2O %		2.21	2.25	3.70	0.33	3.15		3.05
K_2O %		1.04	2.19	1.86	0.15	1.80		0.85
P_2O_5 %		0.36	0.30	0.80	0.22	0.22		0.33
LOI %		3.64	4.17	0.40	7.28	3.68		2.95
Total %		100.4	101.1	100.0	100.6	99.7		100.8
XRF data (trace elements)								
V ppm		154	71	165	70	86		219
Cr ppm		267	59	72	42	69		221
Ni ppm		197	35	50	25	29		89

Table 3.0-1 (continued)

Part 2 (continued)								
Sample	R9-282.6	R9-285.5	R9-292.7	R9-297B	R9-595	R9-616.5	R9-688.6	R9-690.4
lithology	alkalic basalt tephra	alkalic basalt tephra	old alluvium	alkalic basalt in alluvium	tuff ash in Puye Formation	sandstone	soil in Miocene basalt	Miocene basalt
XRF data (trace elements) (continued)								
Zn ppm		96	70	96	70	61		81
Rb ppm		32	75	38	10	30		13
Sr ppm		537	545	959	364	794		569
Y ppm		31	23	30	<7	20		26
Zr ppm		166	323	216	217	240		136
Nb ppm		17	21	38	26	17		12
Ba ppm		714	772	948	274	2536		462
INAA data								
Na_2O %	1.48				0.39		1.54	
K_2O %	0.78				0.59		2.28	
CaO %	9.40				3.65		11.74	
Fe_2O_3 %	11.41				5.56		6.65	
Sc ppm	24				11		18	
Cr ppm	212				42		73	
Co ppm	42				13		38	
Zn ppm	163				97		107	
As ppm	2.93				1.23		4.29	
Rb ppm	29				12		75	
Sr ppm	807				379		406	
Zr ppm	<181				213		226	
Sb ppm	0.30				0.25		0.86	
Cs ppm	1.65				3.53		6.72	
Ba ppm	998				232		1100	
La ppm	46				40		32	
Ce ppm	90				86		61	
Nd ppm	44				30		31	
Sm ppm	9.07				5.20		6.50	
Eu ppm	2.23				1.20		1.37	
Gd ppm	7.11				3.74		5.42	
Tb ppm	0.97				0.52		0.84	
Tm ppm	0.46				0.23		0.45	
Yb ppm	2.81				1.33		2.92	
Lu ppm	0.41				0.20		0.42	
Hf ppm	4.31				5.85		4.86	
Ta ppm	2.30				2.20		1.27	
W ppm	3.36				-0.35		4.86	
Th ppm	6.18				11.60		8.38	
U ppm	18.70				0.90		5.80	

The Cerros del Rio basalts at the Laboratory are mostly of ~2.3 to 2.6 Ma age (WoldeGabriel et al. 1996, 54427) and varied in composition. Those encountered at R-9 are tholeiitic to alkalic in composition. Radiometric ages of basalts from R-9 are summarized in Table 3.2-1. The ages of the upper and lower Pliocene basalts are constrained within a range of 2.15 to 2.45 Ma, a spread of ages that, given the high analytical precision, suggests multiple eruptive events that are nevertheless close enough in age to support hypotheses of genetic continuity.

Table 3.2-1
Geochronology of Basalts in R-9

Sample Number[a]	Basalt Flow Unit	Age (Ma)[b]	2σ Age Uncertainty
R9-50.5D	Cerros del Rio basalt, upper tholeiitic flow	2.15	0.02
R9-273.7	Cerros del Rio basalt, lower alkalic flow	2.45	0.10
R9-690.4	Santa Fe Group basalt	8.63	0.24
R9-699.1	Santa Fe Group basalt	8.45	0.21

[a] Numerical value in sample number indicates depth in feet at bottom of sampled interval.

[b] Ages from WoldeGabriel (1998, 58705); ages determined using the Ar^{40}/Ar^{39} method by W. McIntosh at the New Mexico Institute of Mining and Technology.

Chemical and petrographic analyses define a sequence of four compositional groups: lower and upper alkalic basalts overlain by lower and upper tholeiites. Each group is assumed to represent a separate eruption of basalt, although some geochemical trends indicate a genetic relationship between all four groups. Beneath these lavas, the thin basaltic tephra, at 282- to 289.8-ft depth, represents the initiation of the eruptive sequence but is in several respects distinct from the subsequent lavas.

Based on the data in Table 3.0-1, several chemical trends in the Cerros del Rio basalt of R-9 are evident. These trends, from lower to upper flow units, include increasing silica content and increasing indices of evolution (i.e., increasing olivine fractionation resulting in lower Mg, Ni, and Cr). Other elements such as Sr reflect the difference between alkalic and tholeiitic character, and higher ratios of K_2O/P_2O_5 reflect greater crustal contributions to magma sources. Relevant plots of SiO_2, K_2O/P_2O_5, Sr, and Mg# [representing the cation ratio Mg/(Mg+Fe)] are compiled in Figure 3.2-1. In addition, chondrite-normalized lanthanide data for the basalts (Figure 3.2-2a) are typical of alkalic and tholeiitic basaltic lavas from comparable continental settings in that both have essentially no Eu anomaly and the alkalic compositions are more enriched in light lanthanide elements than the tholeiitic composition. Only when clay forms a significant amount of the sample, as in the tephra shown in Figure 3.2-2a, is a moderate negative Eu anomaly developed. These lanthanide features of the basalts are compared in Figure 3.2-2 with other lithologies and with smectite separates that are discussed in more detail in Sections 3.4, 3.6, and 3.7 of this report.

In addition to bulk chemical composition, compositions of certain minerals within the basalts can be used as a guide to host-rock composition. Altered basalts can retain plagioclase when secondary minerals have largely replaced other phenocryst phases, such as olivine. Figure 3.2-3 compares plagioclase phenocryst compositional data, collected by electron microprobe, for two representative basalts from drill hole R-9. One of these samples is from the lower alkalic basalt in R-9; the other is from the tholeiitic Miocene basalt in R-9 that contains lesser amounts of alkali and alkaline-earth elements. Plagioclase compositions shown in Figure 3.2-3 reflect these differences in higher Sr and higher K + Ba compositions for the alkali versus the tholeiite host, over comparable ranges in the plagioclase series. Distinctly higher Fe_2O_3 content is also recorded in the feldspars of the alkalic basalt. Distinctions such as these allow small rock fragments and even single feldspar crystals to be used to identify different basaltic lava types. This is an important consideration when drilling produces only small cuttings or when there is a need to determine the source of a small rock fragment, such as a basaltic pebble in sediment.

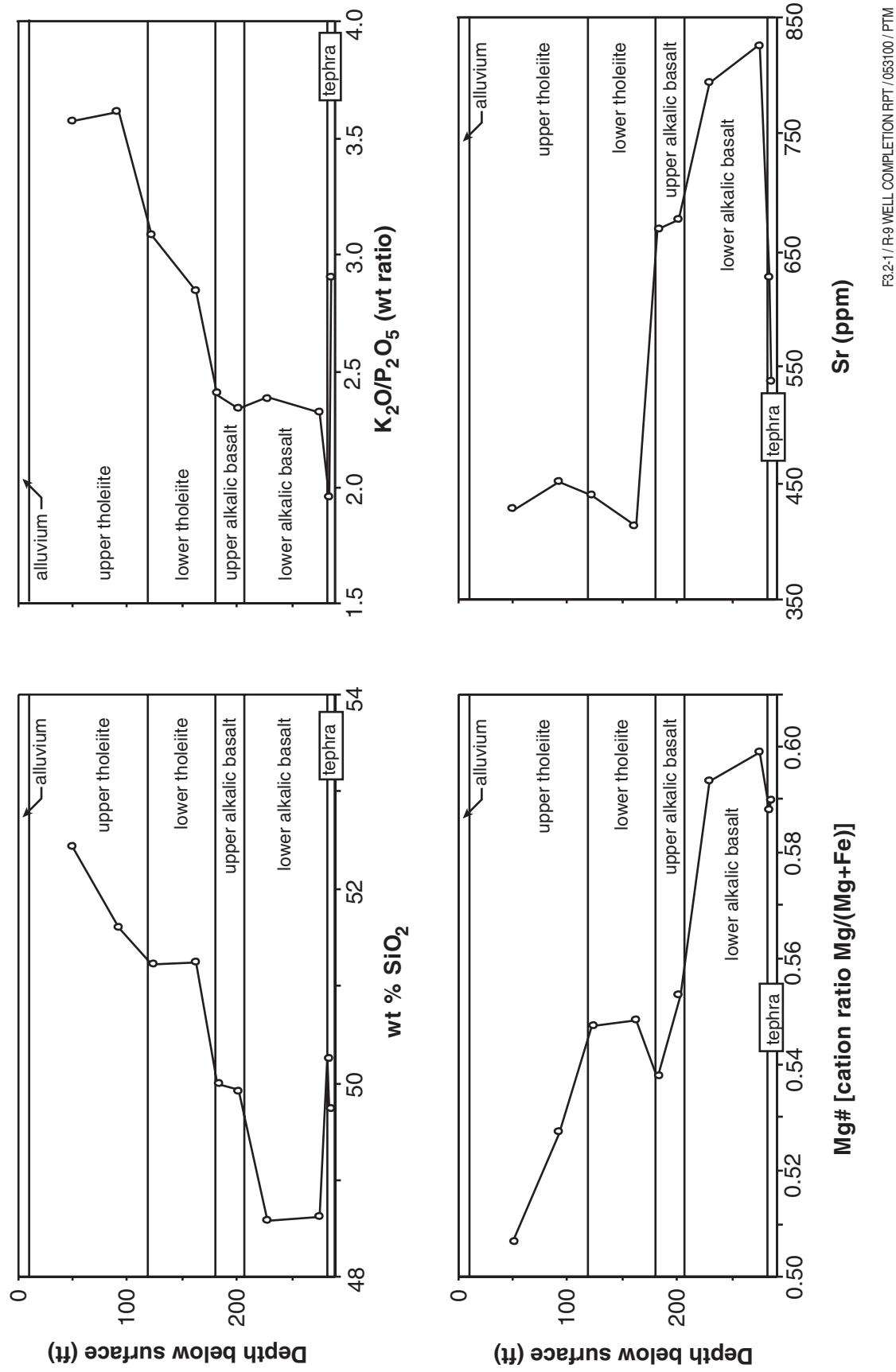

Figure 3.2-1. Variations in SiO_2, K_2O/P_2O_5, Sr, and Mg# [cation ratio of Mg/(Mg+Fe)] with stratigraphic depth in the sequence of Pliocene basalts sampled at R-9. Data for these plots are in Table 3.0-1.

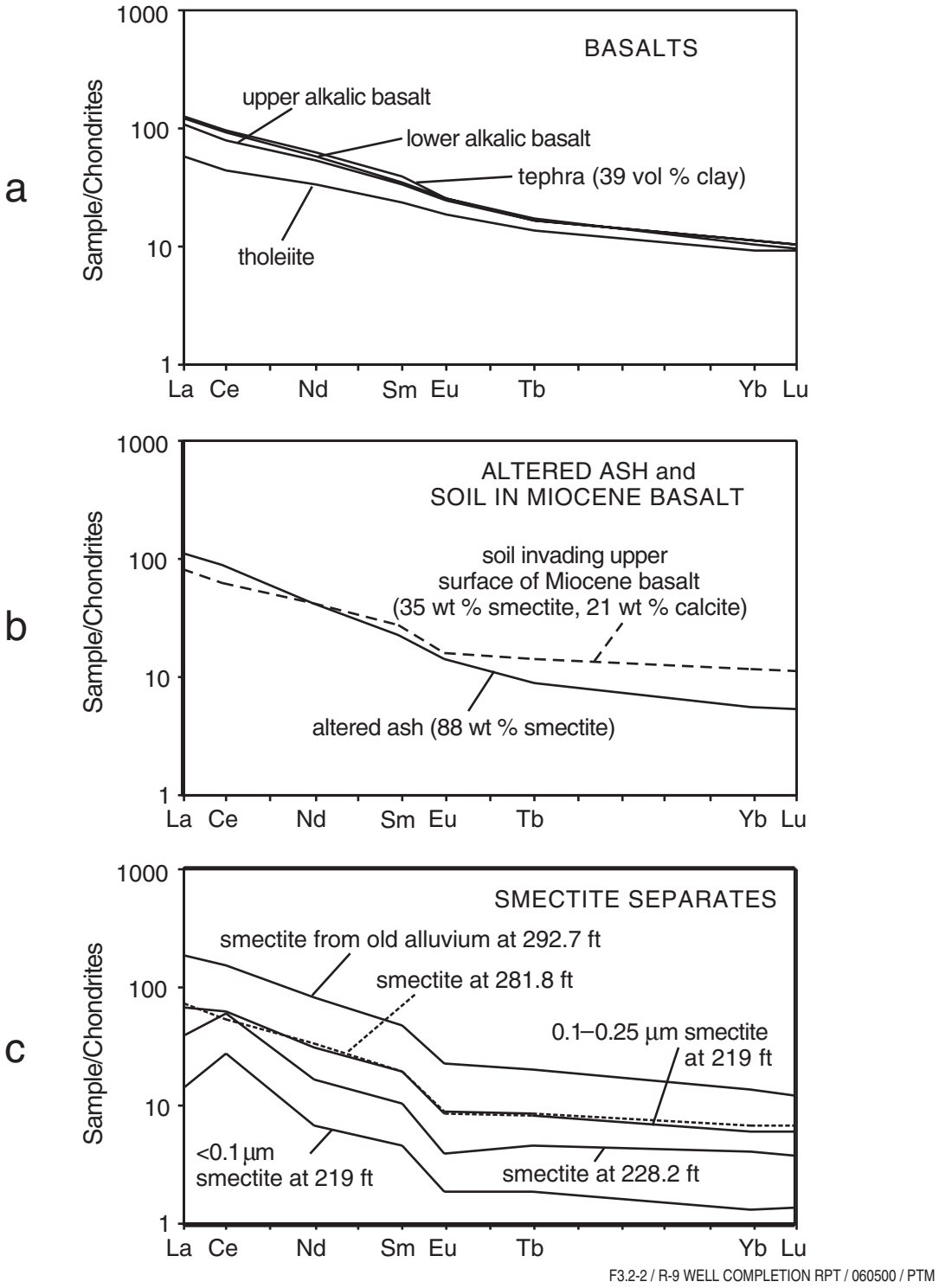

Figure 3.2-2. Chondrite-normalized lanthanide-element profiles for R-9 samples from (a) unaltered tholeiitic and alkalic basaltic lavas and clay-altered (39 vol % clay) tephra, (b) clay-altered tuffaceous ash of the Puye Formation and clay-rich (35 wt % smectite) top of the Miocene basalt, and (c) smectite separates from alkalic basalt at 219- to 281.8-ft depth as well as from the old alluvium at 292.7-ft depth. Data for these plots are in Tables 3.0-1 and 3.7-1.

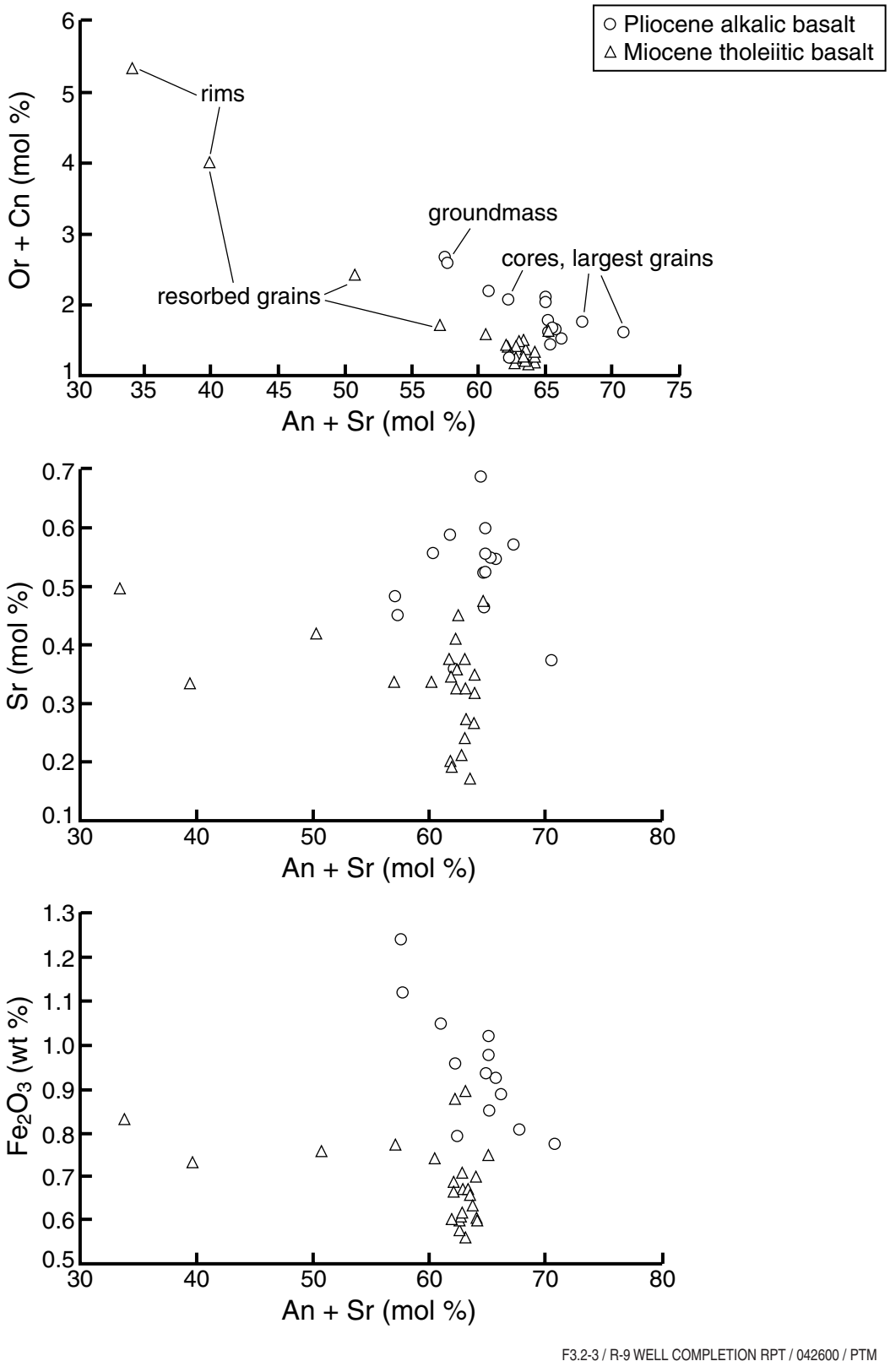

Figure 3.2-3. Variations of K + Ba (Or + Cn), Sr, and Fe_2O_3 content in plagioclase phenocrysts from the lower alkalic basalt and from the Miocene tholeiite in drill hole R-9

Petrographic and chemical character is discussed for each of the four Pliocene basaltic lava series (Sections 3.2.1 to 3.2.4) and for the tephra (Section 3.2.5).

3.2.1 Upper Tholeiite (10- to 118.5-ft depth)

The upper tholeiite in R-9 is relatively well characterized by geophysical logging and by borehole video examination. Video examination and field examination of cuttings from the nearby drill hole R-9i (30 ft west of R-9) have provided additional information on this unit. The borehole video logs from R-9 and R-9i show that the upper tholeiite consists of vesicular and variably fractured lava flows separated by breccia zones at depths of 29.7–45.5 ft, 50–52 ft, 78.5–80.5 ft, 93–99 ft, and 107–116 ft. The borehole videos support the natural gamma and caliper logs (Figure 5.8-2) in indicating a physical and compositional transition at ~24-ft depth, which correlates with a transition from pale-gray aphyric basalt to darker porphyritic lavas more characteristic of the upper tholeiite. At greater depth (~75–88 ft) there is a prominent fracture and rubble zone, visible in the caliper and compensated density logs of Figure 5.8-2, separating two flow subunits within the upper tholeiite. Olivine in this zone is more altered than in the flows above and below. Samples R9-50.5D and R9-92D, on either side of this transition at ~75- to 88-ft depth, were selected for more detailed analysis of the upper tholeiite series.

The upper tholeiite is relatively K-rich, relative to average tholeiitic compositions, and it contains common plagioclase and scarce to common olivine phenocrysts. Compared to the underlying flows (Figure 3.2-1), this basalt has the highest silica content and lowest Mg# ratio. Both of these parameters indicate significant evolution through fractional crystallization. Phenocryst contents for R9-50.5D (Table 3.2-2) distinguish this flow as having the highest plagioclase and lowest olivine content among the four lava sequences. The depth for the lower contact corresponds to a slight downward rise in the natural gamma log (Figure 5.8-4b) at 118-ft depth. The lower ~12 ft of the upper tholeiite and the upper ~10 ft of the lower tholeiite contain abundant vesicle-filling clay.

3.2.2 Lower Tholeiite (118.5- to 180-ft depth)

The lower tholeiite series, from 118.5- to 180-ft depth, shows relatively little variation in natural gamma logging (Figure 5.8-4b) but appears to be fractured, brecciated, and rather extensively clay-altered within a few feet of the basal contact (caliper and resistivity logs at ~173–180 ft, Figure 5.8-3). Relevant to this observation is evidence for the first encounter with perched water as drilling penetrated the base of this unit at 180 ft (Figure 2.3-1), with a rapid rise of water to 137 ft after this water-bearing zone was encountered (see section 4.1 below).

Two samples analyzed from the lower tholeiite, at 122- and 162-ft depth, are relatively constant in composition and less evolved (higher in Mg#) than the samples from the upper tholeiite. A thin breccia zone that contains abundant clay defines the position of the lower contact with the upper alkalic flow. A distinguishing feature of the lower tholeiite is common olivine phenocrysts in an ophitic texture. The transition from lower tholeiite to alkalic basalt compositions at 180-ft depth is marked by prominent increases in Sr, Ba, and light lanthanide-element contents below this depth (see Sr, Figure 3.2-1).

3.2.3 Upper Alkalic Basalt (180- to 206-ft depth)

The upper alkalic basalt in R-9 is a thin unit (26 ft thick) that includes the fracture, breccia and clay zone below the lower tholeiite and a horizon of prominent caliper excursion at 206-ft depth, below which magnetic susceptibility rises and resistivity decreases (Figure 5.8-3). The entire sequence of upper alkalic lava, from 180- to 206-ft depth, contains abundant clay. In gamma logs, the expected higher count rate attributable to K, Th, and U in crossing the boundary between the lower tholeiitic and upper alkalic basalts

is apparently obscured by clay alteration of basaltic glass at the margins of both flows, although a modest rise in the natural gamma below 180 ft is visible in Figure 5.8-4b. Pervasive fractures in the upper alkalic basalt may provide small-scale communication within the perched horizon that completely saturates the upper alkalic basalt (Figure 2.3-1).

Table 3.2-2
Normalized Mineral Content from Detailed Petrographic Analyses of R-9 Samples

Sample Number	VO	CY	MX	PL	OL	GF	GM	GX	AP	Xtln	Norm fact	PN
Upper Tholeiite												
R9-50.5D	6.6	0	6.6	12.9	2.4	46.3	21.6	3.1	0	86.3	1.071	0.22
R9-92D	2.1	7.8		4.6	5.6	53.0	19.9	1.7	0.33	85.1	1.109	
Lower Tholeiite												
R9-122D	3.1	3.4		0.1	4.3	60.1	24.6	2.0	0.33	91.5	1.070	
R9-162D	1.4	6.2		0.7	4.5	61.4	26.6	0.7	0	94.0	1.082	
Upper Alkalic Basalt												
R9-201.5	9.5	0	4.1	7.1	3.7	50.6	16.5	3.4	0	81.4	1.104	0.25
Lower Alkalic Basalt												
R9-219	13.9	8.2		0.10	7.2	29.2	5.0	0.038	0	41.6	1.284	0.41
R9-228	4.2	0		0.08	8.8	56.4	19.8	5.9	0.37	91.4	1.044	0.40
R9-273.7	3.4	0		0.05	8.1	59.5	17.4	5.0	1.93	91.9	1.035	0.40
Basaltic Tephra												
R9-282.6	20.7	39	3.7	0.62	7.6	21.8	0.12	0.012	0	30.2	2.479	0.53
Miocene Basalt												
R9-690.4		3.8		3.8	5.5	64.2	21.2	2.4	0	96.9	1.065	

Note: Except for voids (VO), clay (CY), and cryptocrystalline residue, or mesostasis (MX), all mineral contents are normalized free of VO and CY. Minerals are plagioclase phenocrysts (PL), olivine phenocrysts (OL), groundmass feldspar (GF), mafics (GM), and Fe-Ti oxides (GX), apatite (AP), and total crystalline material reported (Xtln). Values for spinel (PN) represent their concentration within OL. All values are in volume percent. Palagonitic clay matrix and unrecognizable secondary minerals cannot be confidently distinguished from microscopic voids and so are undetermined. Samples with the lowest crystalline totals (xtln) have the highest contents of palagonitic clay matrix.

The upper alkalic basalt is represented by samples R9-181.3 and by R9-201.5 in Table 3.0-1. This is a relatively K-poor alkalic basalt with scarce to common plagioclase and common olivine phenocrysts. Compared to the bounding flows, this flow has intermediate contents of both refractory elements such as Cr and elements readily assimilated from crustal rocks, such as Ba, K, Rb, and Sr. The plagioclase phenocryst content of this basalt (Table 3.2-2) is higher than in the overlying tholeiite and underlying alkalic flows, and the olivine phenocryst content is lower.

3.2.4 Lower Alkalic Basalt (206- to 282-ft depth)

The lower alkalic basalt is a 76-ft thick unit that contains both the base of the upper perched horizon in the basalts (at ~225- to 236-ft depth) and a thin perched horizon at the base of this unit and above the basaltic tephra. Perching in the lower of these saturated sequences is directly related to clay alteration at the base of the lower alkalic basalt and in the tephra; perching in the upper saturated zone is also associated with clay development in breccia zones and in fractures within flow interiors. Clays have been

separated from samples at three levels within the lower alkalic flow for x-ray diffraction (XRD) analysis (see Section 3.7 of this document). The dominant alteration mineral is smectite, which has banding in thin section that documents the process of deposition within voids. The alteration mineral assemblage in the basalts from which the clays have been separated includes minor amounts of quartz, kaolinite, clinoptilolite, illite/mica, and apatite. Calcite (or any carbonate) is absent in XRD analyses of the clay separates and also was not observed in thin sections.

The lower alkalic flow is represented chemically and petrographically by samples R9-219, R9-228 and R9-273.7. These are moderately potassic alkalic basalts with very rare plagioclase and common to abundant olivine; phenocryst content (Table 3.2-2) distinguishes the lower alkalic basalt as having the lowest plagioclase and highest olivine content among the four Pliocene basaltic groups in R-9. Two samples, R9-228 and R9-273.7, represent the interior of the lower flow. These samples contain no basaltic glass or its finely crystalline equivalent (termed “mesostasis” and listed as “MX” in Table 3.2-2) and have very low estimated porosities (based on optical microscopic examination of visible pore spaces). At the other extreme R9-219, sampled near the top of the lower alkalic flow, is very porous and poorly crystalline, with an original porosity (estimated optically) of at least 22% and a content of 42% primary crystals. This upper sample also contains a large amount of palagonitic clay that formed from original basaltic glass during cooling of the basalt. Locally abundant light-colored clay fills voids and may represent a later cycle of alteration.

Compared to the upper alkalic basalt, the lower alkalic basalt has the highest content of refractory elements such as Cr and Ni but the indicators of crustal assimilation (K_2O/P_2O_5 ratios) are similar in both alkalic basalts. The Mg# is considerably higher in the lower alkalic basalt than in the upper. This high Mg# indicates relatively little olivine fractionation in the lower alkalic basalt compared to the overlying basalts. This is in accord with the abundant olivine (7–9%) in the lower alkalic basalt (Table 3.2-2).

3.2.5 Basaltic Tephra (282- to 289.8-ft depth)

A basaltic tephra at the base of the lower alkalic flow unit, believed to be a maar deposit, is characterized by fine-grained, well stratified beds of silt-sized basaltic glass, and downsection it contains increasing proportions of material derived from older sediments. The tephra is petrographically and chemically represented by samples R9-282.2, R9-282.6, and R9-285.5. Sample R9-282.6 had an original porosity (estimated by optical microscopic methods) of at least 60%: 21% voids and 39% clay that filled original voids, plus perhaps additional microscopic, undeterminable voids. This sample is poorly crystalline (30% primary crystals, normalized to the volume of matrix around voids) and consists in large part of a palagonitic clay matrix that formed from original basaltic glass during cooling of the basalt. A small fraction of the original glass (4% of the total rock) remains as cryptocrystalline material. Otherwise the petrographic analysis of the tephra matches well with analyses from the overlying alkalic basalt flow. However, the tephra samples are higher in SiO_2, lower in Al_2O_3, and lower in all alkali and alkaline-earth elements than the overlying flow. Although some of the chemical differences between the tephra and the overlying flow may be attributable to glass alteration in the tephra, other differences (such as the difference in Al_2O_3 content) are not as readily explained by alteration and indicate underlying primary differences. Nevertheless, the tephra samples are alkalic in nature and mark the initiation of the basaltic eruptive cycle that produced the overlying lavas.

3.3 Old Alluvium (289.8- to 329-ft depth)

Old alluvium was defined by Griggs (1964, 8795) as riverine deposits of unconsolidated sands and gravels deposited on a pediment surface cut on the Puye Formation. The old alluvium in R-9 is readily distinguished from the underlying Puye Formation by an abundance of basaltic clasts from boulder to silt size, recognized from detailed petrographic analysis of sample R9-292.7 (Table 3.3-1). About half the

clasts in this sample were derived from a single, petrographically distinctive basalt with conspicuous quartz xenocrysts. The other half of the clasts in sample R9-292.7 are primarily feldspar-poor dacitic lava. A very small fraction (about 1%) of the clasts are small fragments of granitic rock. Rare tiny fragments of garnet also occur within the matrix of sample R9-292.7. Granitic rocks and garnet fragments have not been recognized in any samples of Puye Formation at greater depth; these small fragments in the old alluvium probably were transported from distant sources by the nearby ancestral Rio Grande and delivered in trace abundances to the R-9 site by eolian processes.

Table 3.3-1
Summary of Petrographic Character for Lithic Clasts in Sedimentary Units of R-9

Depth in R-9 (ft) or Sample Number	Stratigraphy	Clast Lithology	% of Lithics	Total Felsics %	Relative % Felsics			Biotite %	Hornblende %	Orthopyroxene %	Clinopyroxene %	Olivine %	Sphene (ppmv)	Alteration State	Lithic Coatings
					Quartz	K feldspar	Plagioclase								
Older Alluvium															
292.7	Pliocene lava	basalt	48	2.1	11	0	89	0	0.02	0	0.01	4.3	0		
292.7	Miocene lava	basalt	1												
292.7	Tschicoma	silicic to intermediate lava	48	1.8	0	0	100	0.03	0	0	0	0	0		
292.7	Precambrian	granite	1												
Upper Puye Formation															
359	Tschicoma	silicic lava	100	3.4	5	0.1	95	0.6	1.2	0.4	0.4	0	0	glass	
414	Tschicoma	silicic lava	60	2.6	8	0	92	0.8	0.5	0.4	0.2	0	13	glass	
414	≅Rendija Cyn.	silicic lava	40	2.4	18	16	67	0.4	0.01	0.03	0.08	0	60	glass	
454	≅Rendija Cyn.	silicic lava	100	3.7	15	9	76	0.8	0.3	0.3	0.4	0	44	glass	opal
509	≅Rendija Cyn.	silicic lava	100	4.6	26	4	70	0.4	0.6	0.3	0.03	0	220	glass	opal
Lower Puye Formation															
564	Tschicoma	silicic lava	98	6.1	0.7	0	99	0.4	1.0	0.9	0.6	0	0	clay	calcite
564	?	basalt	1												
564	?	siltstone	1												
Rhyodacite from Rendija Canyon															
11/19/84/3	Rendija Cyn.	silicic lava		25.4	18	25	57	0.3	0.1	0.01	0.02		89		

Notes: 1. Felsics (quartz, K feldspar, and plagioclase) are reported both as a total and relative to each other.

2. Clasts include Pliocene basalt similar to that of OT1 at 440- to 470-ft depths; Miocene basalt; Tschicoma Formation lavas; rhyodacite similar to that of Rendija Canyon; and Precambrian granite. Sample 11/19/84/3 from Rendija Canyon is included for comparison.

3. ppmv = parts per million by volume; all other entries are volume percent.

X-ray diffraction analysis of the old alluvium sample R9-292.7 (Table 3.3-2) shows the abundance of detrital quartz (25%), which is far more abundant than in any of the underlying Puye Formation samples. This abundance of quartz is also reflected in the high silica content of this sample (Table 3.0-1). The high quartz abundance is accounted for not by the fragments of quartz-xenocryst basalt, which contributes only a small percentage quartz, but by quartz sands in the alluvial deposits.

Table 3.3-2
Quantitative X-Ray Diffraction Analyses of Representative Lithologies, Drill Hole R-9

Sample ID	Sample Type	Lithology	Glass	Calcite	Smectite	Kaolinite	Zeolite*	Quartz	Cristobalite	Tridymite	Feldspar	Hematite	Mica	Amphibole	Total %
Old Alluvium															
R9-292.7	core	siltstone			20(6)	1(1)	2(1)	25(2)	2(1)	2(1)	45(6)	1(1)	1(1)		100(9)
Upper Puye Formation															
R9-359D	cuttings	sandy gravel	19(8)			tr		2(1)	17(1)	5(1)	56(8)	1(1)	tr	tr	100(8)
R9-414D	cuttings	sandy gravel	25(7)		tr			4(1)	12(1)	6(1)	52(7)	1(1)	tr	tr	100(7)
R9-454D	cuttings	conglomerate	21(8)		tr			5(1)	11(1)	5(1)	54(8)	2(1)	1(1)	1(1)	100(8)
R9-509D	cuttings	sandy gravel	28(7)		tr			7(1)	8(3)	5(1)	50(7)	1(1)	1(1)	tr	100(8)
Lower Puye Formation															
R9-564D	cuttings	pebbly sand			25(8)			6(1)	11(1)	2(1)	54(8)	1(1)	tr	1(1)	100(12)
R9-587.4	core	tuffaceous sandstone			52(16)	1(1)	tr	4(1)	2(1)		41(6)	1(1)	tr	1(1)	103(17)
R9-595	core	bedded tuff			88(26)	2(1)	tr				4(1)	4(1)			98(26)
R9-606.4	core	bedded tuff		3(1)	94(28)		0	tr			2(1)				99(28)
R9-616.5	core	sandstone/ conglomerate		1(1)	24(7)	1(1)	1(1)	4(1)	10(1)	1(1)	47(7)	1(1)	tr	tr	91(10)
R9-621.3	core	sandstone/ conglomerate		(1)	28(8)		4(1)	3(1)	9(3)	1(1)	48(7)	1(1)	1(1)	1(1)	96(11)
R9-639.8	core	tuffaceous sandstone			37(11)	tr	tr	6(1)	2(1)		50(7)		1(1)	1(1)	98(13)
R9-645.3	core	tuffaceous sandstone		1(1)	61(18)	tr	1(1)	14(1)			32(5)	1(1)	tr	1(1)	111(19)
R9-661	core	tuffaceous sandstone			74(22)	tr	tr	2(1)	1(1)		26(4)		1(1)	3(1)	108(22)
R9-679	core	tuffaceous sandstone	14(10)		16(5)		0	9(1)	3(1)	tr	58(8)		tr	tr	101(14)
Soil															
R9-688.6CY	core	flow top		21(2)	35(11)	1(1)	9(1)	4(1)			33(5)	1(1)	tr		104(12)

Notes: 1. All entries are in weight percent with approximate 2σ uncertainties in parentheses.

2. tr = trace (<1%; plotted as 0.25% in Figure 3.4-1).

* The zeolite mineral present in these samples is tentatively identified as clinoptilolite.

3.4 Puye Formation (329- to 686.4-ft depth)

The Puye Formation at R-9 consists of gravelly to sandy sediments from volcanic source rocks, as described by Griggs (1964, 8795) and Waresback (1986, 58715). These deposits originated principally from Tschicoma Formation volcanic centers to the west and northwest. Core and cuttings samples of the Puye Formation at R-9 show a lack of clasts larger than pebble size. Thus the unit generally contains much finer clasts than reported at other drill holes west of R-9, such as OT4 (Stoker et al. 1992, 58718), or in outcrop throughout the region (Griggs 1964, 8795; Waresback 1986, 58715; Dethier 1997, 49843). Most

of the Puye Formation at R-9 evidently consists of subaerial mudflows (compare pp. 120–122 in Waresback 1986, 58715). Above 539-ft depth in R-9, the Puye deposits consist of unconsolidated sand, pebbly sand, and gravel (see borehole log in Appendix A. Below 539 ft the Puye Formation is more consolidated and consists of sandstone, pebbly sandstone, and conglomerate with some layers of volcanic tephra. A prominent distinction between the upper and lower parts of the Puye Formation in R-9 is the almost complete preservation of volcanic glass in the upper Puye Formation, contrasted with pervasive alteration of originally glassy constituents in the lower Puye to smectite (Figure 3.4-1). On these criteria the Puye Formation in R-9 is subdivided at 539-ft depth into distinctive upper and lower sediment series.

3.4.1 Upper Puye Formation (329- to 539-ft depth)

Petrographic analysis of the >2-mm fraction of five samples from the upper Puye Formation in R-9 shows no basaltic, plutonic, or metamorphic rocks (Table 3.3-1). Instead, virtually all of the clasts consist of various intermediate to silicic lavas. The virtual absence of basalt clasts contrasts markedly with the abundance of basalt clasts in the old alluvium (Table 3.3-1), and also contrasts with a 12% abundance of basalt clasts reported for the Puye Formation at Guaje Canyon in Figure 17 of Waresback (1986, 58715). Additionally, Figure 17 of Waresback reports 28% andesite, whereas only one fragment of andesite was recognized within the five thin sections of Puye Formation from R-9. The clasts within the upper Puye Formation at R-9 and those in Guaje Canyon, 5 km NNE from R-9, apparently originated from different sources.

The >2 mm fragments in thin sections of the upper Puye Formation at R-9 show that >90% of the lithic clasts represent one unit or perhaps two units of the Tschicoma Formation, with one or two additional units that account for <10% of the clasts. Taken as a whole, the lithic clasts are fairly phenocryst-poor, with systematically downward increasing contents of quartz in the upper Puye Formation in R-9 (Table 3.3-1). Like a distinctive rhyodacite exposed in the headwaters of Rendija Canyon, lithics in the upper Puye Formation of R-9 have a relatively high quartz content, and a dominance of hydrous mafics (biotite and hornblende) over anhydrous mafics (pyroxenes); they also contain sphene. The petrographic resemblance to the Rendija Canyon rhyodacite is poor near the top of the upper Puye Formation, but becomes increasingly stronger with depth. Although the rhyodacite from Rendija Canyon is phenocryst-rich, evolved lavas are frequently phenocryst-poor in distal portions, so it is considered likely that the otherwise similar lithics in the upper Puye Formation of R-9 represent volcaniclastic sediments related to the rhyodacite from Rendija Canyon (Table 3.3-1). This contrasts with the sample from the lower Puye Formation, at 564-ft depth, with rare quartz, no sphene, and equal amounts of hydrous and anhydrous mafics, representing an unrelated source unit. The generally uniform petrographic character for lithics from the upper Puye Formation suggests emplacement by processes that are dominantly volcanic rather than sedimentary. The lithics probably represent fragments within mudflows spawned from the margins of growing volcanic domes. If so, the clasts provide stratigraphic markers within the Puye Formation. The rhyodacite from Rendija Canyon has an unpublished K/Ar age, by F. D. McDowell, of 4.55 ± 0.44 Ma (2σ) (McDowell 1987, 65418).

3.4.2 Lower Puye Formation (539- to 686.4-ft depth)

In contrast to the upper Puye Formation at R-9, the lower Puye Formation has only rare conglomerate or fanglomerate deposits and instead contains abundant tuffaceous sandstones with bedded tuffs that are absent in the upper Puye (Appendix A). Fine grain size (sand-size detritus), extensive smectite development, and pervasive loss of original glass are key features of the lower Puye Formation in R-9. Tschicoma clast lithologies in the lower Puye Formation differ from those of the upper Puye Formation in the absence of quartz-rich intermediate lavas (Table 3.2-1). An additional difference from the upper Puye Formation is a general lack of the silica mineral tridymite (Figure 3.4-1), which is less stable in low-temperature hydrous systems than quartz or cristobalite.

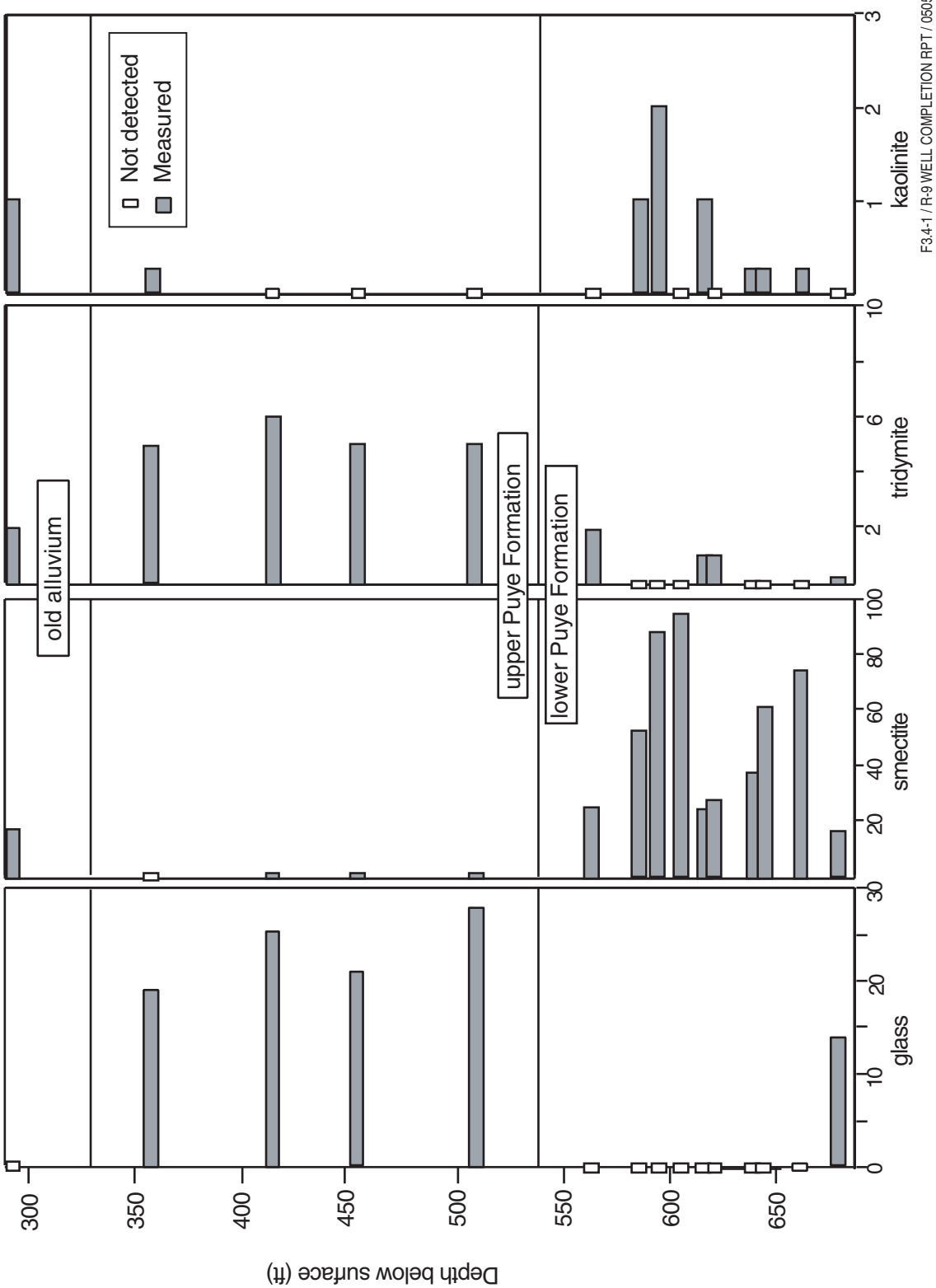

Figure 3.4-1. Abundances of glass, smectite, tridymite, and kaolinite in representative samples from the old alluvium and the Puye Formation in R-9. Note variable scales of horizontal axes (weight percent; quantitative x-ray diffraction data from Table 3.3-2).

The lower Puye Formation contains numerous thin horizons of primary or slightly reworked tuffaceous ash. One of the nonwelded tuffaceous ashes in the lower Puye Formation, at 595.1- to 595.25-ft depth, was sampled and analyzed by x-ray diffraction. This ash consists of 88% smectite with 2% kaolinite, 4% feldspar, 4% hematite, and traces of a zeolite mineral that is probably clinoptilolite (Table 3.3-2). The sample thus represents an almost complete clay replacement of an originally vitric ash bed. The lanthanide-element signature of this sample (Figure 3.2-2b) shows a much greater enrichment of light over heavy lanthanide elements than seen in the basalts (Figure 3.2-2a). This signature, when considered with the other chemical characteristics of this sample (Table 3.0-1), indicates that an intermediate lava (perhaps dacitic) was the precursor. Analysis of immobile elements and their ratios might be used to relate such deposits to potential sources in the Tschicoma Formation or to more distant volcanic centers.

The tuffaceous deposits in the lower Puye Formation probably correlate with waxy tuffs described by Cooper et al. (1965, 8582) between the depths of 795 and 836 ft in nearby water supply well PM-1. Cooper et al. assigned these tuffs to the Tesuque Formation, but their dacitic lithology suggests these tuffs were derived from Tschicoma volcanic sources to the west. Therefore, these tuffaceous deposits are considered part of the Puye Formation.

3.5 Puye Formation (Axial Faces)

Axial deposits of the ancestral Rio Grande (Totavi Lentil of Griggs [1964, 8795]), characterized by abundant clasts of quartzite plus plutonic and metamorphic rocks, were predicted to occur at the base of the Puye Formation, based on lithologic logs from nearby water supply wells. These deposits are not present.

3.6 Late Miocene Basalt (686.4- to >710-ft depth)

A tholeiitic basalt of Late Miocene age occurs beneath the Puye Formation at 686.4 ft to 771 ft (total depth) in R-9. Two samples of this basalt within 10 ft of each other yield ages of 8.63 and 8.45 Ma (Table 3.2-1); the analytical uncertainties on these ages are larger than those for the Pliocene basalt samples and can be interpreted as a single age of ~8.5 to 8.6 Ma. Only three other Late Miocene Cerros del Rio basalts west of the Rio Grande are potentially related tholeiites. A sample of tholeiitic basalt from 2219- to 2231-ft depths in Otowi-1 (Purtymun et al. 1993, 15371) that has been dated with 2σ uncertainty at 12.9 ± 0.3 Ma (WoldeGabriel et al., in preparation) provides a poor chemical match with R9-690.4 and is significantly older. Based on these differences, this basalt in Otowi-1 is not considered to correlate with the basalt beneath Puye Formation in R-9. However, tholeiitic basalt samples DN/97/7 and Otowi-4-1210D provide a fair match with R9-690.4. Both samples have Late Miocene ages via $^{40}Ar/^{39}Ar$; DN/97/7 has been dated at 8.77 ± 0.09 Ma (unpublished analysis by Heizler) and Otowi-4-1210D at 8.81 ± 0.08 Ma (WoldeGabriel et al., in preparation). Although the chemistry differs among R9-690.4, DN/97/7, and Otowi-4-1210D, the generally small differences could be attributed to a combination of alteration, a multiplicity in flow units of this age, and intraunit zonation.

Vesicles and fractures within the uppermost foot of the Late Miocene basalt of R-9 have been filled by thick accumulations of clay and calcite with some drusy quartz. Calcite veins extend downward in hairline fractures an additional 0.8 ft below this depth. A deeper sample of unweathered Miocene basalt at 690.4-ft depth was collected and analyzed for major-element and XRF-suite trace elements (Table 3.0-1); this basalt is significantly lower in SiO_2 and higher in CaO than the Pliocene tholeiites at higher stratigraphic levels in R-9. It also has somewhat higher Sr and Ba. These features, especially the higher Si and Ca contents, distinguish the Miocene tholeiite from the younger basalts.

The lanthanide-element composition of a soil developed on the Miocene tholeiite (sample 688.6) has a light-lanthanide element enrichment and minor negative Eu anomaly that differ from the lower light lanthanides and lack of Eu anomaly in the Pliocene tholeiite (Figure 3.2-2a,b). The pattern in the soil sample is common to many soils containing eolian materials that have compositions similar to calculated crustal averages (Vaniman et al. 1999, 65655). The soil sample consists predominantly of detritus of feldspar (33%) and quartz (4%) with smectite (35%) and calcite (21%). These features indicate soil formation in a moderately arid environment with significant eolian input of calcareous material.

3.7 Relations Between Clay Zones and Hydrostratigraphy

The principal alteration phase throughout the lavas and sediments of R-9 is clay. The predominant clay mineral is an interstratified dioctahedral illite/smectite with smectite predominant (hence referred to simply as smectite in this text). Kaolinite occurs but only in minor amounts (e.g., Figure 3.4-1). These clays may form either by alteration of the host rock in situ or by alteration elsewhere followed by transport to their present location. Both processes may have occurred during generation of the clay occurrences in R-9, but geochemical evidence suggests that most of the clays, particularly those analyzed from the basalts, formed predominantly by alteration of the local host rock.

Samples from four horizons where clay is abundant were processed for clay-mineral extraction and analysis. These four samples are from R9-219 (clay from vesicles, lower alkalic basalt), R9-228.2 (clay from vesicles, lower alkalic basalt), R9-281.8 (clay from a fracture at the base of the lower alkalic basalt), and R9-292.7 (clay matrix of siltstone in the old alluvium). The sample from the alkalic basalt at 219-ft depth was analyzed as two size fractions, one of 0.25–0.1 μm and one of <0.1 μm. Results of INAA analyses are listed in Table 3.7-1.

All clay samples separated from the alkalic basalt and from the siltstone are smectites with approximately 25% to 30% collapsed (illitic) layers. One of the guides to smectite origin is major-element content, but the use of smectite composition to infer origin requires careful consideration. For example, the iron content in the separated smectites from the Fe-rich basalt is lower (3.5–4.5% Fe_2O_3) than in the smectite from the siltstone (9% Fe_2O_3). Thus the Fe content of smectite is not necessarily higher in Fe-rich source rocks and lower in Fe-poor source rocks. As another example, smectites that halo opaque oxides and Fe-rich silicates in the Bandelier Tuff can have exceptionally high Fe contents (18% Fe_2O_3) even though the bulk tuff is not Fe-rich (2–3% Fe_2O_3; Vaniman, in preparation). Moreover, more than one composition of smectite can occur in a single lithologic type, depending on specific minerals or glasses within the sample that are targeted by different stages of alteration. Electron microprobe analysis of clays associated with altered olivine in the Miocene basalt at 690.4-ft depth in R-9 (Table 3.7-2) are far more iron rich (22% Fe_2O_3) than clays separated from vesicles and fractures in the Pliocene alkali basalt (3.5–4.5% Fe_2O_3). Thus other factors, beyond major-element composition, need to be considered in studies of clay origins and of water-clay interactions.

Trace elements in smectites can provide more explicit constraints on origin. In particular, lanthanides and other heavy metals can preserve ratios indicative of source rocks and deviations from those ratios indicative of the alteration process. Where lanthanide analyses have been obtained for the clays in the Pliocene alkalic basalts, chondrite-normalized patterns generally parallel those of the host basalts but have pronounced negative Eu anomalies and may or may not have positive Ce anomalies (Figure 3.2-2c). Parallel patterns and negative Eu anomalies can reflect alteration of basalt mesostasis or glass where calcic (Eu-rich) feldspar crystals are not altered. However, as with the range of Fe contents, this is not definitive evidence for origin by alteration of local basaltic components. The case for local basalt sources is strengthened by other indicators such as U/Th trends in the smectites that parallel those in the basalts (Figure 3.7-1); however, further data are needed to fully constrain the smectite origins.

Table 3.7-1
INAA Chemical Analyses of Clay Separates from Drill Hole R-9

	R9-219CY4	R9-219CY5	R9-228.2CY4	R9-281.8CY4	R9-292.7CY4
	clay from lower alkalic basalt (0.1–0.25 µm)	clay from lower alkalic basalt (<0.1 µm)	clay from lower alkalic basalt (0.1–0.25 µm)	clay from lower alkalic basalt (0.1–0.25 µm)	clay from old alluvium (0.1–0.25 µm)
Na_2O %	0.121	0.131	0.112	0.173	0.068
K_2O %	1.10	0.75	1.47	1.41	0.90
CaO %	2.00	2.18	1.40	1.50	2.83
Fe_2O_3 %	4.48	3.52	4.16	4.42	8.98
Sc ppm	15	13	11	12	17
Cr ppm	34	21	27	30	18
Co ppm	33	42	6	23	67
Zn ppm	118	97	118	112	165
As ppm	2.09	0.96	1.39	1.83	1.72
Rb ppm	104	61	115	108	87
Sr ppm	150	101	99	101	142
Zr ppm	141	86	228	127	330
Sb ppm	0.42	0.17	0.43	0.44	0.31
Cs ppm	7.01	3.22	6.88	8.39	6.13
Ba ppm	228	95	188	177	241
La ppm	25	5	14	26	68
Ce ppm	60	27	56	51	143
Nd ppm	22	5	12	23	57
Sm ppm	4.45	1.06	2.43	4.57	10.80
Eu ppm	0.76	0.16	0.35	0.77	1.93
Gd ppm	3.99	0.98	2.34	3.79	8.57
Tb ppm	0.49	0.11	0.26	0.51	1.18
Tm ppm	0.25	0.05	0.17	0.28	0.53
Yb ppm	1.48	0.33	1.04	1.70	3.34
Lu ppm	0.23	0.05	0.15	0.26	0.48
Hf ppm	3.52	2.69	4.93	2.92	7.96
Ta ppm	1.08	0.38	1.41	0.84	2.89
W ppm	2.49	26.56	8.23	6.72	6.71
Th ppm	9.08	2.57	7.61	8.51	16.40
U ppm	6.30	3.27	4.88	5.44	5.34

Note: Clay sample R9-219CY4 is 98% smectite with 1% kaolinite and traces of clinoptilolite, quartz, and feldspar; clay sample R9-219CY5 is pure smectite; clay sample R9-228.2CY4 is 98% smectite, 1% kaolinite, and 1% feldspar, with traces of mica, clinoptilolite, and quartz; clay sample R9-281.8CY4 is 97% smectite with 1% each of kaolinite, quartz, and feldspar; clay sample R9-292.7CY4 is 99% smectite with 1% apatite and a trace of kaolinite. Clay purity and abundances of associated minerals are determined by x-ray diffraction.

Table 3.7-2
Electron Microprobe Analysis of Clay in Miocene Basalt, R9-690.4

Na_2O %	MgO %	Al_2O_3 %	SiO_2 %	K_2O %	CaO %	TiO_2 %	MnO %	Fe_2O_3 %	SrO %	BaO %	Total %
0.08	12.0	7.11	43.9	0.52	2.85	0.04	0.09	22.0	0.02	0.11	88.72

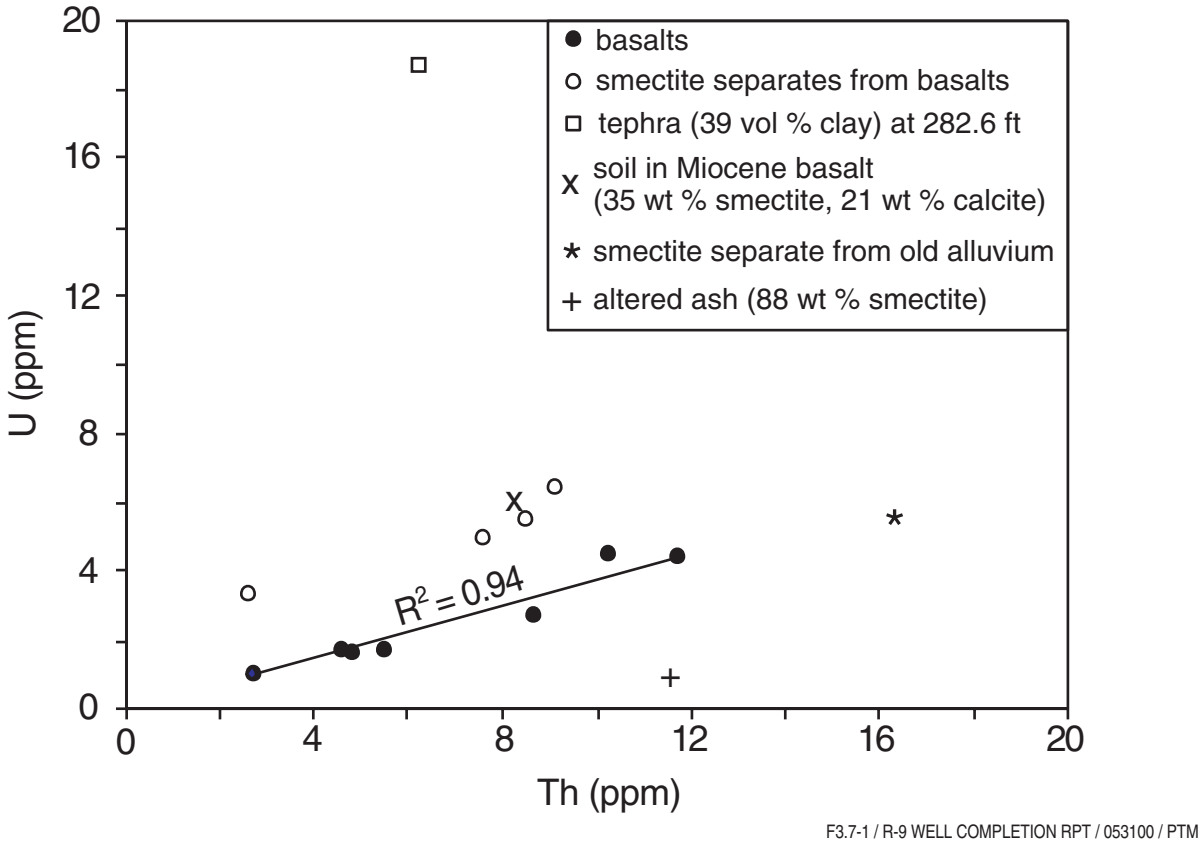

Figure 3.7-1. U versus Th systematics at R-9 for unaltered basalts, clay-altered basalts, and clay separates from basalts, as well as from an altered ash in the Puye Formation

Aside from the limited evidence for smectite origins, the chemical data provide more definitive evidence for interactions of groundwater with the clays. Key among these observations is the development of positive Ce anomalies in smectites at 219- and 228.2-ft depths in the lower alkalic basalt (Figure 3.2-2c). There is evidence from other smectite associations in the Bandelier Tuff for Ce accumulation through oxidation of Ce^{3+} to Ce^{4+} on the surfaces of oxide minerals that are commonly intergrown with smectites in these environments (Vaniman et al., in preparation). The implication of this phenomenon is that the clay-oxide association is effective in fixing metals from solution through oxidation reactions. The importance of this process in removing Pu from groundwater has been demonstrated through combined microautoradiography and synchrotron XANES studies (Duff et al. 1999, 65654). It is noteworthy that the development of positive Ce anomalies in clays is seen in some but not all of the clay separates from the lower alkalic basalt, and that no Ce anomaly is seen in the clay separated from the old alluvium below the basalt. Because the property of Ce fixation is linked to clay-oxide intergrowths (particularly with

Mn-oxides), these variations likely reflect the presence or absence of such intergrowths in the various clay separates.

Reactions of clay systems with some other heavy metals can be examined through the relationships of U and Th in various samples. Figure 3.7-1 shows the correlation of U and Th in the Pliocene alkalic and tholeiitic basalts. Clays derived from these basalts and from the soil in the Miocene basalt all lie at higher U content for a given Th content. This deviation from the trend for basalts reflects both alteration and soil-forming processes. The higher Th content in the clay separated from the old alluvium indicates a very different alteration system, as does the very low U content of the clay-altered tuff ash in the Puye Formation. A particularly interesting outlier is the sample of clay-altered Pliocene basaltic tephra with very high U content (18.7 ppm). This high U content, at a relatively low Th content (6.2 ppm), is highly unusual for either a basalt or a smectite derived from basalt. The sample with this anomalous composition, the tephra at 282.6-ft depth, forms the perching layer above which groundwater with an anomalously high U content occurs in R-9 (see Sections 5.2.2.5 and 5.2.2.6 of this document). It is likely that the U accumulated in this clay is anthropogenic.

4.0 OCCURRENCES OF GROUNDWATER

Four saturated groundwater zones were encountered during drilling operations. All but one of these represent perched conditions. Figure 2.3-1 shows the occurrences of these saturated zones.

4.1 Perched Zones

The first perched zone encountered occurs in the middle of basaltic rocks of the Cerros del Rio volcanic field (Figure 4.1-1). This perched system is one of the thickest occurrences of intermediate-depth groundwater identified in the eastern part of the Laboratory. Water was first encountered at a depth of 180 ft and quickly rose to a depth of 137 ft after the top of the water-bearing zone was penetrated. These conditions suggest two different interpretations.

One interpretation is that the upper perched zone is relatively permeable and confined. In this interpretation, the top of the perched zone occurs at 180 ft in a thin clay-rich basaltic breccia separating two basalt flows. It is uncertain whether the upper confining bed is the clay-rich basaltic breccia or overlying massive lower tholeiitic basalt because coring operations did not begin until the zone was first detected. The upper alkalic basalt flow beneath the breccia is highly fractured, and these fractures probably provide the permeability in this perched zone. The base of the perched zone is believed to occur between 225 and 236 ft. The water occurs in the highly fractured basalt above the massive unfractured basalt below, which is the suspected perching horizon. Rare fractures in the perching layer are notably clay-poor compared with clay-rich fractures in the overlying saturated zone.

A second interpretation is that the upper perched zone is not confined. Instead, the first appearance of water at 180 ft corresponds to the point at which the borehole wall was permeable enough to allow water from the surrounding saturated zone to readily enter the borehole. The 180-ft depth corresponds to the contact between the lower tholeiitic and underlying upper alkalic flows of the Cerros del Rio basalts. The upper alkalic flow is apparently more permeable at this location than the overlying tholeiitic flow. Fractures in the overlying tholeiitic basalt may be less abundant and poorly connected, thus limiting flow to the borehole.

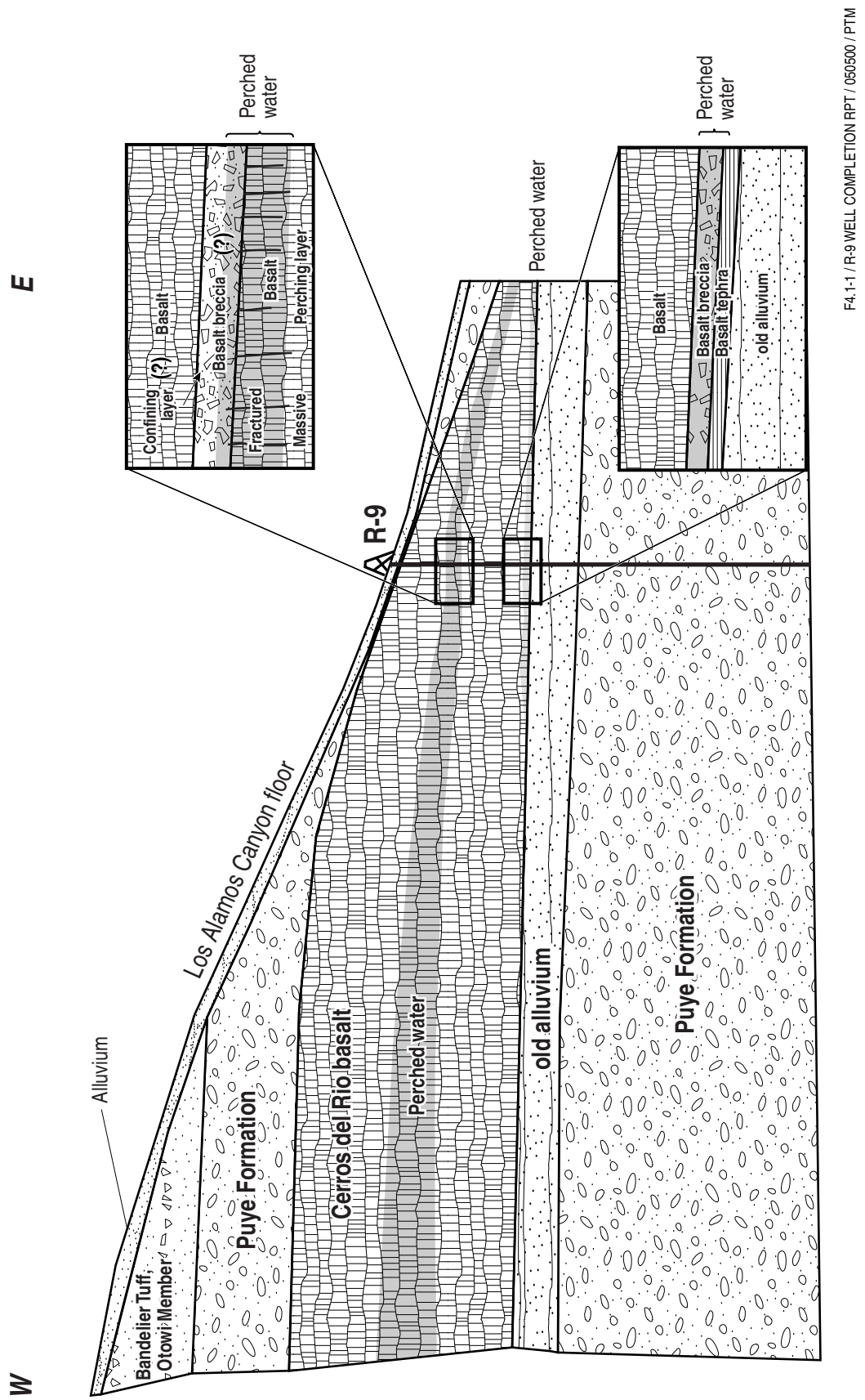

Figure 4.1-1. Setting of perched water in the basaltic rocks of the Cerros del Rio volcanic field in R-9

A second perched zone was encountered in a breccia zone at the base of the basaltic rocks of the Cerros del Rio volcanic field (Figure 4.1-1). Saturation was first recognized at a depth of 275 ft and water slowly rose to a static level of 264 ft. As discussed for the upper perched zone, two interpretations are possible. One is that the water is confined by massive unfractured basalt that overlies a saturated clay-rich basaltic breccia. The basaltic breccia appears to constitute the permeable interval within the second perched zone. The perching layer occurs at a depth of 282 ft within fine-grained, highly stratified basaltic tephra. These tephras occur immediately above the old alluvium of Griggs (1964, 8795). Another interpretation is that water in this zone is not confined. Rather, local permeability conditions are such that water entered the borehole more slowly above 275 ft and was not recognized during drilling. Hydraulic conductivity of the second perched zone appears to be significantly less than in the first perched zone, as evidenced by the slow recovery of water levels in the borehole after the samples were collected and the resistance to injection of water during hydraulic-property testing.

In the third saturated zone, three permeable intervals were encountered in the lower part of the Puye Formation at depths of 579, 615, and 624 ft. These intervals are thin, transmissive sand and gravel beds intercalated within a thick sequence of clay-rich, tuffaceous sedimentary deposits. When the top of the permeable interval was penetrated at a depth of 579 ft, the water level rapidly rose 55 ft to a depth of 524 ft. The base of the 579-ft interval occurred at a depth of 580.5 ft. For the permeable interval at 615 ft, water rose slowly while the borehole rested over the weekend. By the following Monday, the SWL was 524.7 ft. The slow seepage of water into the 615-ft interval indicates that it is not as transmissive as the other two permeable intervals. The permeable interval at a depth of 624 ft consists of transmissive sand and gravel. The base of this interval occurs at a depth of 626.8 ft. When the top of this interval was penetrated, the water level rapidly rose 100 ft in the borehole to a depth of 524 ft. The similar static water levels encountered in all three permeable intervals indicate that they are hydraulically connected and constitute a single saturated zone. The water may be confined between the low-permeability clay-rich deposits in this zone. Alternatively, the water may be unconfined and saturation was not recognized because the clay-rich beds limit flow into the borehole. Currently, these three intervals are each believed to be perched.

4.2 Regional Aquifer

The fourth saturated zone occurs within the top of a basalt that is identified as the top of the Santa Fe Group. This zone occurs at a depth of 688 ft and is unconfined. Saturation occurs in highly fractured basalt and extends beyond the total depth of the borehole. This saturated zone is believed to be associated with the regional aquifer based on the similarity of its water chemistry to that from nearby supply wells PM-1 and PM-3 as well as Test Well 3. However, the elevation at the top of this zone (5694.8 ft) is lower than SWLs for the regional aquifer in wells PM-1 (5758 ft) and Otowi-1 (5724 ft), and it is lower than the elevation predicted based on regional water-table maps (5780 ft) (Figure 1.0-1).

The SWL for the regional aquifer in the R-9 borehole was recorded for a one-year period. The water-level measurements were taken with a transducer that was placed inside the temporary 4-in. polyvinyl chloride (PVC) casing and screen installed in the R-9 borehole. Water level and atmospheric pressure were recorded at 15-min intervals from March 3, 1998, to March 8, 1999. Figure 4.2-1 shows the relationship between atmospheric pressure and the static water level in the regional aquifer. A rise in atmospheric pressure results in a lowered SWL. Conversely, the SWL rises during periods when the atmospheric pressure decreases. As shown on Figure 4.2-1, the change in atmospheric pressure over a period of a few days in February 1999 resulted in a 1-ft change in the static water level. The one-year record collected in borehole R-9 indicates an average annual change of less than 0.15 ft for the SWL in the regional aquifer.

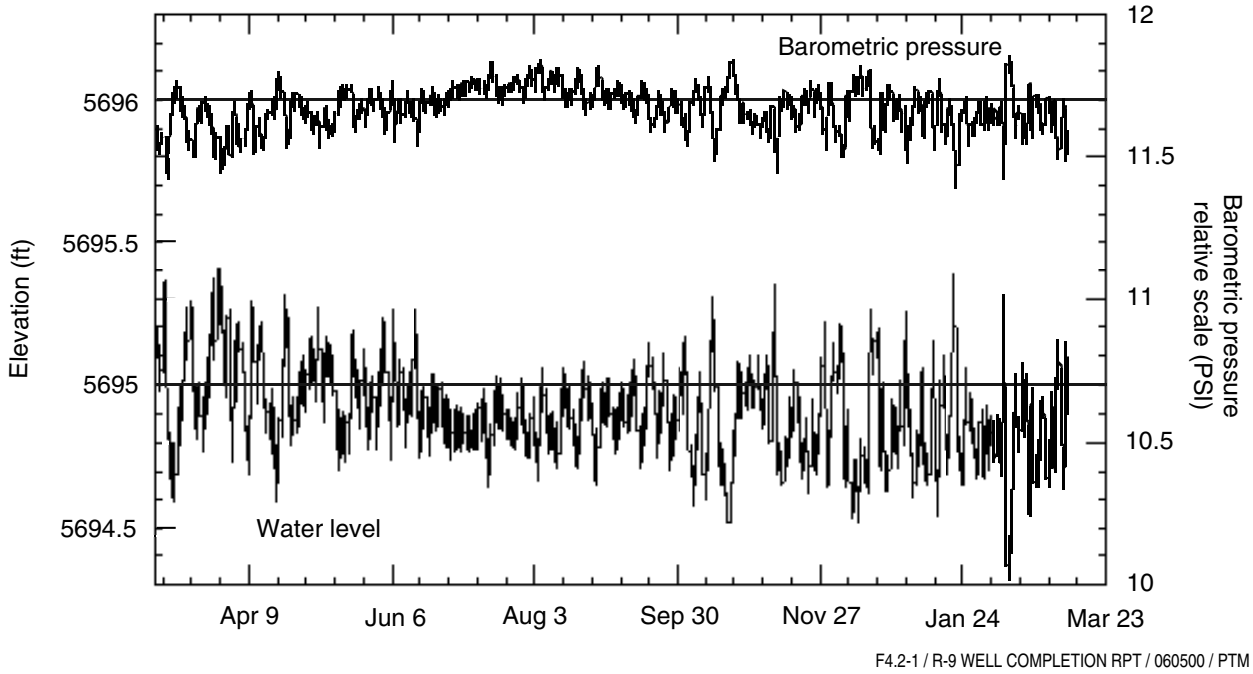

Figure 4.2-1. Water level for the regional aquifer in borehole R-9 from March 3, 1998, to March 8, 1999

5.0 SAMPLING AND ANALYSIS

5.1 Contaminant Characterization of Core and Cuttings

Samples of core and cuttings were collected and analyzed for Resource Conservation and Recovery Act (RCRA) metals, volatile organic compounds (VOCs), semivolatile organic compounds (SVOCs), and radionuclides. Results of chemical and radiochemical analyses are used to determine both naturally occurring elements and contaminant distributions. Contaminants of concern in upper Los Alamos Canyon include americium-241; cesium-137; plutonium-238; plutonium-239,240; strontium-90; tritium; uranium-235; and uranium-238 (LANL 1995, 50290).

5.1.1 Methods

Fifteen samples of core and cuttings were collected for geochemical and contaminant characterization. Five samples of cuttings were collected from the following depth intervals: 41 to 50.5 ft, 50.5 to 55.5 ft, 172 to 178.5 ft, 568 to 569.7 ft, and 570 to 571.5 ft. Ten samples of core were collected from the following depth intervals: 181.1 to 182.5 ft, 185.3 to 187 ft, 205 to 206 ft, 230.4 to 231.3 ft, 236.5 to 237.3 ft, 237.3 to 238.1 ft, 268.5 to 270.8 ft, 280.5 to 281 ft, 291.2 to 292.6 ft, and 582 to 583.5 ft. Approximately 500 to 1000 g of core and cuttings samples were placed in appropriate sample jars in protective plastic bags before being shipped to analytical laboratories. The locations of the samples and the stratigraphic units from which they were collected are shown in the column labeled “Field Analytical Sample Number” in the borehole log in Appendix A.

Samples of core and cuttings were analyzed using a variety of analytical methods specified by the EPA (1997, 57589). Field screening for VOCs was conducted using a photoionization detector (PID) instrument. No VOCs were detected with the field instrument. Solid samples were partially digested using hot HNO_3 (EPA method 3050) before metal analyses. Samples of core and cuttings were shipped to Paragon Analytics, Inc., in Fort Collins, Colorado, for metal and radionuclide analyses. Analyses for aluminum, antimony, arsenic, barium, beryllium, cadmium, calcium, chromium, cobalt, copper, iron, lead, magnesium,

manganese, molybdenum, nickel, potassium, selenium, silver, sodium, thallium, uranium, vanadium, and zinc were determined by inductively coupled plasma emission spectroscopy (ICPES). Concentrations of uranium, using an ICPES method, were biased high in the core and groundwater samples because of matrix interference from iron. Therefore, uranium concentrations determined from ICPES are not included in this report for either core or groundwater samples. Mercury content was analyzed using cold vapor atomic absorption (CVAA). Core samples were washed with deionized water for 16 hr before anion analyses of the leachate. Sulfate, fluoride, bromide, sulfate, nitrate, and chloride contents were determined by ion chromatography (IC). Cyanide content was determined by colorimetry. The precision limits for analysis of major anions and trace elements were generally ±10%. Analyses for occurrence of VOCs and SVOCs was conducted using gas chromatography-mass spectrometry by RECRA Weston.

Radionuclide activities in core samples were determined by alpha spectrometry (americium-241; plutonium-238; plutonium-239,240; uranium-234; uranium-235; and uranium-238), gamma spectrometry (cesium-137 and other isotopes), and gas proportional counting (strontium-90) at Paragon Analytics, Inc. Sample duplicates were collected and analyzed in accordance with EPA procedures (EPA 1997, 57589).

5.1.2 Results

Radionuclides (including americium-241; cesium-137; plutonium-238; plutonium-239,240; strontium-90; uranium-235; and uranium-238) were discharged into Los Alamos Canyon beginning in the early 1940s. Accordingly, distributions of these radionuclides in R-9 are addressed in this section.

Table 5.1-1 provides summaries of radionuclide distributions within the Cerros del Rio basalt and the Puye Formation. Isotopes of uranium (uranium-234, uranium-235, and uranium-238) were detected at activities less than 1 pCi/g in most core samples. These low activities are consistent with low concentrations of naturally occurring radionuclides (e.g., uranium isotopes) in basalt and suggest that little if any Laboratory contamination is present in these samples. Further comparisons with background data will be made when ongoing background studies for basalts are completed. Activities of americium-241; cesium-137; plutonium-238; plutonium-239,240; and strontium-90 generally are less than minimum detectable activity in the samples of core and cuttings, indicating that no Laboratory-derived contamination is detectable in these samples.

Samples of core and cuttings were analyzed for metals including copper, iron, manganese, nickel, and zinc; however, they are not contaminants of concern in upper Los Alamos Canyon. Transition metals, including cobalt, copper, iron, manganese, and nickel, occur naturally within the basalt flows at concentrations above those for the Bandelier Tuff. Background distributions of metals within basalt are being assessed and will be added to the Laboratory background data set.

No VOCs or SVOCs were detected in the two cuttings samples collected from depths of 41 to 50.5 ft and 50.5 to 55.5 ft, indicating that no Laboratory-derived contamination for organic compounds is detectable in these samples.

5.2 Water Quality Determinations

Borehole groundwater samples were collected from the four saturated zones during drilling. These borehole samples provided an initial characterization of water quality in each groundwater zone and were used to target zones for long-term monitoring. Samples were analyzed for inorganic and organic chemicals and radionuclides to determine natural solute and contaminant distributions within the different saturated zones. Telescoping casing and bentonite seals isolated individual groundwater zones from one another so that representative water samples could be collected. In addition, these seals prevented downward migration of potential contaminants to deeper perched zones and to the regional aquifer. Some analytical results may be affected by high turbidity and the disturbed state of the borehole. Additional characterization of the regional aquifer will take place within the developed well.

Table 5.1-1
Radionuclide Activities in Samples of Core and Cuttings from R-9

Depth (ft)	41–50.5	50.5–55.5	172–178.5	181.1–182.5	185.3–187	205–206	230.4–231.3	236.5–237.3
Geologic Unit	CR basalt[a]	CR basalt	CR basalt	CR basalt	CR basalt	CR basalt	CR basalt	CR basalt
Strontium-90[b]	0.04 ± 0.39	0.30 ± 0.43	0.43 ± 0.50	0.03 ± 0.47	0.18 ± 0.47	0.22 ± 0.53	0.10 ± 0.49	0.06 ± 0.50
Cesium-137	0.007 ± 0.052	<0.050	<0.041	<0.061	0.017 ± 0.065	<0.033	0.019 ± 0.039	0.112 ± 0.075
Plutonium-238	0.0094 ± 0.0130	0.0088 ± 0.0170	<MDA[c]	0.0095 ± 0.00158	0.0036 ± 0.0118	<MDA	<MDA	<MDA
MDA	0.025	0.036	0.044	0.033	0.011	0.033	0.030	0.039
Plutonium-239,240	<MDA	0.0077 ± 0.0142	0.0085 ± 0.0150	0.0100 ± 0.0112	0.0167 ± 0.0162	0.0034 ± 0.0110	0.0089 ± 0.0102	0.0138 ± 0.0158
MDA	0.022	0.030	0.032	0.017	0.022	0.010	0.0089	0.028
Americium-241	0.127 ± 0.040	0.0104 ± 0.0104	0.0190 ± 0.0154	0.078 ± 0.030	0.038 ± 0.024	0.038 ± 0.024	0.077 ± 0.032	0.052 ± 0.026
MDA	0.017	0.0078	0.0095	0.027	0.026	0.036	0.031	0.028
Uranium-234	0.205 ± 0.060	0.336 ± 0.082	0.221 ± 0.066	0.236 ± 0.066	0.138 ± 0.048	0.257 ± 0.070	0.393 ± 0.094	0.415 ± 0.096
MDA	0.029	0.031	0.033	0.043	0.031	0.035	0.041	0.037
Uranium-235	0.0190 ± 0.0168	0.030 ± 0.022	0.025 ± 0.022	0.026 ± 0.020	0.0081 ± 0.0128	0.029 ± 0.022	0.026 ± 0.022	0.0198 ± 0.0184
MDA	0.011	0.019	0.022	0.019	0.026	0.026	0.023	0.021
Uranium-238	0.259 ± 0.068	0.248 ± 0.068	0.246 ± 0.070	0.279 ± 0.072	0.184 ± 0.056	0.313 ± 0.078	0.383 ± 0.092	0.402 ± 0.092
MDA	0.027	0.033	0.022	0.029	0.034	0.024	0.013	0.030
Gross Alpha	1.0 ± 1.1	1.5 ± 1.2	0.62 ± 0.81	3.4 ± 1.5	3.0 ± 1.6	3.6 ± 1.8	2.9 ± 1.8	2.7 ± 1.7
Gross Beta	<1.3	0.87 ± 1.6	0.06 ± 0.96	1.8 ± 1.4	2.3 ± 1.7	1.2 ± 1.8	2.0 ± 1.7	2.3 ± 1.7
Gross Gamma	2.30 ± 0.22	2.20 ± 0.23	2.10 ± 0.25	3.35 ± 0.36	3.12 ± 0.36	3.87 ± 0.36	3.86 ± 0.33	5.68 ± 0.47
MDA	0.25	0.26	0.32	0.44	0.46	0.38	0.30	0.41

Table 5.1-1 (continued)

Depth (ft)	237.3–238.1	268.5–270.8	280.5–281	291.2–292.6	568–569.7	570–571.5	582–583.5
Geologic Unit	CR basalt	CR basalt	CR basalt	old alluvium[d]	Puye Fm.[e]	Puye Fm.	Puye Fm.
Strontium-90	0.04 ± 0.47	0.11 ± 0.45	0.27 ± 0.43	0.11 ± 0.65	0.84 ± 0.47	<0.42	<0.34
Cesium-137	<0.046	<0.042	<0.035	0.039 ± 0.050	0.026 ± 0.049	0.002 ± 0.036	<0.069
Plutonium-238	0.0044 ± 0.0156	0.0107 ± 0.0184	0.0147 ± 0.0184	0.0032 ± 0.0160	<MDA	0.027 ± 0.024	0.0069 ± 0.0188
MDA	0.037	0.038	0.035	0.039	0.058	0.039	0.043
Plutonium-239,240	0.0069 ± 0.0112	0.0017 ± 0.0110	0.0005 ± 0.0080	0.0102 ± 0.0130	0.0007 ± 0.0108	0.0014 ± 0.0110	0.0038 ± 0.0124
MDA	0.022	0.029	0.018	0.023	0.026	0.030	0.011
Americium-241	0.037 ± 0.024	0.032 ± 0.024	0.0164 ± 0.0156	0.0139 ± 0.0168	0.0011 ± 0.0086	0.0000 ± 0.078	<MDA
MDA	0.033	0.036	0.023	0.031	0.024	0.023	0.031
Uranium-234	0.391 ± 0.090	0.476 ± 0.110	0.634 ± 0.136	0.993 ± 0.156	0.752 ± 0.108	0.752 ± 0.108	0.660 ± 0.116
MDA	0.038	0.037	0.037	0.027	0.023	0.021	0.029
Uranium-235	0.039 ± 0.026	0.0087 ± 0.0148	0.036 ± 0.028	0.050 ± 0.026	0.047 ± 0.020	0.046 ± 0.022	0.0204 ± 0.0172
MDA	0.020	0.024	0.027	0.022	0.0067	0.018	0.024
Uranium-238	0.521 ± 0.108	0.356 ± 0.092	0.704 ± 0.144	0.952 ± 0.152	0.822 ± 0.128	0.766 ± 0.120	0.650 ± 0.116
MDA	0.024	0.037	0.031	0.027	0.016	0.013	0.026
Gross Alpha	2.1 ± 1.4	2.8 ± 1.8	3.1 ± 1.5	6.4 ± 1.7	3.3 ± 1.3	1.5 ± 1.9	5.1 ± 1.7
Gross Beta	1.9 ± 1.5	2.1 ± 1.9	1.66 ± 0.98	4.1 ± 1.2	2.1 ± 1.1	1.7 ± 1.8	2.5 ± 1.1
Gross Gamma	4.54 ± 0.39	3.87 ± 0.32	4.36 ± 0.36	5.95 ± 0.47	6.41 ± 0.58	6.01 ± 0.51	4.98 ± 0.48
MDA	0.36	0.29	0.32	0.37	0.54	0.43	0.53

Notes: 1. pCi/g.

2. Error of two standard deviations is reported.

[a] CR basalt = Cerros del Rio basalt.

[b] Radionuclides and parameters analyzed by Paragon Analytics, Inc.

[c] MDA = minimum detectable activity.

[d] Old alluvium = old alluvium facies of the Puye Formation.

[e] Puye Fm. = fanglomerate facies of the Puye Formation.

5.2.1 Methods

Groundwater samples for inorganic and organic chemicals and radionuclides were collected using a stainless-steel bailer. Temperature, dissolved oxygen, turbidity, pH, and specific conductance were determined onsite from an aliquot collected during field sampling. Both filtered and nonfiltered samples were collected for chemical and radiochemical analyses. Groundwater samples were collected for analyses of dissolved organic carbon, stable isotopes of hydrogen and oxygen, major cations and anions, metals, and radionuclides. Aliquots of the samples were pressure-filtered through a 0.45-µm Gelman filter and acidified with ultrapure HNO_3 to a pH of 2.0 or less before metal and radionuclide analyses. All groundwater samples collected in the field were stored at 4°C until they were analyzed. Alkalinity was determined in the laboratory using standard titration techniques.

Filtered and nonfiltered groundwater samples were analyzed for different suites of chemicals, including major ions, trace elements, trace metals, stable isotopes, radionuclides, and organic compounds. Groundwater samples were analyzed using a variety of laboratory techniques specified in EPA SW-846 (EPA 1997, 57589) including IC for bromide, chloride, fluoride, nitrate, nitrite, phosphate, and sulfate; graphite furnace atomic absorption (GFAA); colorimetry for total organic carbon; CVAA and ICPES for aluminum, antimony, arsenic, barium, beryllium, boron, cadmium, calcium, cesium, chromium, cobalt, copper, iron, lead, magnesium, manganese, mercury, molybdenum, nickel, potassium, selenium, silver, sodium, strontium, thallium, tin, titanium, vanadium, and zinc. Concentrations of ammonium were determined by using a specific ion electrode. Results of chemical analyses for inorganic species (major cations and anions, trace elements, and trace metals) and radionuclides are provided in Tables 5.2-1, 5.2-2, and 5.2-3.

Radionuclide activity in groundwater was determined by liquid scintillation counting (LSC) for tritium; electrolytic enrichment for low-level tritium; laser-induced kinetic phosphorimetry analysis (LIKPA) for uranium; thermal ionization mass spectrometry (TIMS) for uranium isotopes and total uranium; alpha spectrometry for americium, plutonium, and uranium isotopes; gamma spectrometry for cesium-137 and other isotopes; and gas proportional counting for strontium-90. This work was performed by contract laboratories (Paragon Analytics, Inc., Teledyne, and University of Miami) and by CST-7 for TIMS analysis of uranium.

Sample duplicates, laboratory blanks, and field blanks were collected and analyzed in accordance with EPA and Laboratory procedures. The precision limits for major ions and trace elements were generally ±10%.

Groundwater samples were analyzed for VOCs and SVOCs using gas chromatography and gas chromatography-mass spectrometry through RECRA Weston. Identifiable organic compounds were not detected in the groundwater samples. No organic compounds, except oxalate, have been identified as contaminants of concern in Los Alamos Canyon (LANL 1995, 50290).

The following sections focus primarily on inorganic and radionuclide distributions in groundwater encountered in R-9.

5.2.2 Results

5.2.2.1 Quality of Perched Groundwater Within Cerros del Rio Basalt

Field-measured parameters for the borehole groundwater samples, including pH, temperature, specific conductance, and turbidity, are provided in Table 5.2-4. These parameters were measured at the time of sample collection when groundwater was in contact with the atmosphere. Dissolved oxygen (DO) was also measured; however, DO values are not reported because of potential atmospheric contamination with the electrode and interferences from suspended particles that contributed to very high turbidity values.

Table 5.2-1
Quality of Groundwater Samples Collected at R-9

Part 1						
Depth (ft)	180	180	275	275	579	579
Geologic Unit	CR basalt[a]	CR basalt	CR basalt	CR basalt	Puye Fm.[b]	Puye Fm.
Sample Treatment	Filtered	Unfiltered	Filtered	Unfiltered	Filtered	Unfiltered
Date Sampled	10/06/97	10/06/97	10/16/97	10/16/97	12/18/97	12/18/97
Ag	<0.001	<0.001	<0.001	0.08 ± 0.01	<0.001	<0.001
Al	0.13 ± 0.01	282 ± 3	0.27 ± 0.01	1129 ± 20	0.08 ± 0.01	14.9 ± 0.1
As	0.0008	0.017	0.0013	0.077	0.0004	0.0012
B	0.023 ± 0.002	0.15 ± 0.01	<0.01	1.16 ± 0.02	0.030 ± 0.001	0.048 ± 0.003
Ba	0.017 ± 0.002	1.34 ± 0.02	0.005 ± 0.002	7.23 ± 0.02	0.064 ± 0.001	0.19 ± 0.01
Be	<0.002	0.018 ± 0.002	<0.002	0.067 ± 0.002	<0.002	<0.002
Br	0.16	0.16	0.10	0.08	0.20	0.19
Ca	14.1 ± 0.1	91 ± 0.6	2.91 ± 0.07	1090 ± 10	25.4 ± 0.2	34.1 ± 0.1
Cd	0.0004 ± 0.0002	0.0004 ± 0.0002	0.001 ± 0.0002	0.0053 ± 0.0005	<0.0002	0.0006 ± 0.0002
Cl	29.2	29.5	25.5	26.3	13.2	13.2
ClO_3	<0.02	<0.02	<0.02	<0.02	<0.02	<0.02
Co	<0.002	0.022 ± 0.002	<0.002	1.11 ± 0.02	<0.002	0.003 ± 0.002
CO_3	0	0	7.0	32.6	0	0
Cr	<0.002	0.12 ± 0.01	0.002 ± 0.002	1.22 ± 0.01	<0.002	0.012 ± 0.002
Cs	<0.002	0.020 ± 0.002	<0.002	0.047 ± 0.002	<0.002	0.002 ± 0.002
Cu	0.004 ± 0.002	0.27 ± 0.02	0.017 ± 0.002	11.3 ± 0.1	<0.002	0.012 ± 0.002
F	0.71	0.67	1.27	1.38	0.74	0.74
Fe	0.06 ± 0.01	142 ± 1	0.19 ± 0.01	1460 ± 30	0.06 ± 0.01	9.76 ± 0.2
HCO_3	78.5	93.0	105	400	110	117
Hg	<0.00005	0.00045	<0.00005	0.00035	<0.00005	<0.00005
I	0.17	0.17	<0.01	ND[c]	<0.01	<0.01
K	4.54 ± 0.03	30.6 ± 0.1	5.22 ± 0.02	105 ± 1	2.93 ± 0.02	3.94 ± 0.01
Li	<0.01	0.23 ± 0.01	0.02 ± 0.01	0.68 ± 0.01	0.03 ± 0.01	0.04 ± 0.01
Mg	5.29 ± 0.02	46.2 ± 0.2	1.18 ± 0.01	1083 ± 15	1.24 ± 0.01	4.80 ± 0.06
Mn	0.051 ± 0.001	1.98 ± 0.01	0.013 ± 0.002	31.5 ± 0.3	0.041 ± 0.001	0.33 ± 0.01
Mo	0.025 ± 0.002	0.038 ± 0.002	0.10 ± 0.01	0.34 ± 0.01	0.028 ± 0.002	0.02 ± 0.002
Na	26.1 ± 0.2	51.8 ± 0.1	100 ± 1	400 ± 5	29.8 ± 0.1	29.3 ± 0.1
NH_4	0.03	0.03	0.02	1.34	0.09	0.08
NO_3	<0.02	<0.02	3.61	2.83	10.6	10.7
Pb	<0.002	0.10 ± 0.01	<0.002	0.63 ± 0.01	<0.002	0.01 ± 0.001
PO_4	0.14	0.11	0.61	0.99	<0.05	<0.05
Rb	0.009 ± 0.002	0.27 ± 0.01	0.01 ± 0.002	0.76 ± 0.02	0.005 ± 0.002	0.008 ± 0.002

Table 5.2-1 (continued)

Part 1 (continued)						
Depth (ft)	180	180	275	275	579	579
Geologic Unit	CR basalt	CR basalt	CR basalt	CR basalt	Puye Fm.	Puye Fm.
Sample Treatment	Filtered	Unfiltered	Filtered	Unfiltered	Filtered	Unfiltered
Date Sampled	10/06/97	10/06/97	10/16/97	10/16/97	12/18/97	12/18/97
S_2O_3	<0.01	<0.01	<0.02	ND	<0.05	<0.05
Sb	0.0002	0.0013	0.0012	0.0017	0.0002	0.0010
Se	<0.0002	0.0012	0.0015	0.0017	<0.0001	<0.001
Si	14.1 ± 0.3	120 ± 1	10.4 ± 0.1	230 ± 2	17.2 ± 0.2	51.4 ± 0.3
Sn	<0.005	<0.005	<0.005	<0.01	<0.005	<0.005
SO_4	8.09	8.01	53.8	60.2	12.4	12.1
Sr	0.093 ± 0.002	0.91 ± 0.01	0.033 ± 0.002	13.5 ± 0.1	0.29 ± 0.01	0.36 ± 0.01
Ti	<0.002	3.77 ± 0.01	0.006 ± 0.002	24.0 ± 0.1	<0.002	0.64 ± 0.01
Tl	<0.002	<0.002	<0.002	<0.002	<0.002	<0.002
U	<0.1	<0.1	<0.1	<0.1	<0.1	<0.1
V	<0.002	0.16 ± 0.01	0.004 ± 0.002	1.04 ± 0.01	0.002 ± 0.002	0.009 ± 0.001
Zn	0.01 ± 0.01	0.61 ± 0.01	<0.01	3.17 ± 0.02	0.09 ± 0.01	0.02 ± 0.01
Charge Balance (%)	3.83	n/a[d]	8.44	n/a	-0.35	n/a
Temp. (laboratory, °C)	12.3	12.3	13.2	13.2	15.7	15.7
Conductance (laboratory, µS/cm)	250	256	457	512	273	273
TDS[e]	252.2	1557.5	388.8	11821.4	329.7	544.1
TSS[f]	ND	med	ND	high	ND	low
Hardness ($CaCO_3$)	57.0	417	12.1	7182	68.5	105
Alkalinity (laboratory, $CaCO_3$)	64.3	76.2	97.7	38.2	90.2	95.9
pH (Field, standard units)	8.30	8.30	8.79	8.79	7.9	7.9
pH (laboratory, standard units)	8.02	7.49	8.79	9.09	8.07	8.07
SiO_2 (Calculated)	30.2	257	22.3	492	36.8	110
Oxalate			3.03	2.74	<0.02	<0.02
Acetate	<0.1	<0.1	<0.1	<0.1	<0.1	<0.1
Formate	0.02	0.02	0.04	0.08	0.03	0.04

Table 5.2-1 (continued)

Part 2						
Depth (ft)	615	615	624	624	688	688
Geologic Unit	Puye Fm.	Puye Fm.	Puye Fm.	Puye Fm.	SF basalt[g]	SF basalt
Sample Treatment	Filtered	Unfiltered	Filtered	Unfiltered	Filtered	Unfiltered
Date Sampled	01/12/98	01/12/98	01/14/98	01/14/98	01/20/98	01/20/98
Ag	<0.001	0.005	<0.001	0.002 ± 0.001	<0.001	0.01 ± 0.002
Al	0.17 ± 0.01	543 ± 1	0.43 ± 0.01	193 ± 5	<0.02	196 ± 2
As	0.0002	0.102	0.0018	0.014	0.0025	0.019
B	0.047 ± 0.001	0.20 ± 0.01	0.041 ± 0.003	0.10 ± 0.01	0.046 ± 0.001	0.064 ± 0.002
Ba	0.060 ± 0.001	5.08 ± 0.03	0.028 ± 0.001	0.90 ± 0.01	0.045 ± 0.001	1.38 ± 0.01
Be	<0.002	0.032 ± 0.001	<0.002	0.008 ± 0.001	<0.002	0.003 ± 0.001
Br	0.25	0.24	0.15	0.15	0.05	0.04
Ca	25.1 ± 0.1	611 ± 1	16.6 ± 0.1	139 ± 2	27.1 ± 0.6	132 ± 1
Cd	<0.0002	0.0061 ± 0.0002	<0.0002	0.0008 ± 0.0002	<0.0002	0.012 ± 0.001
Cl	177	180	20.2	20.3	7.67	7.57
ClO_3	<0.02	<0.02	<0.02	<0.02	<0.02	<0.02
Co	<0.002	0.24 ± 0.01	<0.002	0.052 ± 0.002	<0.002	0.11 ± 0.01
CO_3	0	0	0	0	9.2	9.8
Cr	<0.002	1.65 ± 0.03	<0.002	0.13 ± 0.01	<0.002	0.24 ± 0.01
Cs	<0.002	0.029 ± 0.004	<0.002	0.003 ± 0.002	<0.002	0.003 ± 0.002
Cu	0.010 ± 0.002	1.38 ± 0.03	0.003 ± 0.002	0.14 ± 0.01	0.003 ± 0.002	0.82 ± 0.01
F	0.42	0.42	0.56	0.56	0.30	0.32
Fe	0.18 ± 0.01	1051 ± 13	0.43 ± 0.01	121 ± 2	0.01 ± 0.01	170 ± 2
HCO_3	133	910	76.0	177	118	117
Hg	0.00005	0.00038	<0.00005	0.00008	<0.00005	<0.00005
I	0.011	0.015	<0.005	0.005	<0.005	<0.005
K	24.2 ± 0.1	92.4 ± 2.0	2.95 ± 0.01	12.2 ± 0.1	3.87 ± 0.01	10.8 ± 0.1
Li	0.03 ± 0.01	0.44 ± 0.01	<0.01	0.12 ± 0.01	0.03 ± 0.01	0.10 ± 0.01
Mg	1.06 ± 0.01	147 ± 1	0.26 ± 0.01	46.1 ± 0.5	4.09 ± 0.06	60.3 ± 0.5
Mn	0.24 ± 0.01	21.5 ± 0.1	0.03 ± 0.01	2.83 ± 0.02	0.05 ± 0.01	2.88 ± 0.02
Mo	0.05 ± 0.01	0.39 ± 0.01	0.04 ± 0.004	0.04 ± 0.01	0.007 ± 0.002	0.007 ± 0.002
Na	167 ± 3	215 ± 1	41 ± 0.1	45 ± 0.2	20.1 ± 0.5	46.3 ± 0.1
NH_4	0.23	0.94	0.04	0.04	0.06	0.14
NO_3	3.41	<0.02	8.66	7.36	3.42	3.31
Pb	<0.002	2.05 ± 0.01	0.006 ± 0.002	0.12 ± 0.03	<0.002	0.14 ± 0.02
PO_4	<0.05	<0.05	<0.05	<0.05	<0.05	<0.05
Rb	0.011 ± 0.002	0.37 ± 0.02	0.004 ± 0.002	0.077 ± 0.005	0.004 ± 0.002	0.006 ± 0.002
S_2O_3	<0.05	<0.05	<0.05	<0.05	<0.01	<0.01
Sb	0.0003	0.0007	0.0003	0.0003	0.0003	0.0010
Se	<0.0001	0.0007	<0.0001	<0.0001	<0.0001	<0.0001

Table 5.2-1 (continued)

Part 2 (continued)						
Depth (ft)	615	615	624	624	688	688
Geologic Unit	Puye Fm.	Puye Fm.	Puye Fm.	Puye Fm.	SF basalt	SF basalt
Sample Treatment	Filtered	Unfiltered	Filtered	Unfiltered	Filtered	Unfiltered
Date Sampled	01/12/98	01/12/98	01/14/98	01/14/98	01/20/98	01/20/98
Si	4.23 ± 0.03	117 ± 1	9.44 ± 0.07	176 ± 4	31.6 ± 0.1	219 ± 2
Sn	<0.005	<0.005	<0.005	<0.005	0.005 ± 0.005	0.034 ± 0.005
SO_4	64.7	65.8	27.2	29.4	6.37	6.34
Sr	0.28 ± 0.01	4.78 ± 0.04	0.19 ± 0.01	1.52 ± 0.01	0.21 ± 0.01	1.32 ± 0.01
Ti	0.003 ± 0.001	1.99 ± 0.02	0.005 ± 0.001	1.96 ± 0.01	<0.002	4.76 ± 0.10
Tl	<0.002	<0.002	<0.002	<0.002	<0.002	<0.002
U	<0.1	<0.1	<0.1	<0.1	<0.1	<0.1
V	<0.002	0.40 ± 0.01	0.003 ± 0.002	0.12 ± 0.01	0.005 ± 0.001	0.14 ± 0.01
Zn	0.03 ± 0.01	3.85 ± 0.01	<0.01	0.35 ± 0.01	<0.01	0.76 ± 0.01
Charge Balance (%)	6.77	n/a	8.46	n/a	0.63	n/a
Temp. (laboratory, °C)	17.2	17.2	15.3	15.3	17.9	17.9
Conductance (laboratory, µS/cm)	987	1068	281	321	259	266
TDS	550.5	4684.1	276.9	1740.5	386.7	2082.6
TSS	ND	high	ND	med	ND	med
Hardness ($CaCO_3$)	67.0	2131	42.5	537	84.5	578
Alkalinity (laboratory, $CaCO_3$)		746		145		
pH (Field, standard units)	6.95	6.95	8.32	8.32	8.07	8.07
pH (laboratory, standard units)	7.53	7.66	9.16	9.16	8.01	8.04
SiO_2 (Calculated)	9.1	250	20.2	377	67.6	469
Oxalate	2.85	2.71	0.48	0.47	0.30	0.41
Acetate	—[h]	—	—	—	—	—
Formate	—	—	—	—	—	—

Notes: 1. The data in this table should be used only for screening purposes.

2. ppm.

[a] CR basalt = Cerros del Rio basalt.

[b] Puye Fm. = fanglomerate facies of the Puye Formation.

[c] ND = not determined.

[d] n/a = not applicable.

[e] TDS = total dissolved solids.

[f] TSS = total suspended solids.

[g] SF basalt = Santa Fe Group basalt.

[h] A dash in the table means the analyte is present, but in concentrations too low to quantify.

Table 5.2-2
Field-Measured Parameters for Groundwater Samples Collected at R-9

Geologic Unit	Depth (ft)	Date Sampled	pH	Temperature (°C)	Specific Cond. (µSi/cm)	Turbidity (NTU)[a]
Cerros del Rio basalt	180	10/06/97	8.30	9.2	223	17
	275	10/16/97	8.79	13.2	443	—[b]
Puye Formation	579	12/18/97	7.90	15.7	385	142
	615	01/12/98	6.95	17.2	1080	—
	624	01/14/98	8.32	15.2	219	190
Santa Fe Group basalt	688	01/20/98	8.07	17.9	222	—

[a] NTU = nephelometric turbidity unit.
[b] A dash in the table means off the scale because of very high turbidity values for open-borehole groundwater samples.

Table 5.2-3
Radionuclide Activities in Samples of Nonfiltered Groundwater from R-9

Depth (ft)	180	275	579	615	624	688
Geologic Unit	CR basalt[a]	CR basalt	Puye Fm.[b]	Puye Fm.	Puye Fm.	SF basalt[c]
Date Sampled	10/6/97	10/16/97	12/18/97	01/12/98	01/14/98	01/20/98
Tritium[d]	347 ± 25	106 ± 7	2.71 ± 0.58	30.3 ± 1.9	13.93 ± 0.90	14.43 ± 0.96
Strontium-90	0.47 ± 0.28	0.52 ± 0.64	<0.66	<0.68	<0.64	0.36 ± 0.67
Cesium-137	<2.420	1.39 ± 2.44	<2.680	<2.130	<2.420	<2.030
Plutonium-238	0.037 ± 0.044	0.76 ± 0.26	0.0156 ± 0.0194	0.006 ± 0.022	<MDA	0.020 ± 0.028
MDA[e]	0.084	0.23	0.034	0.051	0.039	0.052
Plutonium-239, 240	0.031 ± 0.030	0.011 ± 0.062	<MDA	0.000 ± 0.0154	0.0058 ± 0.0156	<MDA
MDA	0.050	0.110	0.041	0.014	0.035	0.039
Americium-241	0.092 ± 0.046	0.106 ± 0.094	0.029 ± 0.030	0.013 ± 0.024	0.010 ± 0.032	0.042 ± 0.034
MDA	0.047	0.160	0.052	0.051	0.074	0.051
Uranium-234	1.54 ± 0.28	7.94 ± 1.14	1.35 ± 0.22	5.06 ± 0.68	2.14 ± 0.32	2.05 ± 0.32
MDA	0.038	0.096	0.044	0.048	0.043	0.075
Uranium-235	0.043 ± 0.036	0.361 ± 0.158	0.055 ± 0.038	0.132 ± 0.056	0.120 ± 0.054	0.033 ± 0.034
MDA	0.038	0.074	0.05	0.041	0.046	0.058
Uranium-238	1.36 ± 0.26	6.60 ± 0.98	0.949 ± 0.180	2.81 ± 0.40	1.74 ± 0.028	1.47 ± 0.26
MDA	0.057	0.11	0.068	0.053	0.054	0.07
Total Uranium[f,g]	5.45 ± 0.75	112[h]	2.81 ± 0.38	25.08 ± 3.40	4.13 ± 0.57	2.03 ± 0.28
MDA	0.10	0.1	0.10	0.10	0.10	0.10
Gross Alpha	304 ± 56	447 ± 98	1.9 ± 1.7	580 ± 180	270 ± 120	34 ± 35
Gross Beta	351 ± 58	730 ± 120	3.7 ± 1.8	820 ± 230	310 ± 100	113 ± 42
Gross Gamma	212 ± 23	266 ± 16	274 ± 21	340 ± 25	351 ± 25	237 ± 19
MDA	31	18	20	19	18	18

Notes: 1. pCi/L.
2. Error of two standard deviations is reported.

[a] CR basalt = Cerros del Rio basalt.
[b] Puye Fm. = fanglomerate facies of the Puye Formation.
[d] SF basalt = Santa Fe Group basalt.
[d] Tritium analyzed by University of Miami; other radionuclides and parameters analyzed by Paragon Analytics, Inc.
[e] MDA = minimum detectable activity.
[f] µg/L (KPA).
[g] Samples were analyzed for uranium by LIKPA except for the sample collected from the 275-ft perched zone, which was analyzed by TIMS.
[h] Analyzed by TIMS.

Table 5.2-4
Radionuclide Activities in Samples of Filtered Groundwater from R-9

Depth (ft)	180	275	579	615	624	688
Geologic Unit	CR basalt[a]	CR basalt	CR basalt	Puye Fm.[b]	Puye Fm.	SF basalt[c]
Date Sampled	10/6/97	10/16/97	12/18/97	01/12/98	01/14/98	01/20/98
Tritium[d]	(See Table 5.2-3 for results of tritium analyses for the four saturated zones.)					
Strontium-90	0.11 ± 0.25	No sample[e]	<0.69	<0.87	0.13 ± 0.63	<0.84
Cesium-137	<2.070	No sample	<2.31	<2.11	<1.20	0.598 ± 2.180
Plutonium-238	0.039 ± 0.048	No sample	<MDA	0.009 ± 0.024	0.000 ± 0.024	<MDA
MDA[f]	0.093	No sample	0.086	0.058	0.062	0.065
Plutonium-239, 240	0.012 ± 0.024	No sample	<MDA	0.028 ± 0.026	0.0080 ± 0.0162	0.0127 ± 0.0180
MDA	0.055	No sample	0.038	0.017	0.03	0.013
Americium-241	0.037 ± 0.030	No sample	0.0111 ± 0.0180	0.012 ± 0.022	0.019 ± 0.034	0.0135 ± 0.0182
MDA	0.037		0.036	0.044	0.069	0.031
Uranium-234	0.529 ± 0.142	No sample	1.018 ± 0.192	1.30 ± 0.22	0.688 ± 0.154	1.26 ± 0.22
MDA	0.070		0.052	0.050	0.068	0.038
Uranium-235	0.014 ± 0.028	No sample	0.042 ± 0.032	0.016 ± 0.026	0.030 ± 0.028	0.067 ± 0.040
MDA	0.064		0.037	0.052	0.036	0.032
Uranium-238	0.628 ± 0.156	No sample	0.870 ± 0.172	0.698 ± 0.146	0.449 ± 0.118	0.691 ± 0.148
MDA	0.060		0.055	0.047	0.048	0.042
Total Uranium[g,h]	1.22 ± 0.17	48.4[i]	2.08 ± 0.28	2.17 ± 0.30	1.41 ± 0.19	1.63 ± 0.22
MDA	0.10	0.1	0.10	0.10	0.10	0.10
Gross Alpha	0.57 ± 0.65	No sample	0.7 ± 1.0	1.4 ± 1.3	1.20 ± 0.93	<1.3
Gross Beta	3.9 ± 1.0	No sample	4.2 ± 1.7	17.2 ± 2.5	3.3 ± 1.5	2.0 ± 1.5
Gross Gamma	188 ± 30	No sample	274 ± 21	280 ± 21	178 ± 13	252 ± 19
MDA	45		18	17	12	18

Notes: 1. pCi/L.

2. Error of two standard deviations is reported.

[a] CR basalt = Cerros del Rio basalt.

[b] Puye Fm. = fanglomerate facies of the Puye Formation.

[c] SF basalt = Santa Fe Group basalt.

[d] Tritium analyzed by University of Miami; other radionuclides and parameters analyzed by Paragon Analytics, Inc.

[e] No sample = not enough water available for analysis.

[f] MDA = minimum detectable activity.

[g] µg/L (KPA).

[h] Samples were analyzed for uranium by LIKPA except for the sample collected from the 275-ft perched zone, which was analyzed by TIMS.

[i] Analyzed by TIMS.

The water in the upper perched zone in Cerros del Rio basalt at a depth of 180 ft is characterized by a sodium-calcium-chloride-bicarbonate ionic composition with a pH value of 8.30 (Figure 5.2-1 and Table 5.2-4). The water in the lower perched zone in Cerros del Rio basalt at a depth of 275 ft is characterized by a sodium-sulfate-bicarbonate ionic composition with a pH value of 8.79 (Figure 5.2-1 and Table 5.2-2). Water in the lower zone has a higher TDS content (389 ppm) than that in the upper zone (252 ppm), possibly reflecting a longer groundwater residence time.

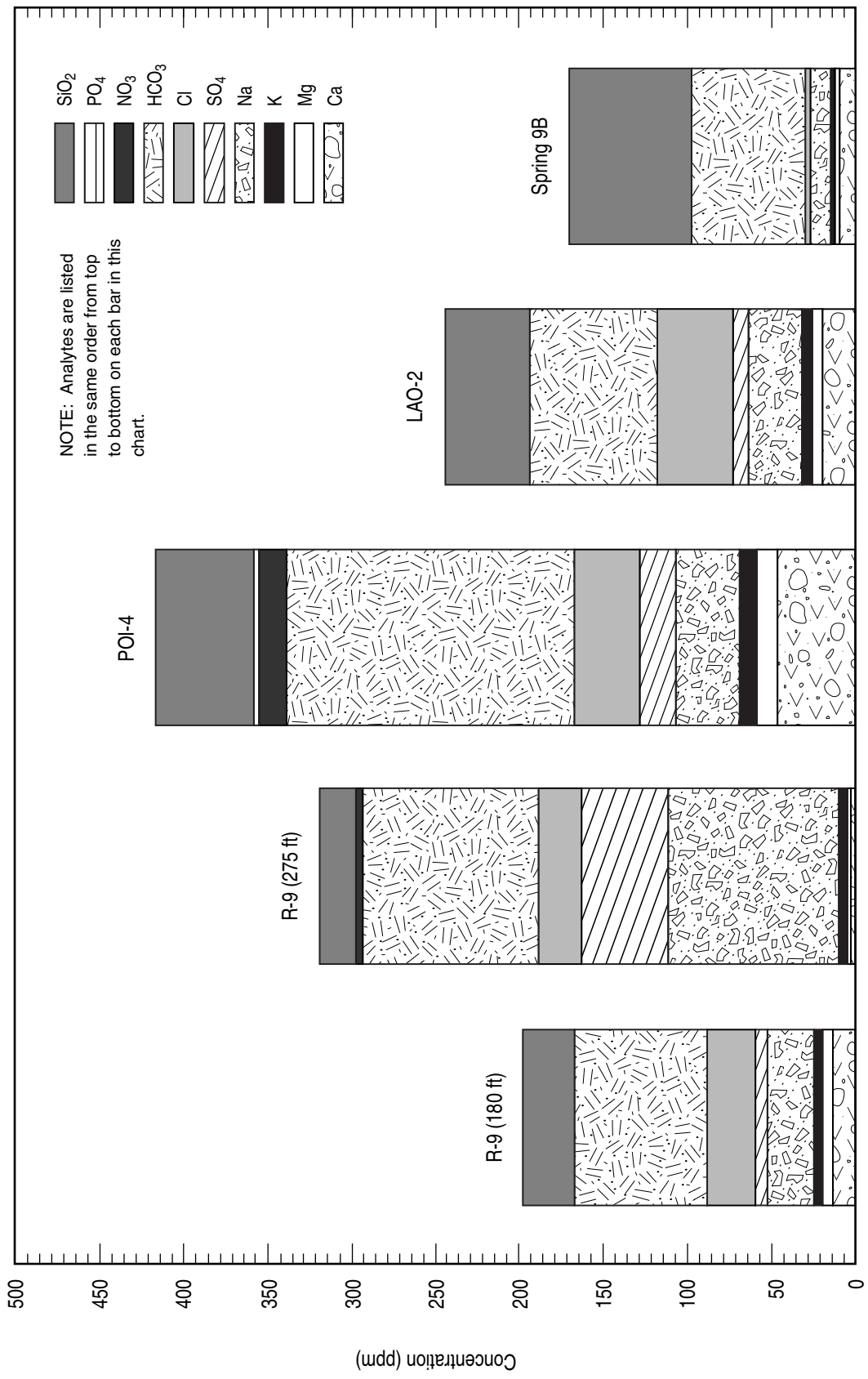

Figure 5.2-1. Comparison of major ion and nutrient chemistry of Cerros del Rio basalt groundwater in R-9 with alluvial groundwater (well LAO-2) and intermediate-depth perched groundwater in basalt (well POI-4 and Spring 9B)

Water quality data for Spring 9B in White Rock Canyon is provided in Figure 5.2-1 as a point of reference for evaluating the water quality data collected from perched water zones in basalt. Spring 9B, which yields water with a calcium-sodium-bicarbonate ionic composition, is the only known spring on the Pajarito Plateau that discharges water from basalt that does not contain elevated concentrations or activities of anthropogenic chemicals, including chloride, nitrate, tritium, sulfate, and uranium. For example, activities of tritium are less than 1 pCi/L at Spring 9B. Concentrations of chloride are 1.93 ppm in Spring 9B (Longmire, in preparation). Although perched groundwater in the basalts of R-9 and Spring 9B water have similar sodium and calcium bicarbonate ionic compositions, concentrations of chloride, sulfate, oxalate, phosphate, and nitrate are higher in the R-9 groundwater (Figure 5.2-1).

The major-ion chemistry of the upper perched zone within the basalt is chemically similar to alluvial groundwater in well LAO-2 (Environmental Surveillance and Compliance Programs 1997, 56684) (Figure 5.2-1), which is located at the confluence of Los Alamos Canyon and DP Canyon (Figure 1.0-1). The two perched groundwater zones within the Cerros del Rio basalt appear to contain a component of alluvial groundwater (LAO-2) based on the presence of above-background concentrations of chloride (29 ppm or mg/L) and tritium (347 pCi/L in the upper zone and 106 pCi/L in the lower zone). Stable isotope data also suggest that basalt groundwater is derived from meteoric sources that recharge through the canyon floor (Table 5.2-5).

Table 5.2-5
Stable Isotopic Data for Nonfiltered Groundwater Samples Collected from R-9

Saturated Zone (depth in ft)	δD (per mil)	$\delta^{18}O$ (per mil)
Basalt		
180	-73	-10.1
275	-74	-10.9
Puye Formation		
579	-70	-9.8
615	-72	-9.8
624	-90	-12.3
Santa Fe Group Basalt		
688	-75	-10.5

Note: The local meteoric line for the Jemez Mountains is $\delta D = 8 \times (\delta^{18}O) + 12$ (Blake et al. 1995, 49931). Precision values for D and ^{18}O are ±1 per mil and ±0.1 per mil, respectively. Isotopic analyses for δD and $\delta^{18}O$ are performed by Geochron Laboratories, Cambridge, Massachusetts.

The perched groundwater in the Cerros del Rio basalt in R-9 is chemically distinct from that found in a similar geologic setting in well POI-4 located in lower Pueblo Canyon (Figures 1.0-1 and 5.2-1). This suggests that the occurrences of perched groundwater in basalts found in Pueblo and Los Alamos Canyons are probably not hydraulically connected. Perched intermediate groundwater beneath Pueblo Canyon probably flows to the east-southeast; some of this water discharges at Basalt Spring.

5.2.2.2 Quality of Perched Groundwater within the Puye Formation

In the Puye Formation, within saturated zone 3 (Figure 2.3-1), the uppermost saturated interval at a depth of 579 ft is characterized by a calcium-sodium-bicarbonate ionic composition with a TDS content of 329.7 ppm (Table 5.2-1). The second permeable interval at a depth of 615 ft is characterized by an overall sodium-chloride ionic composition with a TDS content of 550.5 ppm (Table 5.2-1). This second

permeable interval has unique chemistry as evidenced by elevated dissolved sodium (167 ppm) and chloride (177 ppm) concentrations. Calcium and bicarbonate are present in lower concentrations in the second permeable interval. The third permeable interval at a depth of 624 ft is characterized by a sodium-calcium-bicarbonate ionic composition with a TDS content of 276.9 ppm (Table 5.2-1). Sulfate and chloride are also present in this interval (Table 5.2-1 and Figure 5.2-2), and concentrations of these two solutes are greater than those found in water supply wells PM-1 and PM-3 (Environmental Surveillance and Compliance Programs 1997, 56684). The major ion chemistry of the three permeable intervals in saturated zone 3 (Figure 2.3-1) within the Puye Formation differs from the characteristic calcium-sodium-bicarbonate compositions found in PM-1 and PM-3. Sodium is the dominant cation in the Puye Formation groundwater at R-9, whereas calcium is the dominant cation in PM-1 and PM-3 waters (Figure 5.2-2).

Presence of elevated nitrate, chloride, and sulfate within the Puye Formation waters (Figure 5.2-2) suggests a pathway from the surface to the regional aquifer up-canyon from R-9 (Table 5.2-1). The concentration of dissolved nitrogen (as nitrate) in water from the uppermost permeable interval within the Puye Formation is 10.6 ppm (Figure 5.2-2 and Table 5.2-1). Concentrations of this solute increase from saturated interval 2 to saturated interval 3, from 3.41 to 8.66 ppm.

5.2.2.3 Quality of Groundwater Within the Santa Fe Group Basalt

Water in the saturated zone in Santa Fe Group basalt at a depth of 688 ft is characterized by a calcium-sodium-bicarbonate ionic composition with a TDS content of 387 ppm and a pH of 8.0 (Table 5.2-1). This groundwater is chemically similar to regional aquifer water in wells PM-1 and PM-3 (Figure 5.2-2).

5.2.2.4 Radionuclide Distributions in Groundwater

Activities of total and dissolved radionuclides (americium-241; cesium-137; plutonium-238; plutonium-239,240; strontium-90; and tritium), gross alpha, gross beta, and gross gamma in groundwater samples collected at R-9 are summarized in Tables 5.2-2 and 5.2-3. Activities of most radionuclides, excluding tritium and uranium, are at less than detectable levels in all saturated zones. Natural and anthropogenic isotopes contribute to gross alpha, gross beta, and gross gamma values measured in the basalt perched zones. Natural radioactivity (potassium-40, thorium-232, uranium-234, uranium-235, and uranium-238) found in silicate rocks (Brookins 1984, 12453) contributes to these parameters measured in waters from the Puye Formation and Santa Fe Group basalt.

Activities of measurable tritium are present in all zones, suggesting that there is a component of groundwater less than 50 yr old (Blake et al. 1995, 49931; Adams et al. 1995, 47192) within the Cerros del Rio basalt, Puye Formation, and Santa Fe Group basalt (Table 5.2-2). The sources of tritium are likely to include both atmospheric and Laboratory-derived tritium. The tritium demonstrates that there is a pathway for surface water/alluvial groundwater to recharge perched zones and the regional aquifer within the past 50 yr.

Plutonium-238 was detected at 0.76 ± 0.26 pCi/L (two standard deviations) in a nonfiltered groundwater sample collected from the lower perched zone at a depth of 275 ft (Table 5.2-3). This activity is above the detection limit for the sample. However, the dominant isotope of plutonium in Los Alamos Canyon is plutonium-239,240 derived from weapons research conducted at TA-21. This sample was reanalyzed by Paragon Analytics Inc., which confirmed the analytical results. Plutonium-238 was used at TA-21 for heat source experiments.

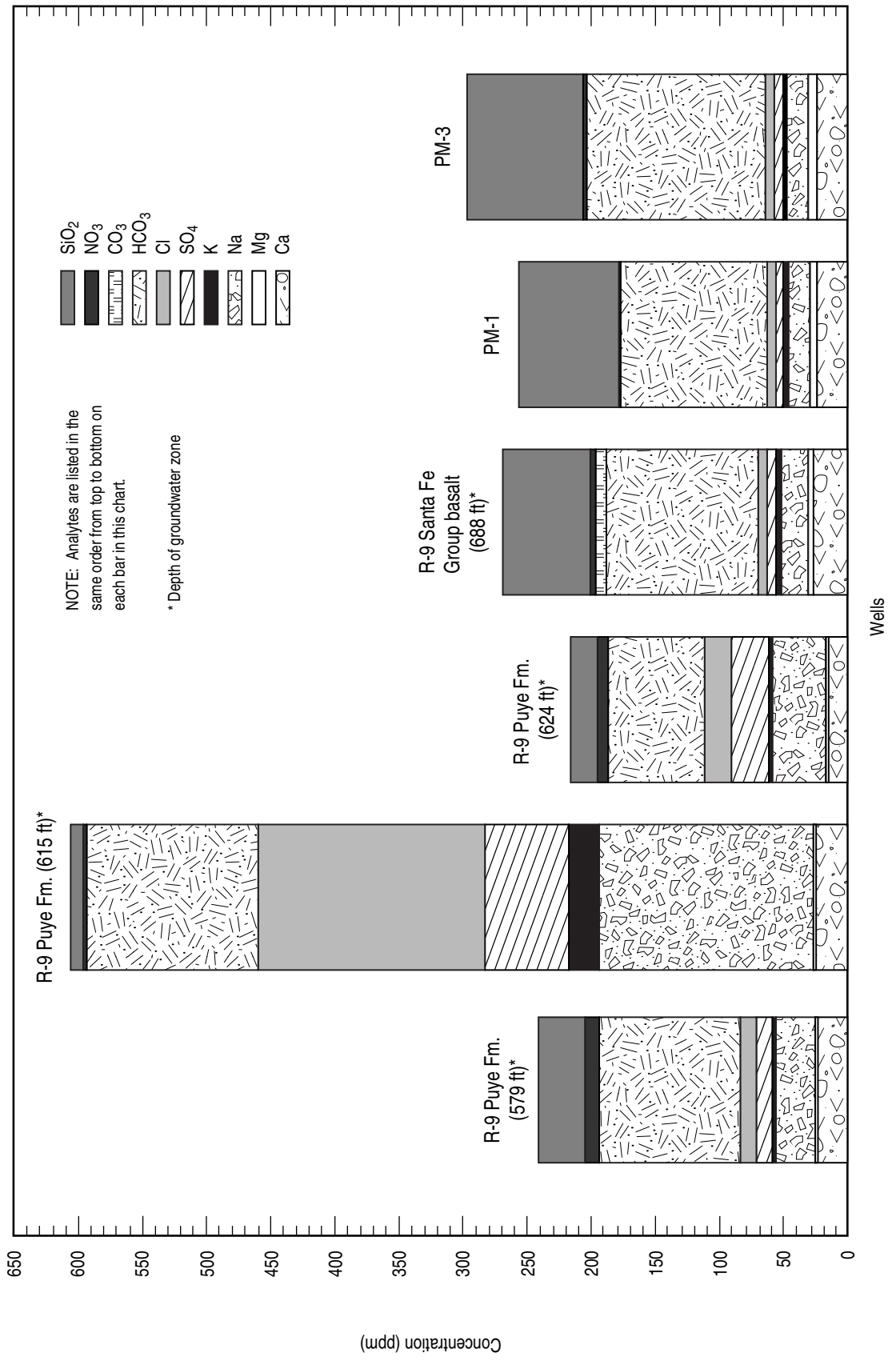

Figure 5.2-2. Comparison of major ion and nutrient chemistry of Puye Formation and Santa Fe Group groundwater in R-9 with regional aquifer groundwater in nearby water supply wells PM-1 and PM-3

5.2.2.5 Uranium and Oxalate Distributions in Groundwater

Dissolved uranium concentration in the upper perched zone within the Cerros del Rio basalt (180 ft deep) is 1.22 ppb or μg/L (Table 5.2-4). Dissolved uranium concentration in the lower perched zone within the Cerros del Rio basalt (275 ft deep) is 48.4 ppb. Under oxidizing conditions for the lower perched zone within the basalt, uranium is predicted to occur predominantly as $UO_2(CO_3)_3^{4+}$ based on model simulations using the computer code MINTEQA2 (Allison et al. 1991, 49930). This uranyl-carbonato complex does not completely adsorb onto mineral surfaces at a pH value of 8.79 (Langmuir 1997, 56037), which probably accounts for its elevated concentration in the lower perched zone water. The total (dissolved and suspended) uranium concentration is 112 ppb for the lower perched zone (Table 5.2-3). The turbidity value for this zone exceeded the maximum readable value for the instrument, suggesting a high particulate content, which likely accounts for a significant portion of the uranium in the unfiltered sample.

Background concentrations of dissolved uranium in alluvial groundwater and surface water at the Los Alamos reservoir in upper Los Alamos Canyon are less than 1 μg/L (Longmire, unpublished data; Longmire et al. 1996, 54168; Environmental Surveillance and Compliance Programs 1997, 56684). Concentrations of uranium in alluvial groundwater are below the proposed EPA maximum contaminant level of 20 μg/L and the New Mexico Water Quality Control Commission standard of 5 mg/L. Above-background concentrations of uranium are observed in groundwater samples collected from observation wells LAO-0.7, LAO-1, LAO-2, LAO-3, LAO-4, and LAO-4.5 (Longmire et al. 1996, 54168; Environmental Protection Group 1990, 6995; Environmental Protection Group 1992, 7004; Environmental Protection Group 1993, 23249; Environmental Protection Group 1994, 45363; Environmental Protection Group 1995, 50285; Environmental Surveillance Program 1996, 55333; Environmental Surveillance and Compliance Programs 1997, 56684) and in surface water (LANL 1981, 6059). Total uranium concentrations are greater than background for some canyon floor sediments near the confluence of Los Alamos and DP Canyons (see discussion in Section E-1.2.25 of Reneau et al. 1998, 59160). Because of uranium processing that took place for Laboratory projects, former TA-1 and TA-21 are potential sources of uranium discharged or released into upper Los Alamos Canyon before the 1950s.

The high uranium content of the Bandelier Tuff, particularly the Guaje Pumice Bed, is an alternative source of the uranium found in this groundwater. However, perched groundwater in the Guaje Pumice Bed in well LAOI(A)1.1 typically has uranium concentrations less than 1 ppb (Longmire, unpublished data). In addition, uranium occurs as a trace element in glass and in zircon and other trace minerals (Broxton et al. 1995, 50121). Although glass has a much higher solubility than the other mineral phases at near-neutral pH values, leaching of uranium from glass and other phases in sufficient quantity is unlikely.

Statistical distributions of uranium within 65 groundwater and spring samples collected on the Pajarito Plateau and surrounding areas are shown in Table 5.2-6. The mean uranium concentration for this sample population is 1.86 μg/L with a standard deviation of 3.78 μg/L. The median uranium concentration is 0.68 μg/L. This distribution is characterized by a right-sided tail (skewness = 3.69). Laboratory test wells, supply wells, springs (west of the Rio Grande), and ER Project groundwater samples typically contain uranium concentrations of less than 2 μg/L.

San Ildefonso Pueblo wells and La Mesita Spring (east of the Rio Grande) contain uranium concentrations ranging from 0.05 to 19.64 μg/L. Uranium concentrations in the La Mesita Spring sample are 10.01 μg/L (Environmental Surveillance and Compliance Programs 1997, 56684). The San Ildefonso Pueblo wells are completed within the Santa Fe Group sediments; groundwater discharging from La Mesita Spring is associated with the Santa Fe Group sediments. Higher uranium concentrations in groundwater are observed near the Rio Grande in the regional aquifer (Santa Fe Group sediments).

Table 5.2-6
Statistical Distribution of Uranium
in Groundwater from the Pajarito Plateau and Surrounding Areas

Statistic	Value (μg/L)
Number	65
Mean	1.86
Standard error	0.47
Median	0.68
Standard deviation	3.78
Kurtosis	14.15
Skewness	3.69
Minimum	0.05
Maximum	19.64
Confidence level (95%)	0.94

Sources: Environmental Surveillance and Compliance Programs, 1991, 56684; Laboratory background groundwater investigation (spring 1998 sampling)

Oxalate is present in groundwater samples collected from the lower perched zone (saturated zone 2, Figure 2.3-1) in the Cerros del Rio basalt at 3.03 ppm (Table 5.2-1). However, oxalate was not detected in the uppermost perched zone. Oxalate was detected within the permeable zones in the Puye Formation and Santa Fe Group basalt (Table 5.2-1). Oxalate is a mobile anion ($C_2O_4^{2-}$), similar to sulfate (SO_4^{2-}), above pH values of 5.

The source of the oxalate is not known with certainty. The oxalate detected in R-9 may be derived from natural sources through bacterial activity in soils and rocks, specifically through the oxidation of carbohydrates to carbon dioxide gas. However, the oxalate detected may be derived from anthropogenic sources. Oxalate and oxalic acid were used during the processing and purification of natural uranium, or tubaloy, to precipitate uranyl oxalate at former TA-1 in the early 1940s. Oxalate was also used in the processing and purification of plutonium ($Pu_2(C_2O_4)_3$) at former TA-1 and TA-21.

5.2.2.6 Summary of Groundwater Chemistry

Solute chemical data show the presence of anthropogenic anions (chloride, nitrate, oxalate, and sulfate) derived from alluvial groundwater in upper Los Alamos Canyon within the four saturated zones identified during the drilling of R-9 (Figure 2.3-1). Measurable activities of tritium within the Puye Formation and Santa Fe Group suggest that a component of groundwater in these saturated zones is less than 50 yr old. The source of this tritium may be atmospheric fallout (Adams et al. 1995, 47192) and/or from Laboratory discharges (Blake et al. 1995, 49931).

Dissolved uranium (48.4 ppb) measured within the lower perched zone (basalt) of R-9 is a statistical outlier with respect to uranium concentrations for 65 groundwater and spring samples (mean value of 1.86 μg/L) collected on the Pajarito Plateau and surrounding areas. R-9 is downgradient from former TA-1 and TA-21; these sites are known to have used uranium during refining and purification and research activities. However, additional data are needed to determine if the elevated uranium concentration detected in the lower perched zone within the basalt was derived from these Laboratory sources.

Dissolved uranium distributions within the groundwater of the Puye Formation and Santa Fe Group are generally less than 2 ppb.

5.3 Anion Profiles

5.3.1 Methods

Anion concentrations (chloride, nitrate, nitrite, oxalate, phosphate, and sulfate) for pore water in samples of core and cuttings were determined and plotted with depth. Samples were collected and analyzed at approximately 10-ft intervals. A few samples were collected on more closely spaced intervals to examine behavior at stratigraphic contacts or changes in moisture content. Anion concentrations were determined by leaching the samples with deionized water and analyzing the leachate using ion chromatography following Newman (1996, 59118). The leaching and analyses were performed at the EES-1 geochemistry laboratory. For each sample, approximately 50 g of rock was crushed using a mortar and pestle. The crushed rock was then oven dried for at least 12 hr at 100°C. The dry sample was weighed and added to an Erlenmeyer flask along with approximately 75 g of deionized water. The flask was agitated for 24 hr on a rotary mixer. After the mixer was turned off and the solid material settled, the supernatant was filtered and analyzed using a Dionex ion chromatograph. Analytical precision of the ion chromatograph is better than 5%.

Pore water chloride concentrations were calculated using leachate concentrations, gravimetric moisture contents, and bulk densities. Moisture content data are reported in Sections 5.2 through 5.2.6 of this document. Bulk densities have not been measured for R-9 samples, so estimates were used that are representative of typical values for the kinds of rock and sediments encountered. Uncertainties in the bulk density estimates increase the uncertainty in the pore water concentrations. However, comparing calculated pore water concentrations from saturated zone samples with those reported in Table 5.2-1 show reasonable agreement, indicating that the bulk density estimates are close to the actual values.

5.3.2 Results

Analysis of the vertical variations in geochemistry of Los Alamos Canyon waters is one of the best ways to understand flow and transport in the subsurface. One important component of the subsurface hydrochemistry is the distribution of anions. Samples of core and cuttings obtained from R-9 were analyzed to obtain the vertical distributions of chloride, nitrate, nitrite, oxalate, phosphate, and sulfate. Bromide was also measured, but concentrations were too low for quantification. In addition, several samples had nitrate, nitrite, and phosphate concentrations below the detection limit. The lack of detection does not mean that these species are not present in the samples. Instead, the leaching procedure results in substantial dilution, and if an anion has a low concentration, the dilution can lower the concentration beyond the detection limit. In general, the anions all showed similar behavior with multipeaked profiles, and the peaks and valleys of the various anion distributions tend to occur at similar depths (Figure 5.3-1). The multipeaked profile is consistent with multiple flow paths and changes in vertical recharge through time. Given the hydrologic contrast between units and the chemical differences between saturated zones (Table 5.2-1), the multiple flow path explanation appears to be the most likely. Pore water concentrations for all the anions are shown in Table 5.3-1.

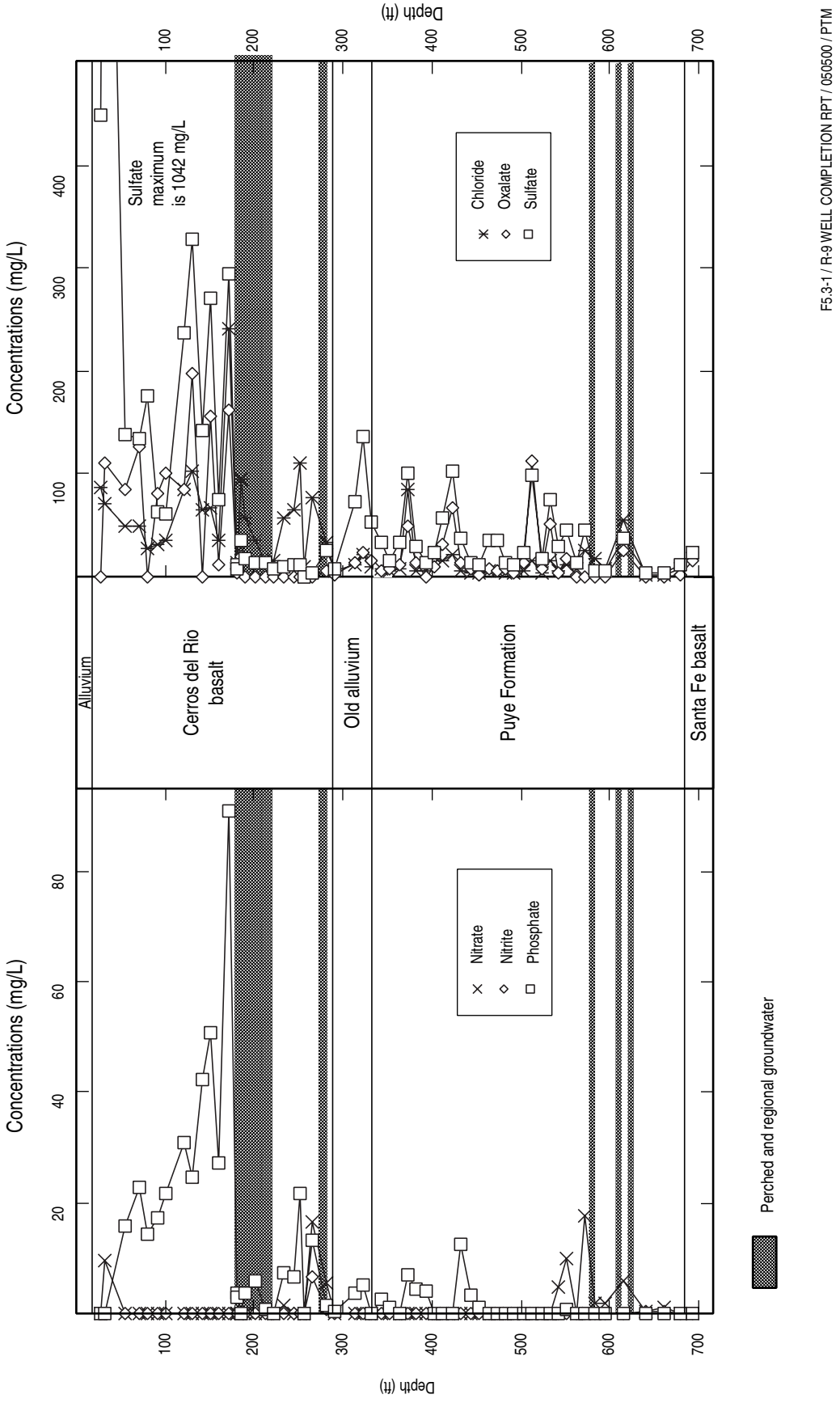

Figure 5.3-1. Pore water anion profiles for R-9

Table 5.3-1
R-9 Pore Water Anion Concentrations

Average Depth of Sample (ft)	Chloride	Nitrate	Nitrite	Oxalate	Phosphate	Sulfate
26.75	87	BD*	BD	BD	BD	449
32.50	72	10	BD	112	BD	1042
54.25	50	BD	BD	85	16	139
71.0	50	BD	BD	126	23	134
81.0	27	BD	BD	BD	14	175
91.0	32	BD	BD	81	17	63
101.0	36	BD	BD	101	22	61
121.50	85	BD	BD	85	31	237
131.0	102	BD	BD	198	25	328
141.0	65	BD	BD	BD	42	142
150.5	68	BD	BD	157	51	270
161.0	36	BD	BD	12	27	74
171.0	240	BD	BD	161	91	295
181.0	15	BD	BD	4	4	12
181.4	7	BD	BD	4	3	8
184.65	95	BD	BD	20	BD	36
189.15	58	BD	BD	BD	4	18
201.35	36	BD	BD	BD	6	14
213.15	14	BD	BD	BD	1	14
222.75	15	BD	BD	BD	BD	8
234.40	57	1	BD	BD	7	10
243.98	64	BD	BD	BD	7	11
252.50	111	BD	BD	BD	22	12
255.25	9	BD	BD	BD	BD	BD
266.48	77	17	7	BD	13	5
281.65	33	6	1	6	2	26
290.60	6	BD	BD	1	0	7
312.75	12	BD	BD	13	4	73
322.75	22	BD	BD	23	5	136
332.75	10	BD	BD	16	BD	54
342.75	8	BD	BD	5	2	33
352.75	5	BD	BD	8	1	17
362.75	8	BD	BD	12	BD	33
372.75	85	BD	BD	49	7	102
382.75	6	BD	BD	14	4	30
392.75	6	BD	BD	BD	4	14
402.75	20	BD	BD	10	BD	24
412.75	16	BD	BD	31	BD	58
422.75	21	BD	BD	67	BD	103
432.75	6	BD	BD	15	12	38
443.5	4	BD	BD	8	3	14

Table 5.3-1 (continued)

Average Depth of Sample (ft)	Chloride	Nitrate	Nitrite	Oxalate	Phosphate	Sulfate
453.5	3	BD	BD	3	1	12
463.5	6	BD	BD	7	BD	35
472.75	5	BD	BD	6	BD	35
482.75	3	BD	BD	8	BD	14
492.75	3	BD	BD	3	BD	12
502.75	6	BD	BD	13	BD	23
512.75	15	BD	BD	113	BD	99
522.75	5	BD	BD	9	BD	19
532.75	17	BD	BD	52	BD	75
541.75	5	5	BD	3	BD	30
551.9	11	10	BD	18	1	46
561.95	7	BD	BD	BD	BD	14
572.95	26	18	BD	BD	BD	46
584.15	17	2	BD	BD	BD	6
595.5	8	2	BD	BD	BD	6
616	56	6	BD	25	BD	37
639.7	3	0	0	BD	BD	5
660.9	2	1	0	BD	BD	4
678.9	8	BD	BD	2	BD	12
692.3	24	BD	BD	16	BD	23

Note: mg/L.

* BD = below detection.

5.4 Moisture Content of Core and Cuttings

5.4.1 Methods

Moisture content was determined on samples of both core and cuttings. Core was collected from 34.4% of the borehole, including all the saturated intervals. Therefore, collecting a vertical profile of moisture content for the entire borehole requires that moisture content analyses be performed on drill cuttings. The drill cuttings were collected from a port that was installed in the cuttings return line at a location before the cuttings entered the cyclone. This was done to prevent the moisture loss that occurs when cuttings are in the cyclone. After core or cuttings were screened for radioactivity, samples were immediately placed in preweighed and prelabeled jars with tightly fitting lids. The moisture content was determined gravimetrically by drying the samples in an oven in accordance with the American Society for Testing and Materials (ASTM) method D2216-90. Data collected for moisture content are listed in Appendix C.

5.4.2 Results

The moisture content in core and cuttings for unsaturated intervals of the borehole are shown in Figure 5.4 1 and Figure 5.4-2. Consistent results were obtained for analyses on both core and cuttings (Figure 5.4 1). The moisture content data are necessary to calculate the transport of water and contaminants through the thick, unsaturated intervals. The moisture content data are also necessary to calculate the pore-water anion concentrations over vertical profiles (see Section 5.3) and to prepare water retention curves.

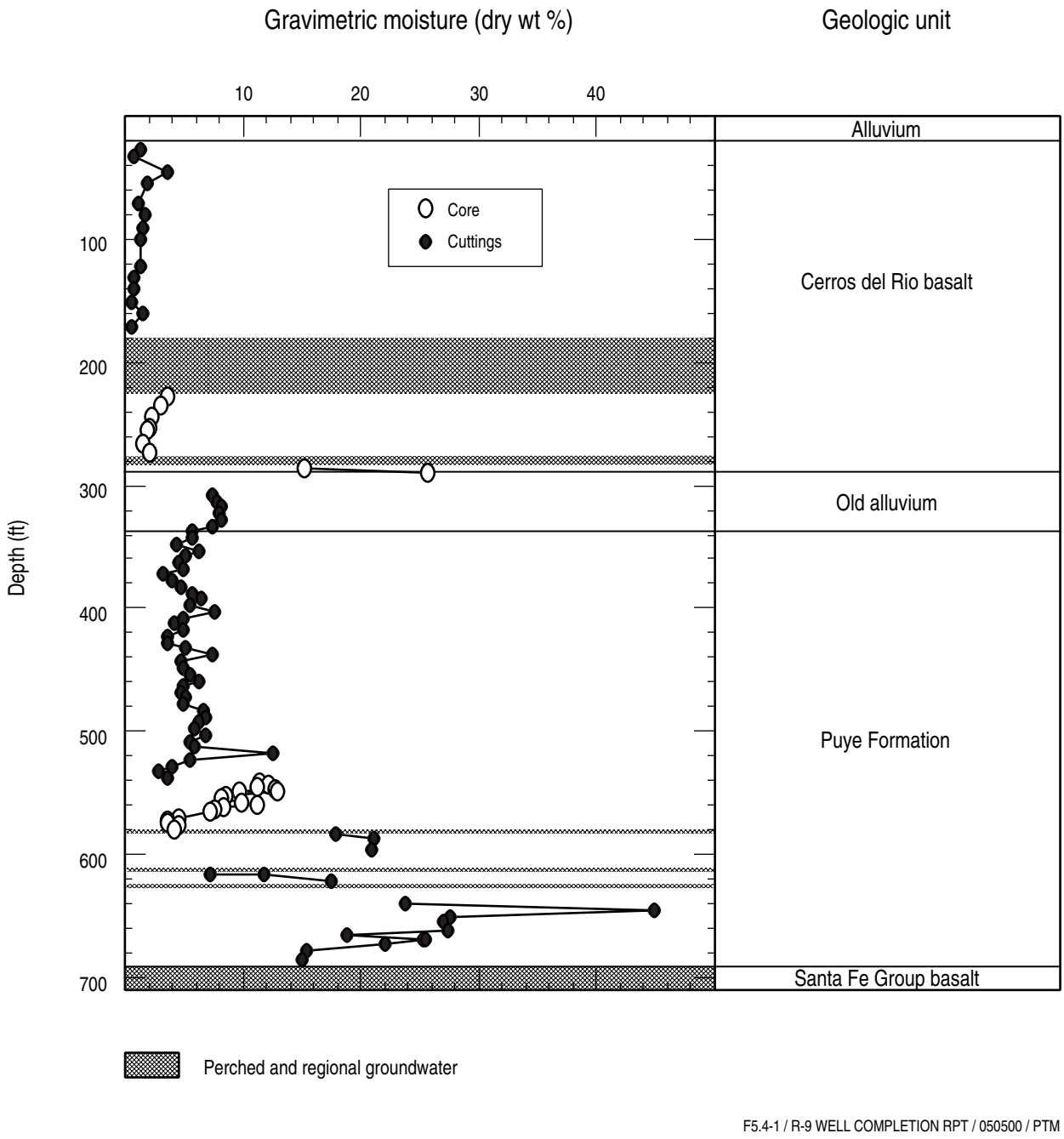

Figure 5.4-1. Moisture content for core and cuttings from R-9

Moisture content is lowest in the Cerros del Rio basalt above the first perched zone at a depth of 180 ft (Figure 5.4-1). Moisture contents are also low in Cerros del Rio basalt in the unsaturated interval separating the upper two perched zones. A marked increase in moisture content occurs in the Puye Formation below the second perched zone. The highest moisture content occurs in the clay-rich tuffaceous sediments in the lower part of the Puye Formation.

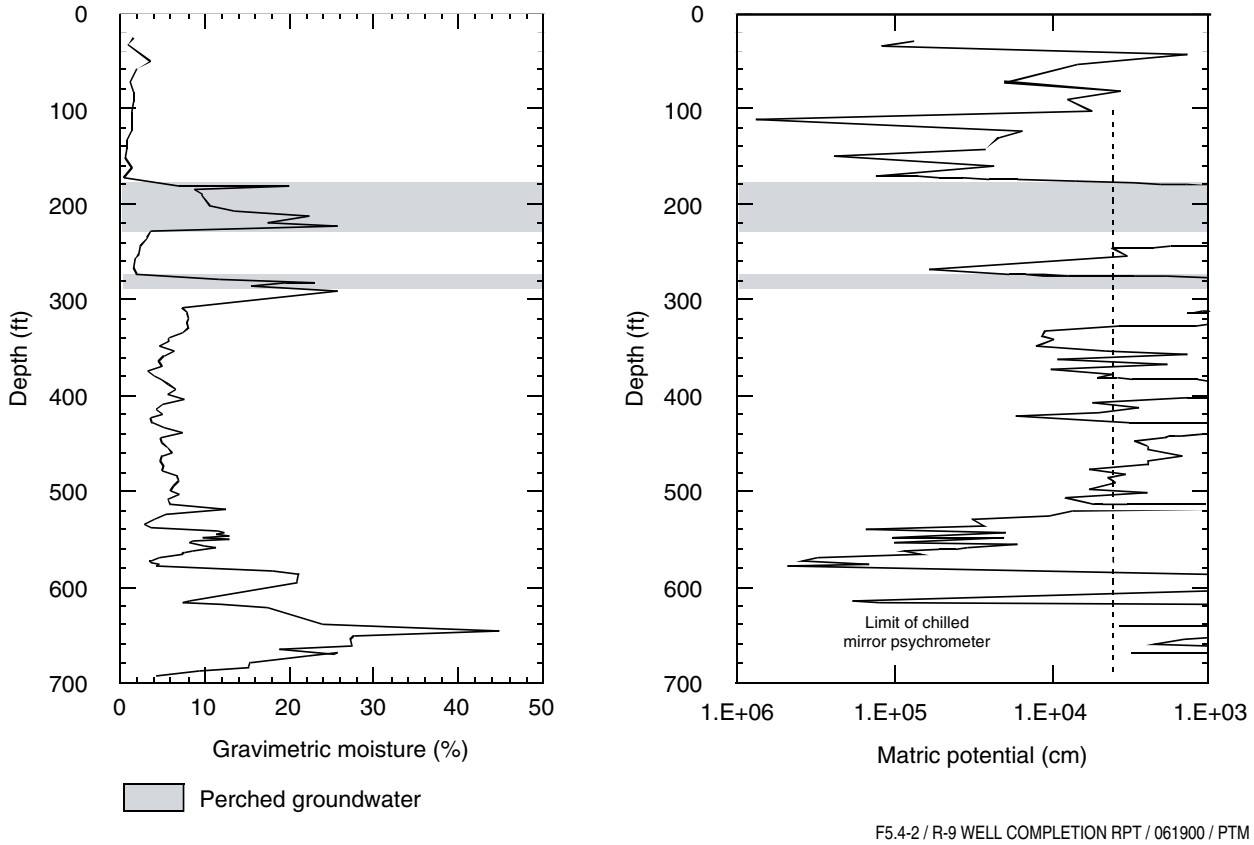

Figure 5.4-2. Gravimetric-moisture and matric-potential measurements in R-9

5.5 Matric Potential

This section concerns the measurement of the water pressure potential, or matric potential. The energy state of water that occupies the pores of a rock is described in terms of the "water potential". When rock pores are not water-filled, the hydrostatic pressure (or matric potential in unsaturated rock), is less than atmospheric pressure. In this case the pressure potential is negative and work is required to remove water from the rock. The matric potential arises from capillary forces holding water in the interstices between grain boundaries, and the forces of adsorption that hold water to particle surfaces. The accompanying figures show the absolute value of the matric potential.

The chilled mirror psychrometer (or water activity meter) is designed for measuring matric potential in dry soils. The meter measures the water activity, which can be converted to matric potential. The units of matric potential may be given as a pressure in Pascals (Pa), or as the height of an equivalent column of water, in cm (10200 cm H_2O = 1 MPa). The best use of the meter is for soils drier than 0.003 water activity units (-0.4 MPa or -4080 cm H_2O). This value is shown on the accompanying plots as the limit of the chilled mirror psychrometer.

5.5.1 Methods

Water potential was measured using a chilled-mirror water activity meter as described by Gee et al. (1992, 58717). Measurement results are presented in Appendix C. Samples were doubly sealed in ziplock bags and wrapped in packing tape immediately following screening of core or cuttings for radioactivity. Storage time ranged from 2 to 49 days. Duplicate measurements were made within 10 min

after loading samples into plastic vials with tight-fitting lids. These vials were directly inserted into the water activity meter. Core was crushed into mm-sized fragments as quickly as possible after breaking the seal to load the vials. Repeat measurements demonstrated that samples produced the same results as long as the measurements were made less than 3 hr after the vials were loaded and the lids were secured. All analytical runs were bracketed by measurements of standards, which demonstrate a 2σ reproducibility of 0.0026 for 114 analyses of the matric potential of distilled water. This is close to the instrumental precision stated in Gee et al. (1992, 58717) of 0.003 water activity units (0.4 MPa or 4080 cm H_2O).

5.5.2 Results

Two methods of displaying the matric-potential data are presented here. The first is a profile of matric potential compared to depth (see Figure 5.4-2). The axis of the matric-potential plot is reversed so that drier values appear to the left on the plot, corresponding to the direction of drier values of moisture content data. In general, the dry values of matric potential correspond to the dry moisture content measurements. The exact correspondence of potential and moisture content depends on rock texture and reflects factors like porosity and pore-size distribution.

The second method of displaying the matric-potential data is shown in Figure 5.5-1 where separate plots of matric potential are compared with moisture content data for each stratigraphic unit. This display represents the drier portion of a moisture retention curve. The moisture retention curve relates the volumetric soil moisture content of unsaturated soils and rocks to the energy state of the soil water. The water content (or gravimetric moisture content) reported here equals the mass of water divided by the dry mass of solids in a sample; to convert to volumetric moisture content, water content is multiplied by the dry bulk density of the sample.

On the figure for the lower argillic portion of the Puye Formation, average moisture retention curves for the soil groups silt loam, silty clay loam, and loam are shown from van Genuchten et al. (1991, 65419). These curves were converted from volumetric moisture content to water content using the porosity and an assumed grain density value. A silt loam with a porosity of 43% and a grain density of 2.6 g/cm^3 would have a calculated dry bulk density of 1.48 g/cm^3. The data for the lower argillic Puye fanglomerate fall near the average values for these fine-grained soil groups.

5.6 Hydraulic Properties

A total of 39 core samples were collected and preserved for hydraulic-property testing and most are currently stored at the FSF. Samples were selected for testing based on data needs identified for numerical flow and transport modeling. Laboratory hydraulic-property testing of samples from unsaturated zones included, but was not limited to, moisture content, particle density, bulk density, porosity, matric potential, saturated hydraulic conductivity, and determination of water retention curves. Field hydraulic-property testing focused on hydraulic conductivity of saturated zones.

5.6.1 Methods

Samples for laboratory hydraulic-property testing were collected as soon as possible after core extraction and were protected from moisture loss by the following methods.

- Samples for hydraulic-property testing were collected in 6-in.-diameter Lexan plastic or stainless-steel liners loaded into the core tube.
- If a core collected without a liner was deemed to warrant hydraulic testing, it was quickly inserted into a liner, intact if possible.

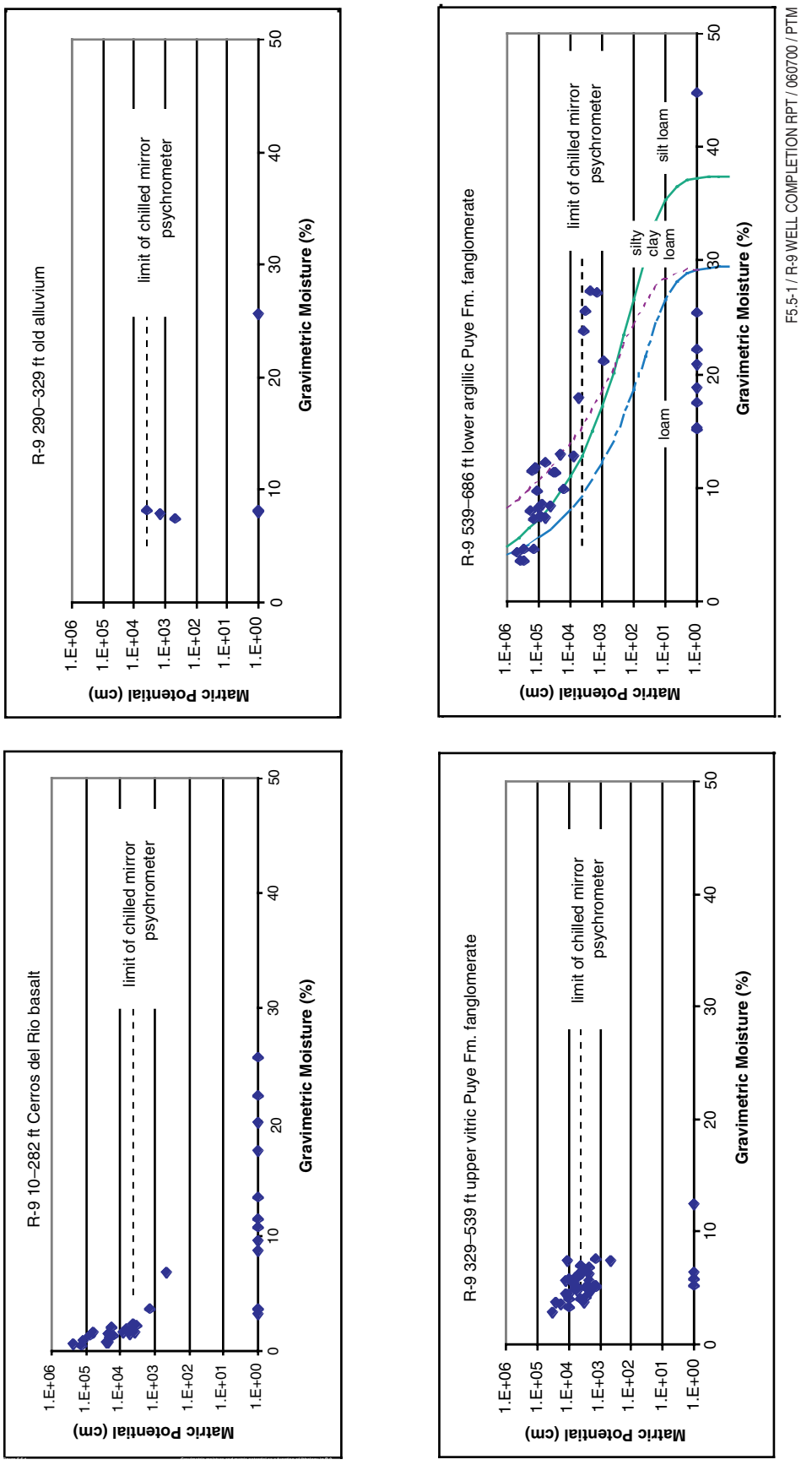

Figure 5.5-1. Gravimetric moisture and matric potential as a function of lithology in R-9

The ends of the Lexan plastic or stainless-steel liners containing core to be preserved were capped with tight-fitting plastic caps and sealed with Teflon nonstick-coated tape.

- The capped ends of the liner were wrapped with clear packing tape.
- The footage interval of the core sample as well as the time and date of collection were recorded on the liner with indelible ink.
- The capped and labeled liner was inserted into a Coreprotec aluminized sleeve labeled with the same sampling information.
- The ends of the Coreprotec sleeve were closed with an electric heat sealer, creating an air-tight seal.
- The protected cores were documented as samples for hydrologic testing, stored to prevent freezing, and transported to the FSF as soon as possible after they were collected.
- Custody of the samples was transferred from the Canyons Focus Area field support team to the FSF using a PC-based Access database and electronic chain-of-custody form.

As R-9 was completed with a single screen, it lent itself to aquifer analysis by pumping. However, discharge with a 7.5-hp pump did not stress the aquifer enough to yield data that could be analyzed. Details of testing at both R-9 and R-9i will be presented in a separate report.

5.6.2 Results

Two samples were selected for laboratory testing of hydraulic properties. This includes one from a perched zone in the Cerros del Rio basalt and one from an unsaturated zone in the Puye Formation (Table 5.6-1). Analysis of the sample of Cerros del Rio basalt by the falling-head method yielded a saturated hydraulic conductivity of 1.1E-06 cm/sec (Stone 2000, 66781). Results of testing the sample of Puye Formation for the full suite of hydraulic properties are given in Appendix D.

Table 5.6-1
Samples from R-9 Selected for Testing of Hydraulic Properties

Sample Number	Geologic Unit	Depth Interval (ft)	Test
8808	Cerros del Rio basalt	187.5–188.2	Ksat[a]
8814	Puye Formation (calcareous sandstone)	642.3–642.8	H Pkg[b]

[a] Ksat = tested for saturated hydraulic conductivity only; results given in text.

[b] H Pkg = tested for hydraulic package (full suite of unsaturated properties); results given in Appendix D.

5.7 Air Permeability and Borehole Anemometry

SEA performed a series of in situ air measurements during the drilling of R-9. These measurements were performed during periods of open-borehole access to determine unsaturated permeability characteristics of the basalt formations.

5.7.1 Methods

The straddle packer permeability measurements were performed within intervals of Cerros del Rio basalt after open-borehole drilling or in intervals where the drill casing was retracted to expose open borehole. Air was injected into a 28-in. interval isolated by two pneumatic packers, and the resulting air-flow rate and injection pressure were used to infer an air permeability using a steady-state, one-dimensional, spherical flow model. The measurement system had been used previously at TA-54 to support characterization of the Bandelier Tuff. R-9 was the system's first application in basaltic rocks.

Two borehole regions were available for measurements. The first was an open region in the upper part of the Cerros del Rio basalt, where individual measurements were made at the depths of 39, 43, 60, and 64 ft. The second region was located in the lower part of the Cerros del Rio basalt where individual measurements were made at depths of 245, 250, and 255 ft.

Straddle-packer permeability measurements have historically been performed to conduct air and water permeability measurements in porous media. For this application, a steady-state spherical flow model is used. If the air injection (or extraction) source can be approximated as a sphere, the steady-state air flow into the source, the source equivalent radius, the source pressure, and the ambient soil-gas pressure can be used to infer the effective air permeability, k (as shown in the equation below) (Keller et al. 1973, 59119; Lowry and Narbutovskih 1991, 59120).

$$k = \frac{\mu R T \dot{m}}{2\pi M\left(P_o^2 - P^2\right)} \bullet \left(\frac{1}{r_o}\right)$$

where:

μ = dynamic gas viscosity
R = universal gas constant
T = absolute temperature
$\dot{m}$ = gas mass flow into soil
M = gas molecular weight
P_o = absolute pressure of source
P = ambient absolute soil gas pressure
r_o = source radius

This model is applied in straddle packer measurements by setting r_o to be the radius of the sphere whose surface area is equal to the area of the exposed borehole wall (Figure 5.7-1).

The packer system is depicted in Figure 5.7-2. Packers are located above and below the injection zone, and their separation distance is variable. Each packer is 6 ft long, is fabricated of a lightweight packer material, and is operated at 5 pounds per square inch (psi) or above internal pressure during the permeability measurement. The primary measurements recorded are the pressure difference between the injection zone and ambient atmospheric pressure (the temperature of the air being injected and the air-flow rate during the injection [measured with an orifice plate flowmeter]). All the sensors are located in an electronics package situated above the packer system, and the data are transmitted uphole to a laptop computer for averaging and recording. The air-permeability system schematic is shown in Figure 5.7-3.

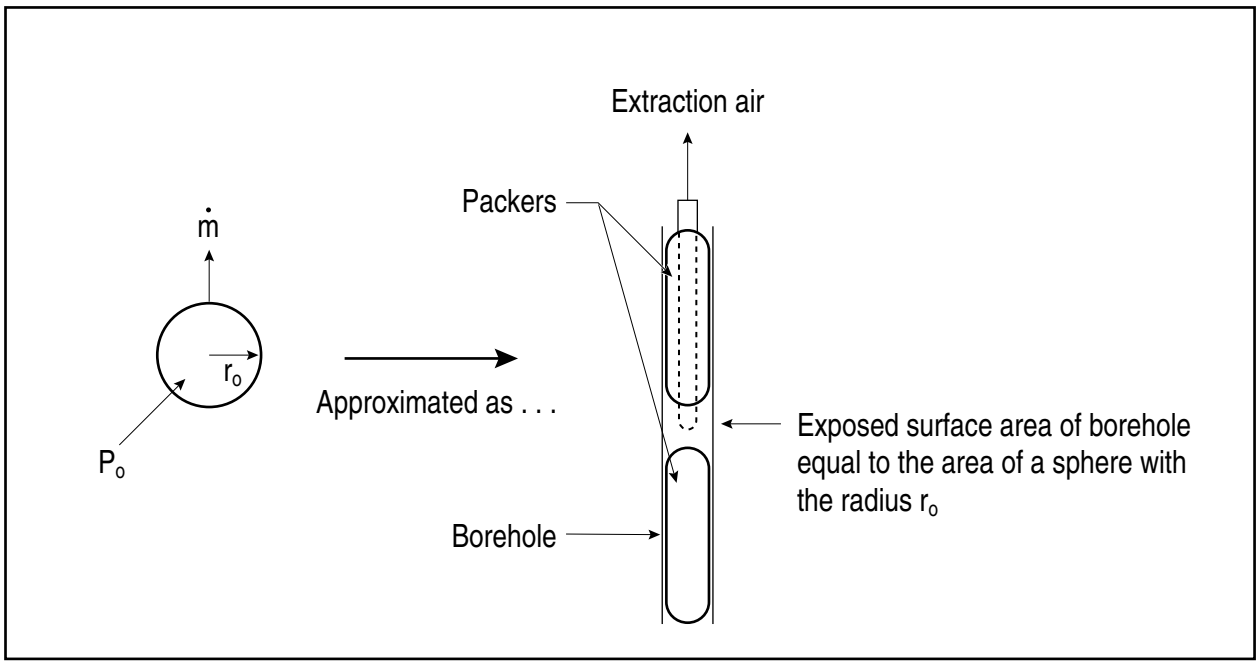

F5.7-1 / R-9 WELL COMPLETION RPT / 060500 / PTM

Figure 5.7-1. Approximation of a spherical air-flow geometry with a conventional straddle packer design for in situ soil gas permeability measurements

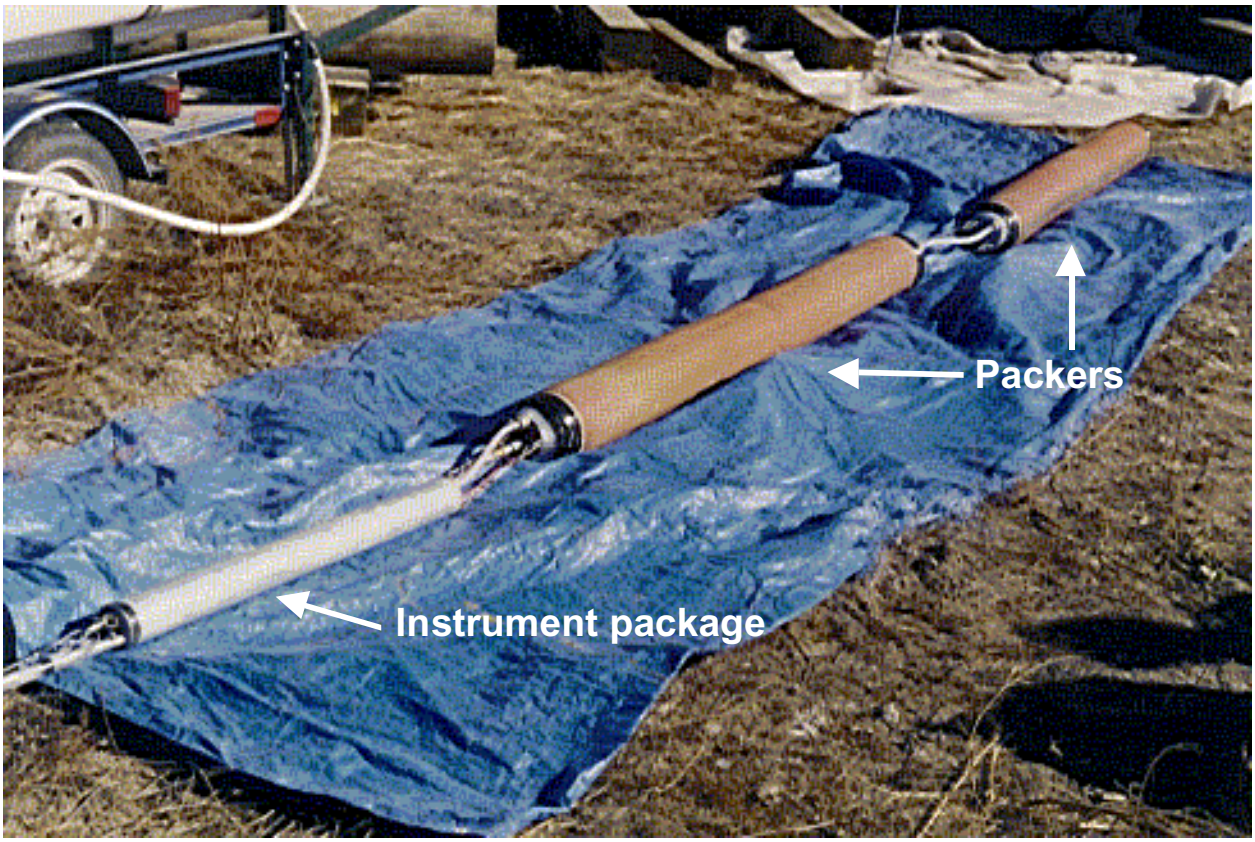

F5.7-2 / R-9 WELL COMPLETION RPT / 042700 / PTM

Figure 5.7-2. Downhole instrument package and packers

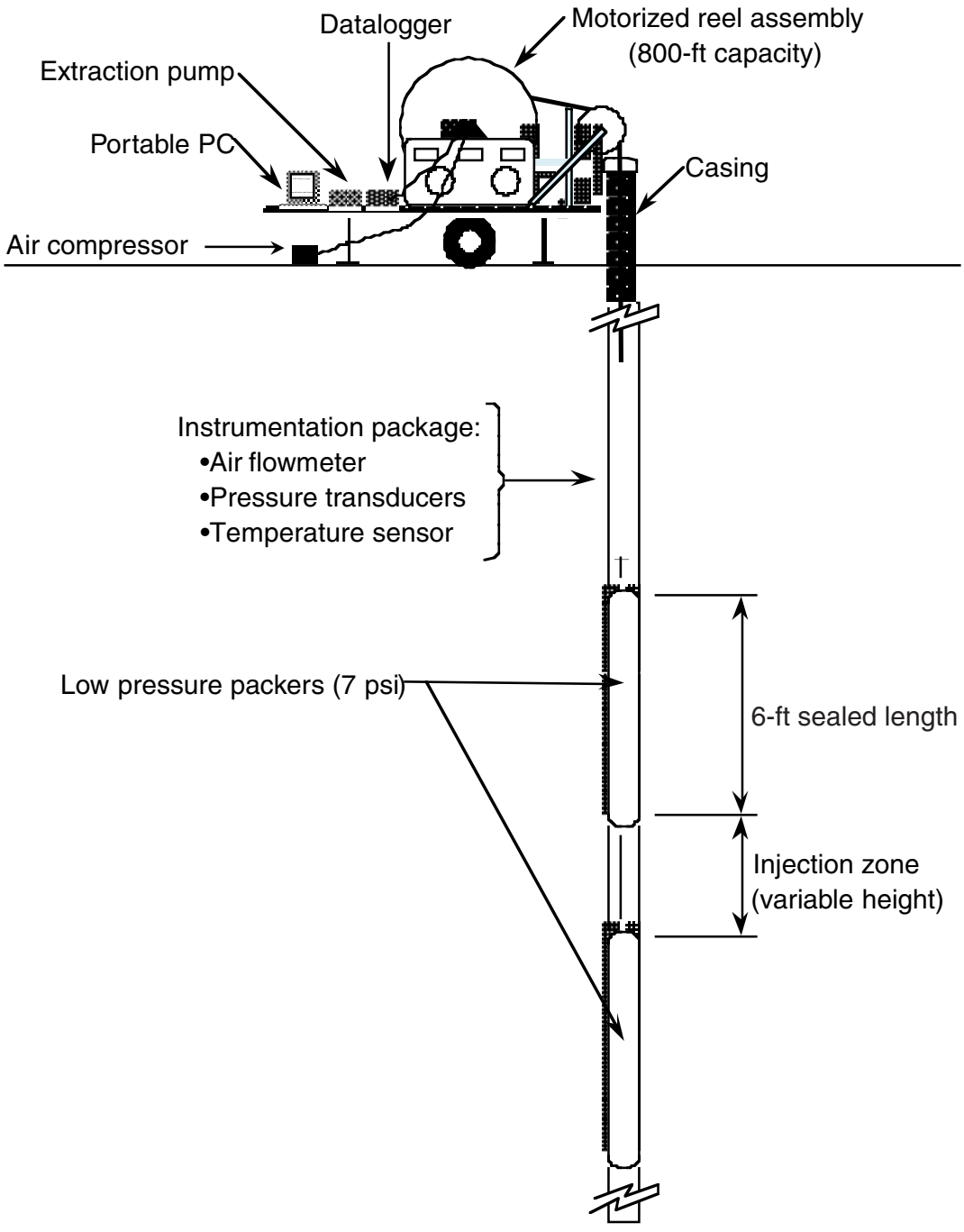

F5.7-3 / R-9 WELL COMPLETION RPT / 050500 / PTM

Figure 5.7-3. Air-permeability measurement system

5.7.2 Results

Data from the upper region, in the upper tholeiite of the Cerro del Rio basalt (39 to 64 ft), showed the higher of the measured values: 2.4 Darcies at 39 ft and 1.2 Darcies at 64 ft. The measurements at 43 and 60 ft indicated permeability higher than the system could sense, probably in excess of several hundred Darcies. This could be due to either a highly fractured and conductive zone or a borehole wall so rough that the packers could not form an adequate seal. Measurements in the lower region of the borehole, in the lower alkalic basalt of the Cerros del Rio basalt, indicated notably lower permeabilities, all at 0.3 Darcies (245-, 250-, and 255-ft depths). Results are summarized in Table 5.7-1.

Table 5.7-1
R-9 Packer Permeability Results for Cerros del Rio Basalt

Date	Depth (ft)	Borehole Diameter (in.)	Air Temp (°C)	Packer Pressure (psi)[a]	Atmospheric Pressure (psia)[b]	Injection Overpress (psia)	Flow Rate (SCFM)[c]	Permeability (Darcies)
9/27/97	39	5.25	14.8	13.0	12.10	0.95	3.0	2.4
9/27/97	43	5.25				—[d]		$>10^2$
9/27/97	60	5.25				—		$>10^2$
9/27/97	64	5.25	13.5	11.0	12.10	1.4	2.2	1.2
10/19/97	245	4.5	18.4	5.4	12.08	1.4	0.5	0.3
10/19/97	250	4.5	18.7	5.7	12.08	1.4	0.5	0.3
10/19/97	255	4.5	18.6	5.7	12.08	1.4	0.5	0.3

Note: Injection zone height was 28 in. in all cases.

[a] psi = pounds per square inch.

[b] psia = pounds per square inch, absolute.

[c] SCFM = standard cubic feet per minute.

[d] A dash in the table means injection zone overpressure too low to measure, hence very high inferred permeability; blank cells indicate no data were collected.

5.8 Borehole Geophysics

5.8.1 Methods

The borehole geophysical methods that were used for measurements during the drilling of R-9 include color videotape, borehole digital image processing system (BIPS), natural gamma radiation (NGR), caliper, electromagnetic induction (EM), magnetic susceptibility (MS), gamma-gamma density (density), thermal neutron (TN), and epithermal neutron (EN). Most measurements were taken in the open borehole, and some measurements were taken inside the drill casing. The borehole geophysical measurements were performed by the borehole geophysics company COLOG, Inc., and by the environmental contractor (SEA). SEA performed measurements using a portable Mt. Sopris geophysical logging system rented from COLOG. The record of borehole measurements is archived at the Facility for Information Management, Analysis, and Display (FIMAD). Borehole measurements were collected according to the schedule presented in Table 5.8-1.

Table 5.8-1
Borehole Measurements at R-9

Date	Depth (ft)[a]	Operator	Borehole Status	Video Camera	BIPS	Caliper	EM	MS	NGR	TN	EN	Density
9/27/97	10–98	COLOG	Open	X	X	X	X	X	X	X	X	X
9/27/97	10–98	COLOG	RC[b] rods						X	X	X	
10/19/97	239–278	SEA	Open				X	X	X			
10/20/97	6–239	COLOG	Cased[c]	X								
10/20/97	239–264	COLOG	Open	X	X							
10/20/97	239–282	COLOG	Open			X			X	X	X	X
10/21/97	119-138	COLOG	Open	X	X							
10/21/97	119–235	COLOG	Open			X			X	X	X	X
10/21/97	7–119	COLOG	Cased[c]							X		
10/21/97	119–225	SEA	Open			X	X	X				

Note: Blank cells indicate no measurements were taken.

[a] See Figure 2.3-1 for geologic units.

[b] Reverse-circulation dual-wall drill casing.

[c] 6-5/8-in.-diameter drill casing.

The borehole video camera and BIPS records are recorded on video tape. A preliminary viewing of these records from R-9 established that they identify changes in basalt lithology from massive to vesicular and they show the presence of fractures. The BIPS videotape record can be processed to calculate the strike and dip of the fractures. Determining the aperture of the fractures would require computer processing of the digital BIPS record.

The neutron borehole measurements include records of two types: TN and EN. The radioactivity source for these measurements was americium-beryllium with a strength of 3 Ci. The EN measurements were collected by placing a cadmium foil shield on the source.

The gamma-gamma density measurements were performed using a cesium-137 radioactive source with a strength of 100 mCi. The borehole probe was a focused design that was decentralized and side collimated. A single caliper arm pressed the probe against the borehole wall. The probe was a compensated design with two detectors (near and far from the radioactive source) to correct for changes in borehole diameter.

The NGR measurements provide a borehole record of the total gamma radiation. The most significant naturally occurring gamma-emitting radioisotopes are potassium-40 and daughter products of the uranium and thorium decay series. NGR measurements in boreholes are used for stratigraphic correlation and for identification of rocks and sediments that have a high abundance of clay. Uranium and thorium are concentrated in clay by the process of adsorption and ion exchange.

The MS measurements are a record of the magnetic susceptibility of the rock matrix, which is related to iron content and importantly, the iron chemistry. Ferromagnetic materials exhibit a very high magnetic susceptibility. The objective of MS measurements is stratigraphic correlation.

Caliper measurements are a record of the diameter of the borehole. The caliper record identifies features such as fractures, joints, collapse zones, and rubbly zones. The caliper record is important to the interpretation of other borehole measurements, such as neutron, density, and air and water permeability (measured with straddle packer systems).

EM measurements are collected in saturated and unsaturated boreholes. The EM probe used for measurements in R-9 is designed to measure the electrical conductivity of the rocks 8 to 39 in. from the borehole axis. The EM measurements are sensitive to the electrical properties of the rocks and the quantity and quality of contained groundwater.

5.8.2 Results

Figures 5.8-1 through 5.8-6 present borehole measurements taken with NGR, caliper, EM, and TN. The measurements were collected as digital records. The figures were generated with the ViewLog software package for interpretation and display of borehole geophysical measurements. The figures also show the borehole stratigraphy and the presence of saturation.

Figures 5.8-1 and 5.8-2 present results for borehole measurements in a 5-in.-diameter open borehole that was drilled in unsaturated rock. The measurements were taken in the depth interval from land surface to 98 ft. Surface casing was present to a depth of 4 ft.

Figures 5.8-3, 5.8-4a, and 5.8-4b present the results of measurements in an open borehole in the depth interval of 199 to 235 ft. At the time of these measurements, the borehole was cased from land surface to 119 ft with 6-5/8-in.-diameter drill casing. The results of TN measurements that were collected in the cased interval are also presented in Figures 5.8-4a and 5.8-4b. During the geophysical measurements, the borehole was unsaturated to a depth of 137 ft and saturated at greater depths. During drilling of the borehole, water first entered the borehole at a depth of 180 ft. The groundwater quickly rose to a borehole depth of 137 ft.

Figures 5.8-5 and 5.8-6 present the results of measurements in an open borehole in the depth interval of 239 to 282 ft. In this interval the borehole was drilled with coring systems and had a diameter of 4.5 in. The borehole was unsaturated to a depth of 264 ft and saturated at greater depths. During the coring operations, water first entered the borehole at a depth of 275 ft. Groundwater then rose in the borehole to a depth of 264 ft.

The figures show that the caliper record is important in identifying massive, competent intervals of basalt; the presence of fractures; and vesicular, rubbly intervals in the basalt.

The NGR measurements generally range in abundance from 40 to 75 counts per second (cps). The local variation to higher abundance in the depth interval of 20 to 25 ft is probably caused by a higher clay content. The general increase in NGR abundance that occurs at depths greater than 238 ft is within the lower alkalic basalt (Section 3.2.4) but may reflect a mineralogic change in the basalt.

The EM measurements collected in R-9 range in value from 20 to 1200 ohm-meters. The low values are measured in saturated intervals; the high values are measured in massive basalt that has a low moisture content. In the unsaturated borehole intervals, the EM measurements vary because of moisture content and clay content.

The MS measurements range in value from 4 to 10 parts per thousand; the highest values were measured in the upper 100 ft of basalt. The application of MS measurements for stratigraphic correlation cannot be determined from the limited measurements performed in R-9.

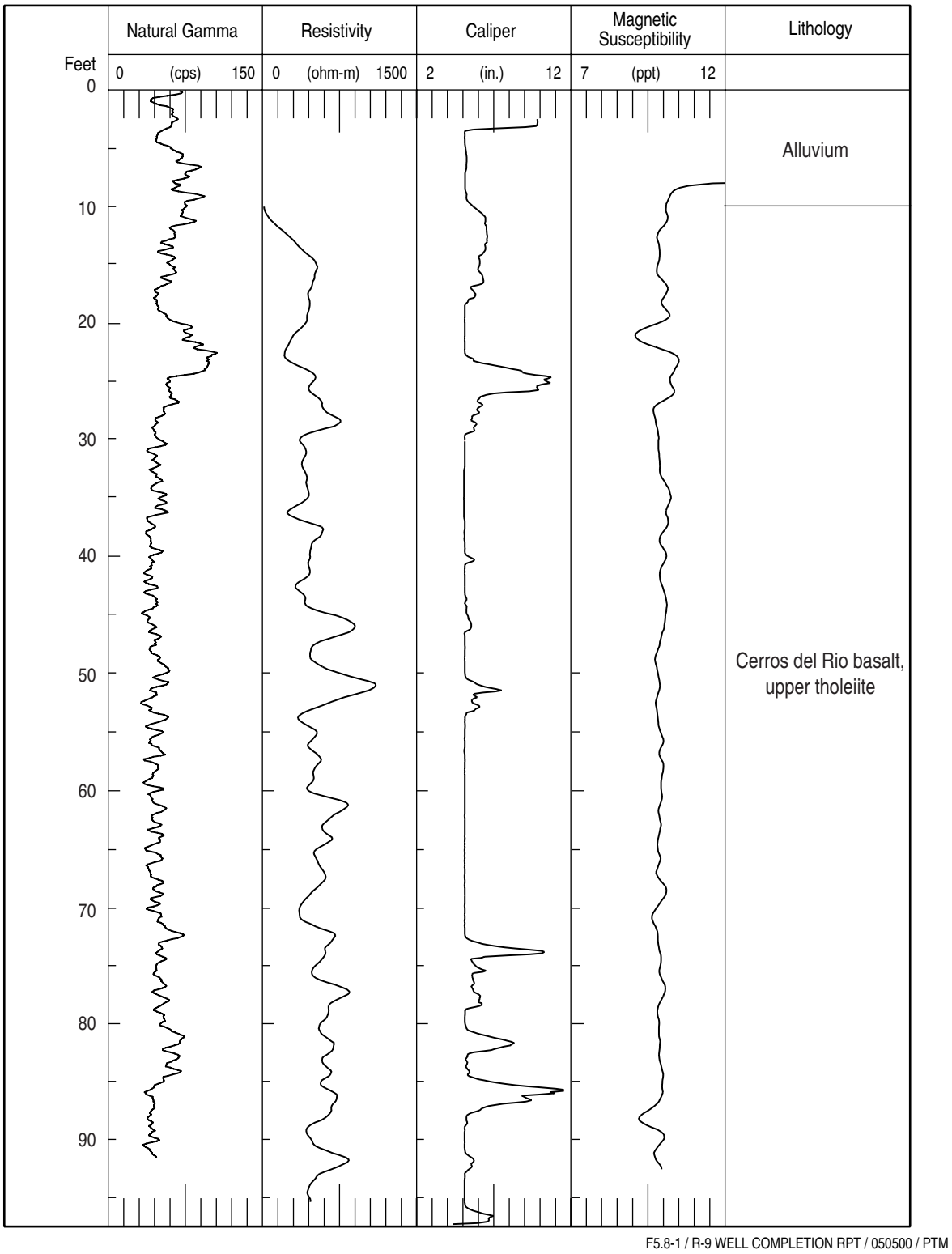

Figure 5.8-1. Borehole geophysical measurements in an open borehole with nonradioactive source tools in R-9 for the depth interval of 10 to 96 ft

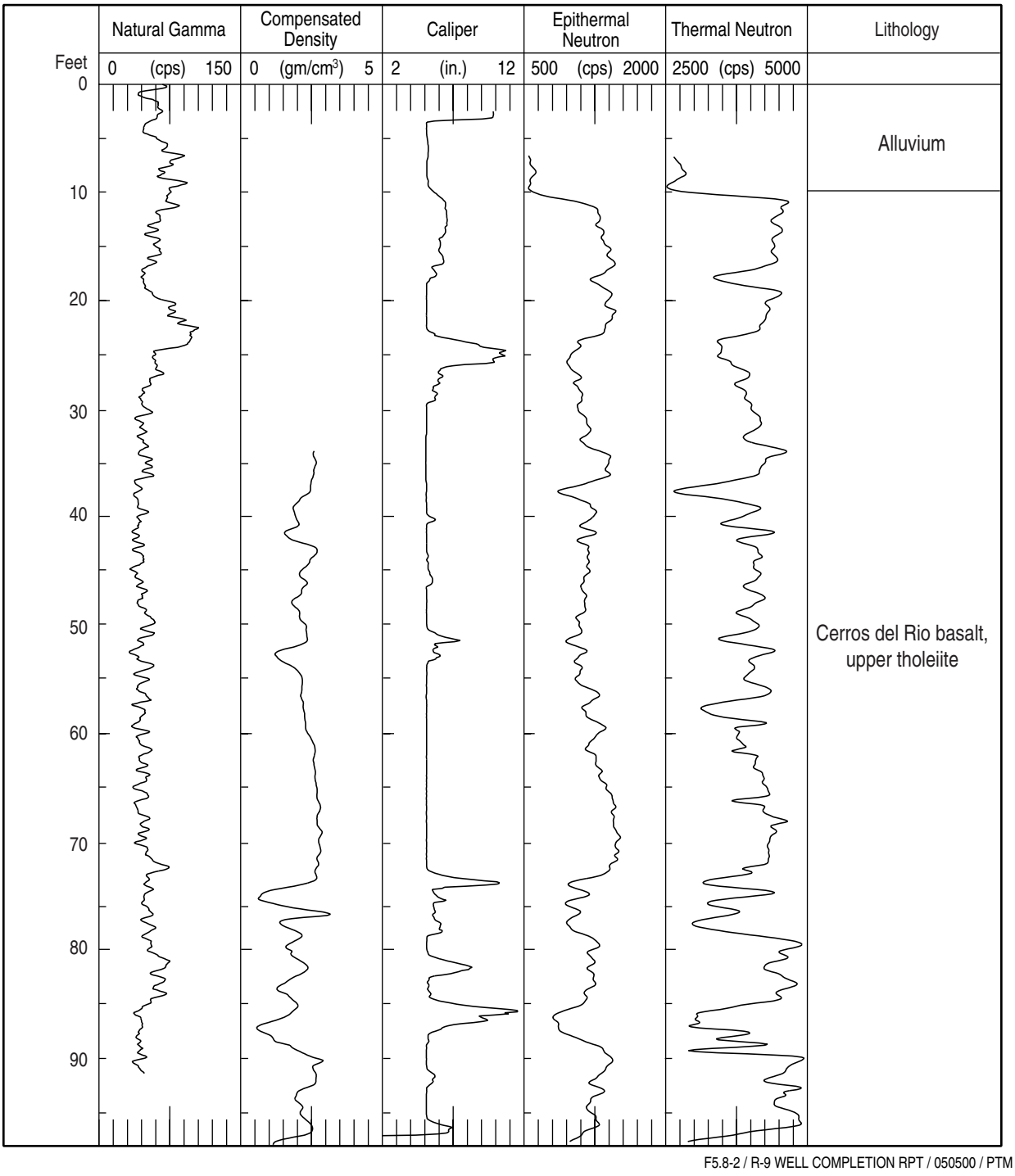

Figure 5.8-2. Borehole geophysical measurements in an open borehole with radioactive source tools in R-9 for the depth interval of 10 to 96 ft

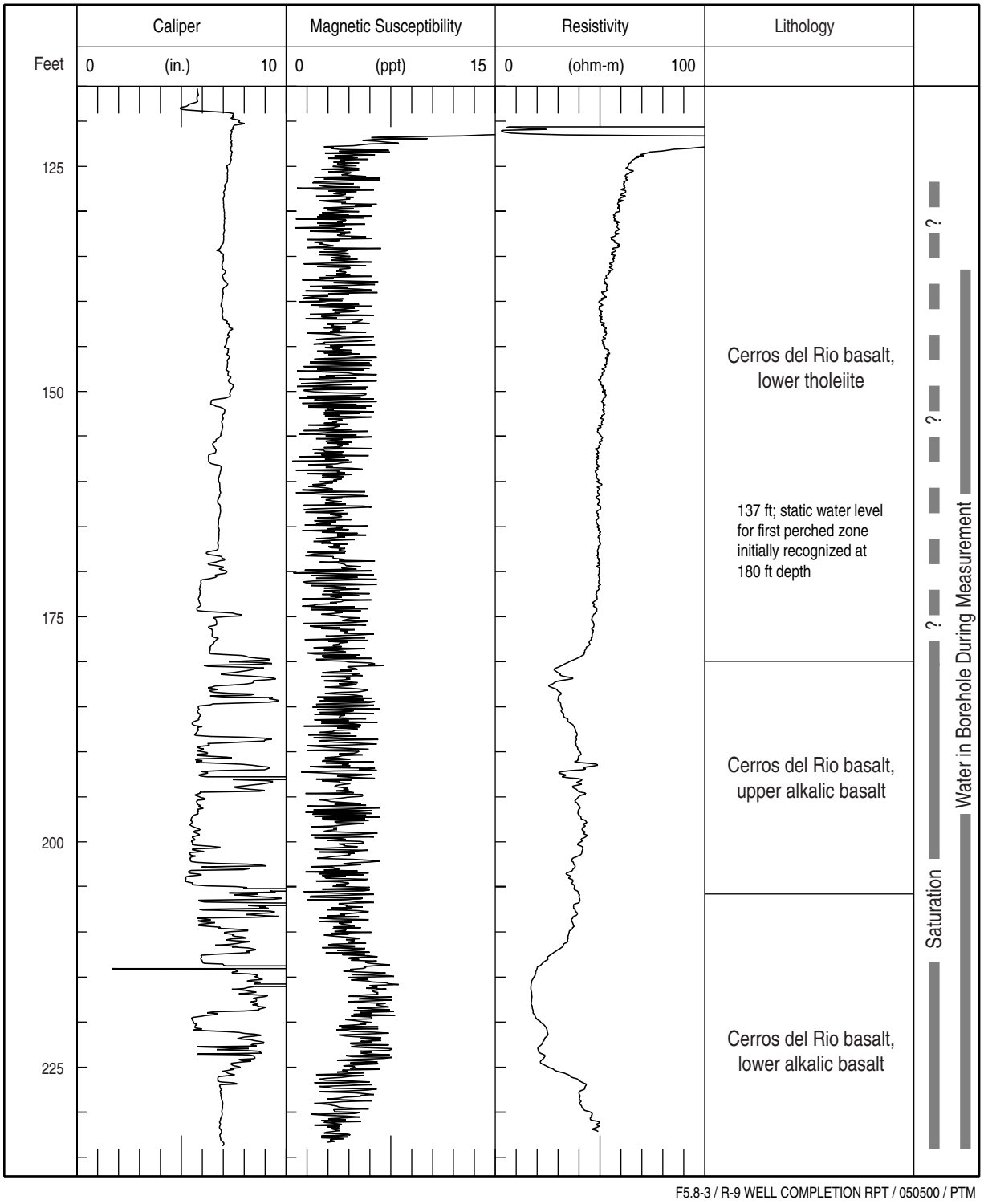

Figure 5.8-3. Borehole geophysical measurements in an open borehole with nonradioactive source tools in R-9 for the depth interval of 120 to 225 ft

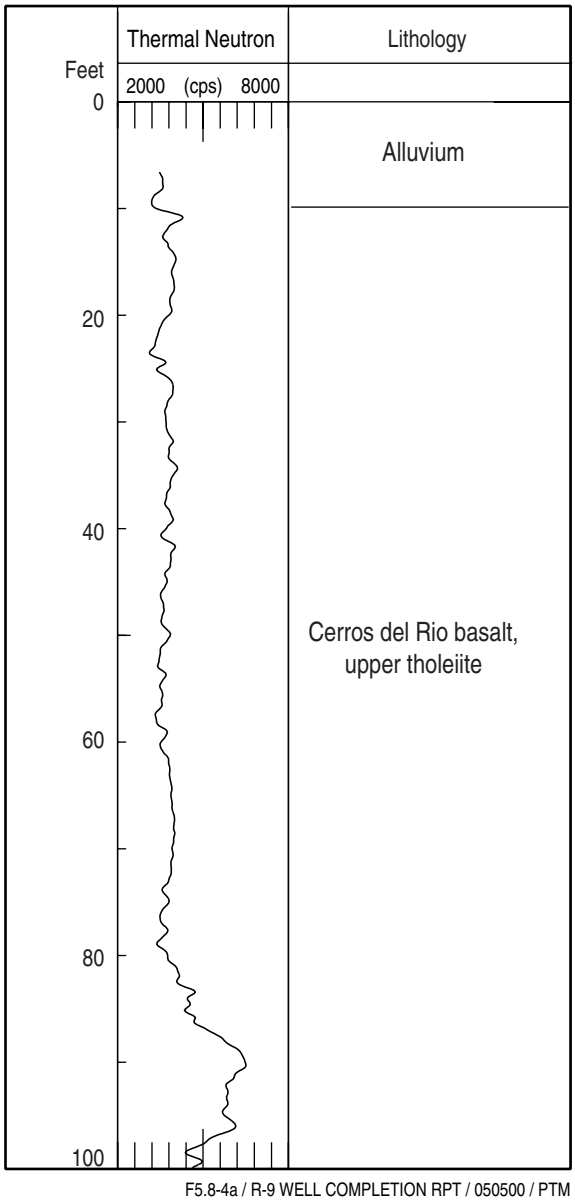

Figure 5.8-4a. Borehole geophysical measurements through steel casing with radioactive source tools in R-9 for the depth interval of 5 to 100 ft

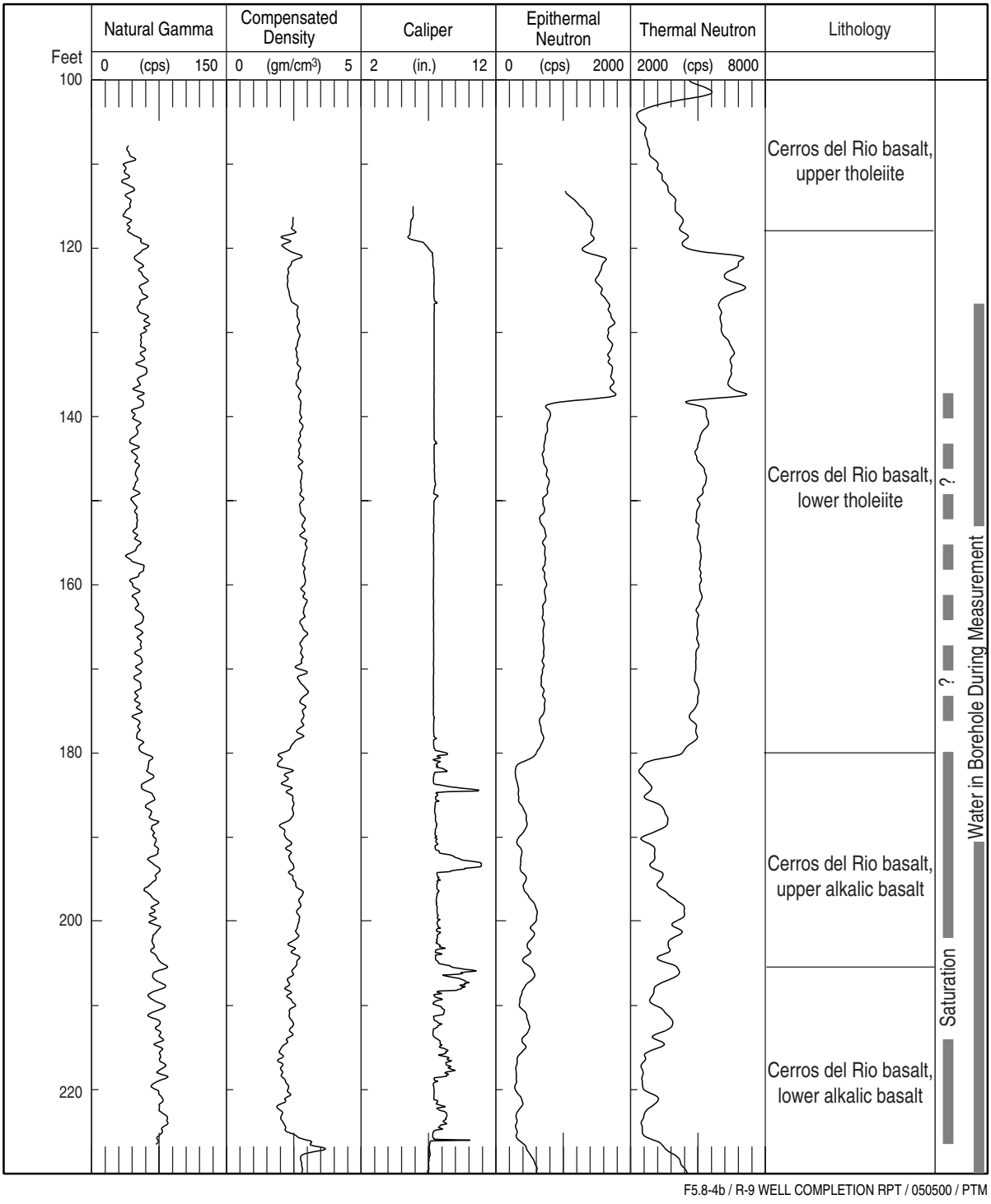

Figure 5.8-4b. Borehole geophysical measurements in an open borehole with radioactive source tools in R-9 for the depth interval of 120 to 226 ft

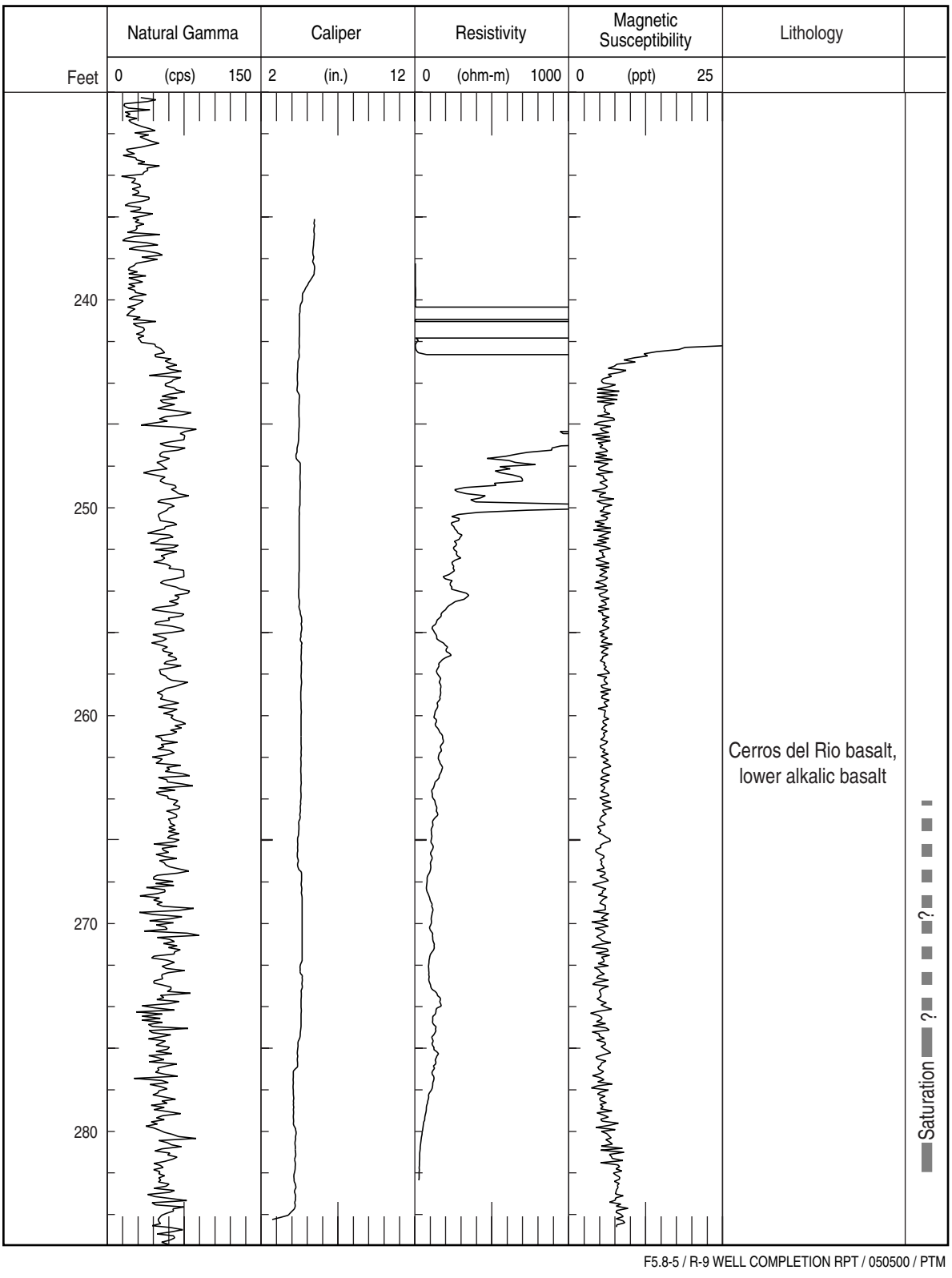

Figure 5.8-5. Borehole geophysical measurements in an open borehole with nonradioactive source tools in R-9 for the depth interval of 224 to 278 ft

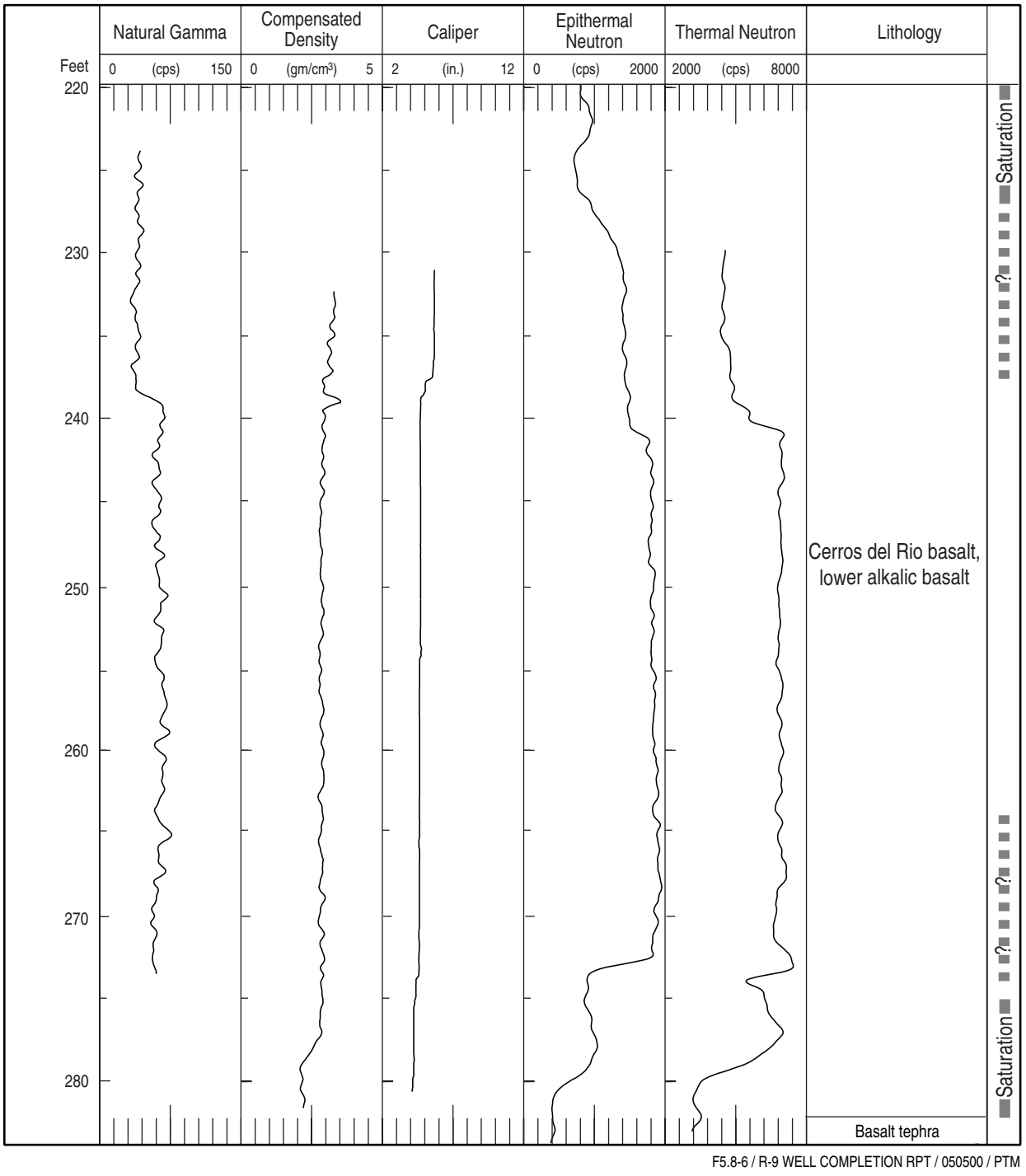

Figure 5.8-6. Borehole geophysical measurements in an open borehole with radioactive source tools in R-9 for the depth interval of 220 to 280 ft

The compensated density measurements show the effect of borehole rugosity on the measured values. It is important to compare density measurements with caliper measurements. Unrealistic low values for density correlate with depth intervals where the borehole exhibits a great change in diameter over a short distance. In competent sections of the borehole, the density measurements range from 2.3 gm/cm^3 to 2.7 gm/cm^3. The lower values of density were measured in highly vesicular basalt, and the higher values were measured in dense, massive basalt. The highest density values were measured in the dense, massive basalt that forms the perching horizon below the first perched zone of saturation.

The EN and TN measurements exhibit an important relationship to moisture content. The neutron measurements trend to higher values as moisture content drops. This trend is illustrated in Figure 5.8-6 at the base of the first perched zone of saturation and at the top of the second perched zone of saturation (273 to 280 ft).

6.0 WASTE MANAGEMENT

The waste generated during R-9 drilling activities included drill cuttings, purge water, decontamination water, personal protective equipment, absorbent pads used beneath the drill rig, and miscellaneous waste. Drill cuttings were collected in 55-gal. drums and transferred daily to a roll-off bin. A total of two 15-cubic yard roll-off bins were generated from the drilling of R-9. When the bins were full, a sample was collected in accordance with the approved waste characterization strategy form (WCSF) and analyzed for metals, gross alpha, gross beta, gross gamma, and tritium. The analytical results for the cuttings samples were reviewed and found to not be regulated as hazardous waste. Using the waste-minimization strategy identified in the WCSF, the cuttings were taken by Parker Brothers Construction to be used as backfill; however, the consistency of the cuttings was not suitable for backfill and they subsequently were disposed of in the Los Alamos County landfill. An additional 1.5 cubic yards of drill cuttings were generated during the second phase of drilling, when the borehole was deepened to accommodate the permanent well casing. These cuttings were characterized based on results from previous sampling of drill cuttings during the initial phase of drilling and spread on the ground surface.

Purge water generated during drilling activities through the first zone of saturation at 180-ft depth was stored in five 3000-gal. portable tanks. In accordance with the approved WCSF, the groundwater analytical results from this zone were reviewed and found to meet discharge requirements. A total of 7800 gal. of water was then discharged though a sprinkler system in accordance with the approved Notice of Intent (NOI) to discharge.

Approximately 3000 gal. of purge water were generated and stored in two tanks during drilling activities through the second zone of saturation at 275-ft depth. This stored groundwater was analyzed and then transported to TA-50 for disposal, based on 48.4 ppb dissolved uranium results.

The regional aquifer was encountered at a depth of 688 ft during the first phase of drilling, and approximately 2400 gal. of purge water were generated and stored in two tanks. The groundwater analytical results were found to meet discharge requirements, as stated in the WCSF, and the water was discharged onsite in accordance with the approved NOI. During the second phase of drilling, an additional 3400 gal. of water were generated while drilling in the regional aquifer; 3000 gal. of water were generated during well development, and 26,700 gal. were generated during hydrologic testing. This water was direct-discharged through a sprinkler system, based on prior characterization of regional groundwater.

Decontamination water (less than 6 gal. per day) was generated when the sampling equipment (i.e., core tubes, bailers, water-level probe tape) was decontaminated onsite. Since no contamination was encountered based on field screening or visual observation, the water was discharged to the site in

accordance with “Decontamination Water Discharge Procedure: Containerized Decon Water” (LANL 1996, 58716) and in accordance with the approved WCSF. Large equipment and a drill pipe were decontaminated at TA-50, as needed.

Miscellaneous waste included nitrile gloves, paper towels, plastic bags, plastic sheeting, and drum liners. A resealable plastic bag was kept at the entrance of the access control zone to contain the miscellaneous waste. When the bag was full, it was sealed and labeled with the well designation, generation dates, borehole depths, and contents. Approximately four 55-gal. drum liners of miscellaneous waste were generated during drilling. A waste profile form was prepared for this waste stream, and the miscellaneous waste was disposed of on November 11, 1997, and March 18, 1998, at the Los Alamos County landfill in accordance with the approved WCSF.

Other miscellaneous waste included approximately 12 drums of soil mixed with diesel fuel from a generator that leaked. Also, eight drums of bentonite and six drums of absorbent pads were generated during drilling activities. The pads were used to absorb any liquids that leaked from beneath the drill rig. All drums were profiled in accordance with the approved WCSF and disposed of accordingly.

7.0 SURVEY ACTIVITIES

7.1 Geodetic Survey

The location of R-9 was determined by geodetic survey on September 19, 2000, using a Wild/Leica TC1600 total station. The 1992/1993 Laboratory-wide control network provided survey control. The survey located the brass monument in the northwest corner of the well pad and the north side of top of well casing (Table 7.1-1). Horizontal well coordinates are based on New Mexico State Plane Grid Coordinates, Central Zone (North American Datum 83) and are expressed in feet. Elevation is expressed in feet above mean sea level using the National Geodetic Vertical Datum of 1929. The Facility for Information Management, Analysis, and Display (FIMAD) location identification number for R-9 is LA-00168.

Table 7.1-1
Geodetic Data for Well R-9

	Northing (ft)	Easting (ft)	Elevation (ft)
Brass Monument	1770847.1	1648236.5	6382.8
Top of Casing	1770843.9	1648241.4	6385.36

7.2 Surface Radiological Survey

A surface radiological survey was conducted by a radiological control technician before drilling activities began at LAOI-7. This predrilling radiation survey consisted of collecting alpha, beta, and gamma background measurements and conducting statistical analyses to calculate action levels that suggest radioactivity elevated above background values. The survey consisted of 15 points on a grid projected over the work area. Each point was surveyed using direct reading alpha, beta/gamma, and dose rate meters. Alpha was measured using a Ludlum 139 with an air proportional probe; beta/gamma was measured using a Ludlum 12 with a 44-9 probe; dose rate was measured using a Ludlum 19 µR/hr meter. Calculated background values for the drill site are 0.4 cpm for alpha, 152 cpm for beta/gamma, and 16.2 µR/hr for dose rate.

8.0 WELL DESIGN, CONSTRUCTION, AND DEVELOPMENT

8.1 Well Design

When the drilling of R-9 borehole was temporarily halted at a depth of 710 ft on February 3, 1998, the depth to the regional water table could not be determined with certainty because several discrete zones of saturation had been encountered in the lower part of the borehole. After discussions between the Laboratory, the Department of Energy (DOE), and the New Mexico Environment Department (NMED), further work on R-9 was halted until relationships at the top of the regional zone of saturation could be better determined. The principal concern at this time was that the well screen might be improperly positioned to sample the top of the regional zone of saturation. As a result, a temporary PVC casing was installed to provide access to sampling water and to provide a stable environment for a pressure transducer to monitor water levels until the completion strategy for the permanent well could be finalized. This temporary well is shown in Figure 8.1-1. The temporary well at R-9 was constructed in the following manner.

- The 8-5/8-in.-diameter casing was landed at 679 ft and sealed with bentonite to prevent water from flowing downhole and mixing with water in the productive zone at 688 ft.
- A 6-in.-diameter hole was drilled to a total depth of 710 ft.
- A temporary 4-in.-diameter schedule 40 PVC casing was hung inside the existing casing strings.
- A 20-ft screen was positioned from 684 to 704 ft, and a 2-ft sump was installed.
- A sand pack (20-40) was tremied in the hole from 6 ft above to 6 ft below the screened interval.
- A pressure transducer was installed to monitor water-table fluctuations because of atmospheric effects, seasonal effects, earth tides, and pumping of nearby water supply well PM-1.

Data collected from drilling activities at R-12 helped clarify groundwater conditions at R-9, and a final completion strategy for R-9 was proposed by the Groundwater Integration Team. This completion strategy was discussed with DOE and NMED, and the completion of R-9 was scheduled for the latter part of fiscal year 1999. The final phase of drilling and well installation at R-9 took place from September 22, 1999, through October 18, 1999.

During the final stages of drilling and well completion, the temporary PVC well was removed, and the borehole was deepened from 710 ft to 771 ft to accommodate the desired length of well screen and sump. After drilling operations were completed, the well string with a single screen was tripped into the hole and operations to install annular materials around the well were initiated. At total depth, the R-9 borehole contained four telescoped drill casings with diameters of 14 in., 12.75 in., 10.75 in., and 8.62 in.

8.2 Well Construction

During well-construction operations, the 8-in. well casing was successfully pulled back in increments while annular materials were placed around the well with a tremie line. The 8.62-in. casing was completely removed from the borehole and the annular materials were installed to the bottom of the 10.75-in. drill casing. However, when attempts were made to pull back on the 10.75-in. drill casing, it was discovered that the 5-in. well casing had become locked to the drill casing. Attempts to decouple the 5-in. well casing from the 10.75-in. drill casing were unsuccessful. Because further attempts to pull back on the 10.75-in. drill casing might cause severe damage to the well completion string, a decision was made to cement in place the 10.75-in. casing and the two other remaining drill casings.

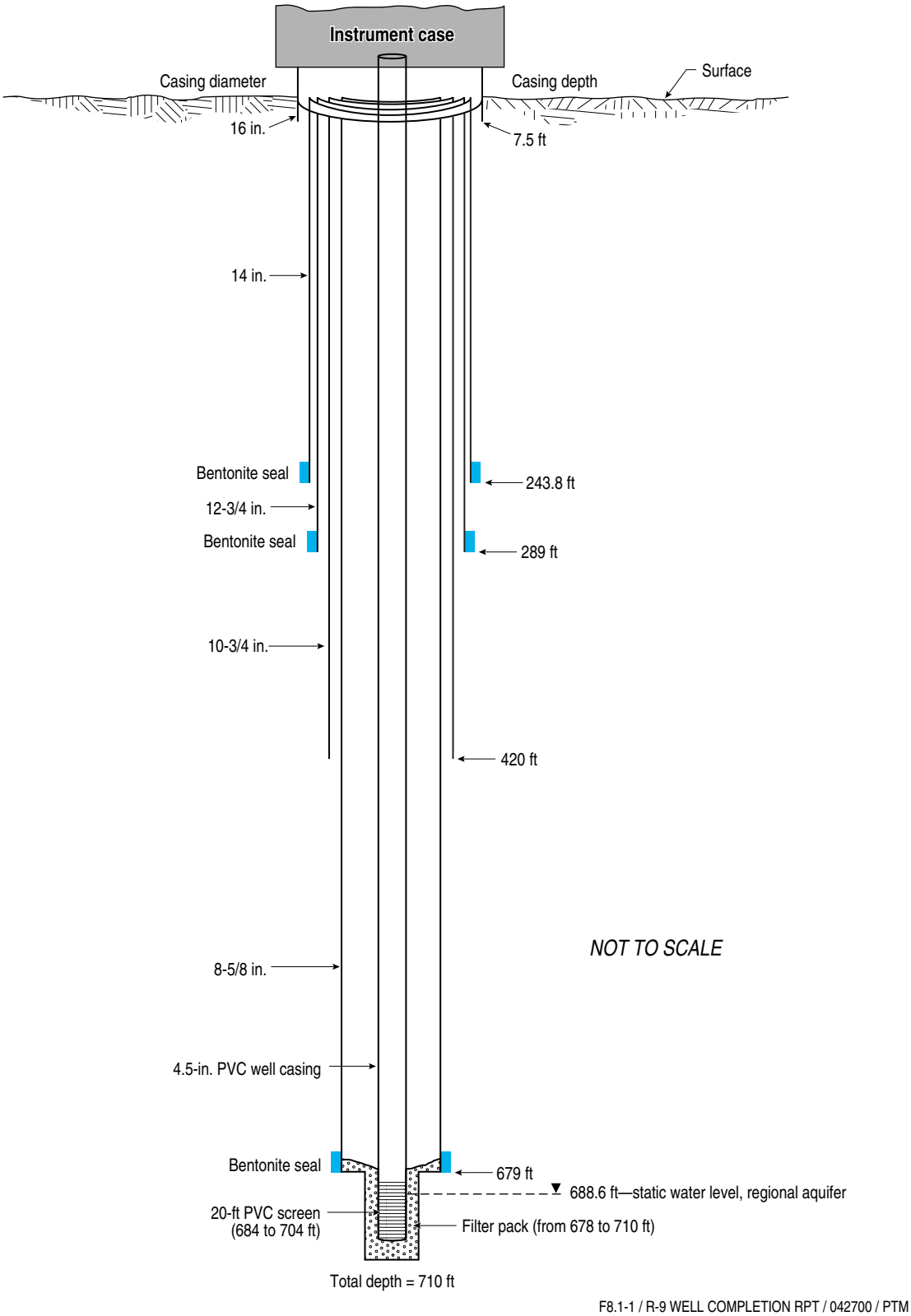

Figure 8.1-1. Configuration of the temporary well for R-9

The annular materials between the top of the regional water table and the bottom of the 10.75-in. casing and the two uppermost drill casings that currently seal off two perched groundwater zones provide adequate protection of the regional saturation from perched groundwater above. In addition, cement was pressure-injected into the annular space between the 14-in. and 12.75-in. casings and between the 12.75-in. and 10.75-in. casings to further isolate the perched water zones in the upper part of the borehole. The driller reported that cement was present in the bottom of the 10.75-in. casing after the pressure injection of grout between the 12.75-in. and 10.75-in. casings, indicating the annulus between the 10.75-in. casing and the borehole wall was successfully sealed. Cement was also placed inside the 10.75-in. casing, sealing in the well casing. The as-built well completion drawing for R-9 is shown in Figure 8.2-1.

8.3 Well Development

Well development was conducted from February 10, 2000, to February 13, 2000. Well-development methods involved jetting and pumping the single screen at the top of the regional water table. The 60-ft screened interval was jetted with water at 20-ft intervals using an underground drill rig (UDR)-20 drill rig and specialized jetting tool on NQ drill rod. A total of 3000 gal. of municipal-supply water was used during the jetting process. Following jetting of the screen, a submersible pump was deployed and the well was pumped to purge introduced municipal water, remove sediment, and reduce turbidity to less than 5 nephelometric turbidity units (NTU). A total of 3000 gal. of water was pumped during development at a rate of 8 to 11 gal. per minute (gpm). Turbidity was reduced to less than 1 NTU at completion of well development. Turbidity with respect to volume of water pumped is shown in Figure 8.3-1. An additional 26,700 gal. of water was pumped from R-9 during subsequent hydrologic testing; removal of this large volume of water also contributed to the development of the well.

8.4 Pump Installation

A submersible pump was installed in well R-9 by Rio Grande Well Supply of Santa Fe, New Mexico. The pump is a 3-horsepower Grundfos™ Model 10S30-34, 4-in.-outside diameter (O.D.), submersible pump that operates on a 460-volt, 3-phase power supply provided by a portable diesel generator. The power cable is No. 12, 3CWG jacketed submersible wire, secured to the pump riser pipe with cable ties. The pump was installed on 1.25-in. 304 stainless-steel NPT riser pipe with 3000-lb couplings. The pump intake was set 774 ft below top of casing (741.4 ft below ground surface); at this depth the intake is approximately 53.4 ft below the static water level in the well. The pump was installed with a check valve and a weep hole drilled in the riser pipe at point near the static water level in the well to allow water to drain from the piping. The pump capacity is approximately 10 gal./min at 700-ft depth.

A 1-in.-inside diameter (I.D.), flush-threaded, schedule 40, PVC pipe with a bottom cap was installed to a depth just above the submersible pump body to serve as a conduit for a pressure transducer. The bottom 20 ft of the PVC pipe was perforated to provide a hydraulic connection with the well. The PVC pipe was secured to the pump riser pipe with cable ties

The pump riser and PVC pipe are securely hung and sealed at the top of the well casing by a 3000-lb capacity landing plate. The pump discharge was completed with a ball valve and threaded nipple to allow connection of appropriate tubing for well purging and sample collection. The pump, power cable, and all piping was washed with Alconox™ detergent and steam-cleaned prior to installation.

8.5 Wellhead Protection

A reinforced concrete vault was installed to provide wellhead protection. Figure 8.5-1 shows plan and profile views of the well-head configuration.

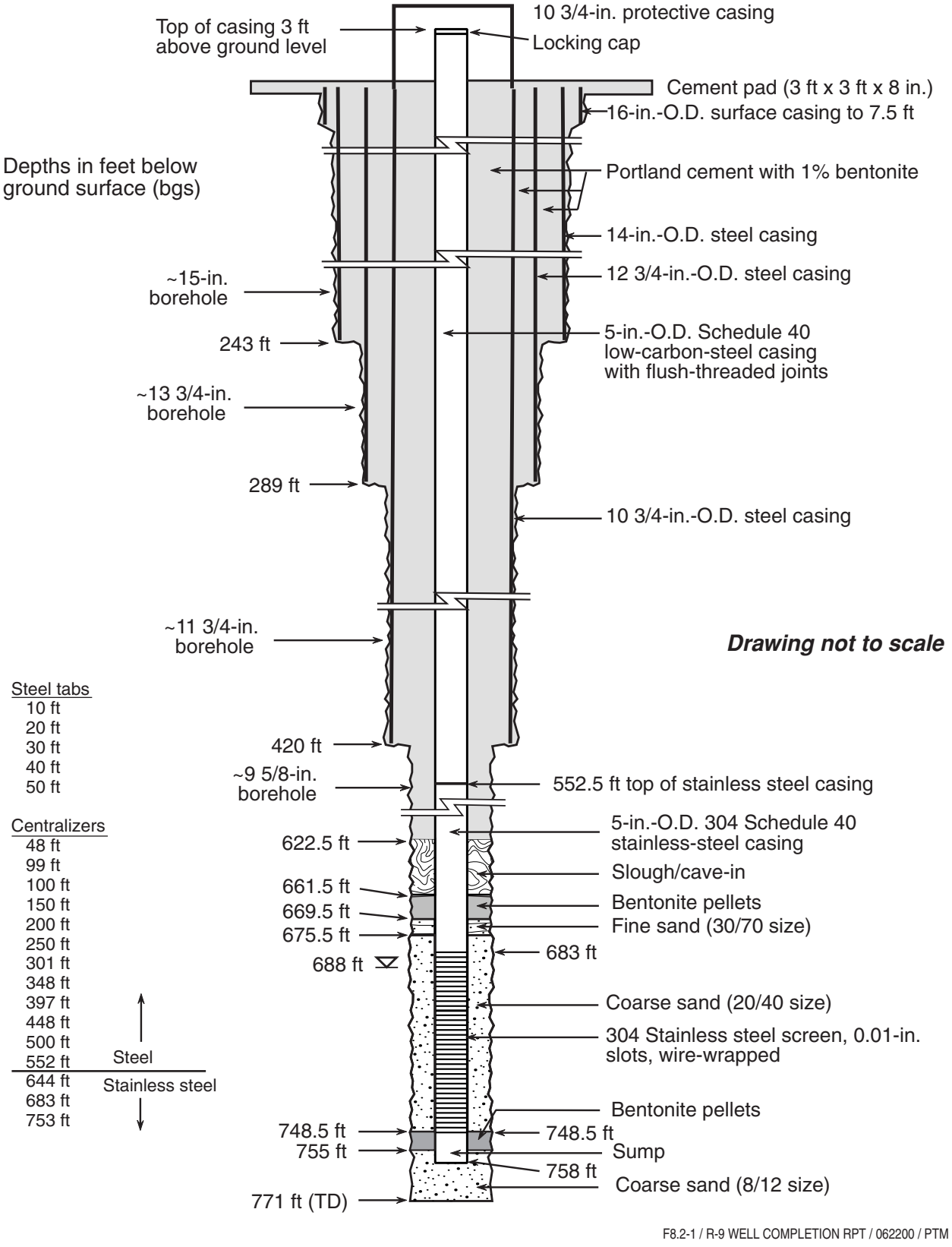

Figure 8.2-1. As-built well completion diagram of well R-9

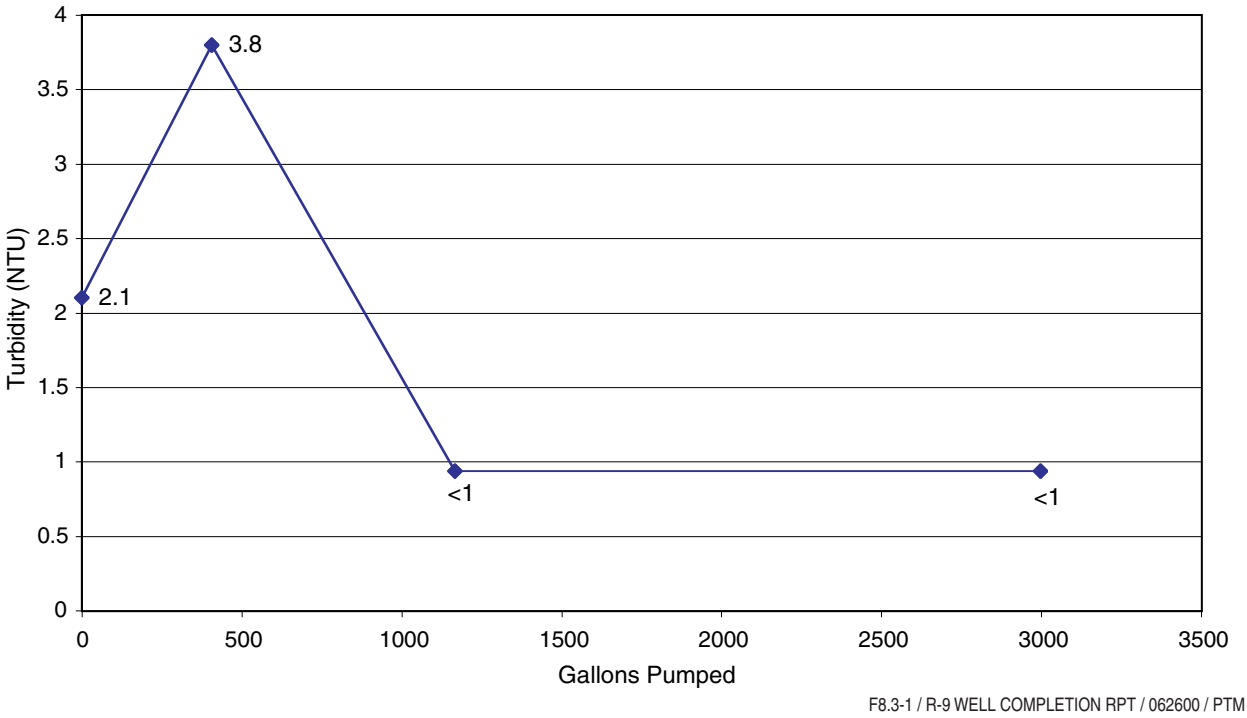

Figure 8.3-1. Well R-9 pumping development

9.0 SITE RESTORATION

The R-9 drill site area was recontoured to match the surrounding topography using a backhoe. The surface of the drill pad was roughened and native dryland seed was applied to the denuded areas. Straw mulch was then spread over the seeded areas and wheel-rolled to crimp in the straw and cover the seed.

10.0 MODIFICATIONS TO WORK PLANS

Table 10.0-1 compares the planned characterization activities in the "Task/Site Work Plan for Operable Unit 1049: Los Alamos Canyon and Pueblo Canyon" (LANL 1995, 50290), the "Hydrogeologic Workplan" (LANL 1998, 59599), the core document (LANL 1997, 55622), and the "Field Implementation Plan for the Drilling and Testing of LANL Regional Characterization Well, R-9" ("the field implementation plan"; LANL 1997, 59163) with characterization activities performed in R-9. The characterization activities in the "Hydrogeologic Workplan" and the core document are the same; therefore, planned characterization activities for these two documents are shown together in Table 10.0-1.

The most significant modification of planned versus actual activities at R-9 was the redesign of R-9 from an intermediate-depth well to a regional aquifer well. In the Los Alamos Canyon and Pueblo Canyon work plan, R-9 (as LAOI-7) was originally designed to detect and characterize the highest intermediate-depth perched groundwater zone near the eastern Laboratory boundary in Los Alamos Canyon. The original depth was not to exceed 150 ft. In the "Hydrogeologic Workplan", the core document, and the field implementation plan, the well was redesigned to penetrate the regional aquifer. R-9 successfully penetrated the top of the regional aquifer at a depth of 688 ft.

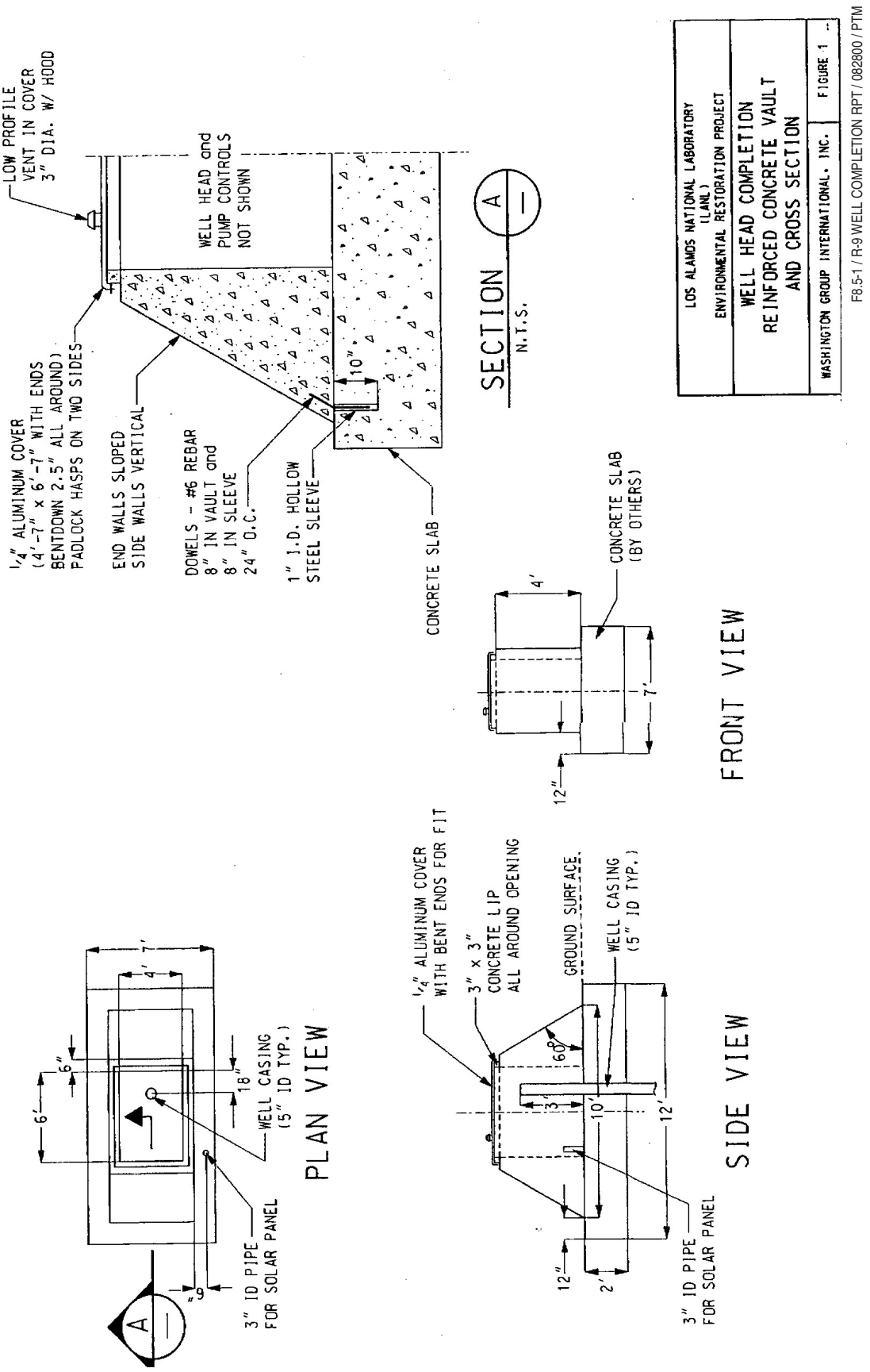

Figure 8.5-1. Well R-9 wellhead diagram

Table 10.0-1
Activities Planned for R-9 Compared with Work Performed

	Work Plan for Los Alamos Canyon and Pueblo Canyon	Hydrogeologic Workplan and Core Document for Canyons Investigations	R-9 Field Implementation Plan	R-9 Actual Work
Planned depth (ft)	Maximum 150	100 to 500 into the regional aquifer	750	771
Drilling method	Auger or rotary drilling	Methods may include, but are not limited to, hollow-stem auger, air-rotary/Odex/Stratex, air-rotary/Barber rig, mud-rotary drilling	Air-rotary methods including downhole percussion hammers on 4.5-in. and 7-in. O.D. dual-wall casings to drill open hole; air-rotary 101-mm Geobarrel system to collect continuous core; air-rotary Holte and Stratex casing advance systems and downhole percussion hammers to simultaneously drill and advance casing in the borehole	Same as field implementation plan
Amount of core	Not specified	10% of the borehole	Approximately 38% of the borehole	31.7 % of the borehole
Lithologic log	Log to be prepared from core, cuttings, and drilling performance	Log to be prepared from core, cuttings, and drilling performance	Log to be prepared from core, cuttings, and drilling performance	Log was prepared from core, cuttings, and drilling performance
Number of water samples collected for contaminant analysis	A water sample will be collected from each saturated zone. Well will be sampled at completion and after six months.	A water sample will be collected from each saturated zone. The number of sampling events after well completion are not specified.	A water sample will be collected from each saturated zone. The geochemistry project leader and technical team will determine the number and locations of samples based on conditions encountered. The number of sampling events after well completion are not specified. Up to seven water samples are planned.	A total of 13 water samples were collected from saturated zones. Of these, 6 were duplicate water samples.
Water sample analytes	**Trace Elements/Metals:** Al, Sb, As, Ba, Be, B, Cd, Ca, Cr, Co, Cu, Fe, Pb, Mg, Mn, Hg, Ni, K, Se, Ag, Na, Tl, Ti, U, V, Zn **Anions:** Br, ClO_3, Cl, F, NO_3, PO_4, HCO_3, SO_4 **Other Inorganic Chemicals:** Si, cyanide **Radionuclides:** ^{3}H, ^{90}Sr, ^{137}Cs, ^{234}U, ^{235}U, ^{236}U, ^{238}U, ^{238}Pu, $^{239,240}Pu$, ^{241}Am **Organic Compounds:** pesticides, PCBs, VOCs, SVOCs **Other Analyses:** ^{14}C, ^{13}C, $^{18}O/^{16}O$, D/H, DOC	Radiochemistry I, II, and II analytes; ^{3}H; gamma spectroscopy scan; general inorganic chemicals; metals; stable isotopes	**Trace Elements/Metals:** Al, Sb, As, Ba, Be, B, Cd, Ca, Cr, Co, Cu, Fe, Pb, Mg, Mn, Hg, Ni, K, Se, Ag, Na, Tl, U, V, Zn, NH_4 **Anions:** Br, ClO_3, Cl, F, NO_3, NO_2, PO_4, HCO_3, SO_4 **Other Inorganic Chemicals:** Si, cyanide, total organic carbon **Radionuclides:** ^{3}H, ^{90}Sr, ^{137}Cs, ^{241}Am, ^{234}U, ^{235}U, ^{238}U, ^{238}Pu, $^{239,240}Pu$, gamma spectroscopy, gross alpha, gross beta, gross gamma **Organic Compounds:** VOCs, SVOCs **Other Analyses:** ^{14}C, ^{13}C, $^{18}O/^{16}O$, D/H, DOC	Same as field implementation plan with additions of Mo, ^{236}U, $^{15}N/^{14}N$

Table 10.0-1 (continued)

	Work Plan for Los Alamos Canyon and Pueblo Canyon	Hydrogeologic Workplan and Core Document for Canyons Investigations	R-9 Field Implementation Plan	R-9 Actual Work
Water sample field measurements	Alkalinity, dissolved oxygen, pH, specific conductance, temperature, turbidity	Alkalinity, pH, specific conductance, temperature, turbidity	Alkalinity, dissolved oxygen (completed well only), pH, specific conductance, temperature, turbidity	Alkalinity, pH, specific conductance, temperature, turbidity
Number of core/cuttings samples collected for contaminant analysis	Collect and preserve seven cores to represent major hydrogeologic units and zones above and below major hydrogeologic contacts	Twenty samples of core or cuttings to be analyzed for contaminants in each borehole.	Up to 21 core/cuttings samples planned.	To date, 15 samples of cores/cutting have been collected for contaminant analysis.
Core sample analytes	**Trace Elements/Metals:** Al, Sb, As, Ba, Be, Br, Cd, Ca, Cr, Co, Cu, Fe, Pb, Mg, Mn, Hg, Ni, K, Se, Ag, Na, Tl, Ti, U, V, Zn **Anions:** B, Cl, F, SO_4 **Other Inorganic Chemicals:** Si, cyanide **Radionuclides:** ^{3}H, ^{90}Sr, ^{137}Cs, ^{230}Th, ^{232}Th, ^{234}U, ^{235}U, ^{238}U, ^{238}Pu, $^{239,240}Pu$, gamma spectroscopy, gross alpha, gross beta, gross gamma	Uppermost sample to be analyzed for a full range of compounds: deeper samples to be analyzed for Radiochemistry I, II, and II analytes; ^{3}H; and metals. Four samples to be analyzed for VOCs.	**Trace Elements/Metals:** Al, Sb, As, Ba, Be, Cd, Ca, Cr, Co, Cu, Fe, Pb, Mg, Mn, Hg, Ni, K, Se, Ag, Na, Tl, Ti, U, V, Zn **Anions:** Br, Cl, F, SO_4, NO_3 **Other Inorganic Chemicals:** Cyanide **Radionuclides:** ^{3}H, ^{90}Sr, ^{137}Cs, ^{241}Am, ^{234}U, ^{235}U, ^{238}U, ^{238}Pu, $^{239,240}Pu$, gamma spectroscopy, gross alpha, gross beta, gross gamma VOCs and SVOCs collected only at depths of 33 and 43 ft, and where PID detects occur	Same as field implementation plan.
Laboratory hydraulic tests	Bulk density, dry density, Kd, porosity, mineralogy, moisture content, moisture potential, saturated hydraulic conductivity	Hydraulic properties will be determined on 5 samples and will typically include moisture content, porosity, particle density, bulk density, saturated hydraulic conductivity, and water-retention characteristics.	The following hydraulic properties will be determined in each of the major stratigraphic units: particle size (sedimentary units), moisture content, matric potential, porosity, particle density, bulk density, saturated hydraulic conductivity, and water retention characteristics.	A total of 120 samples were analyzed for moisture content, 114 for matric potential, 1 for saturated hydraulic conductivity, and 1 for the full suite of unsaturated hydraulic properties. Additional core is preserved for possible future testing.
Geology		Approximately 10 samples of core or cuttings will be collected for mineralogy, petrography, and rock chemistry.	Approximately 10 samples of core or cuttings will be selected by the geology task leader for mineralogy, petrography, and rock chemistry.	Samples were characterized for mineralogy (16), petrography (15), and rock chemistry (17).

Table 10.0-1 (continued)

	Work Plan for Los Alamos Canyon and Pueblo Canyon	Hydrogeologic Workplan and Core Document for Canyons Investigations	R-9 Field Implementation Plan	R-9 Actual Work
Geophysics	Natural gamma, neutron moisture, and density logs may be collected.	In general, open-hole geophysics includes caliper, electromagnetic induction, natural gamma, magnetic susceptibility, borehole color videotape, fluid temperature (saturated), fluid resistivity (saturated), single-point resistivity (saturated), and spontaneous potential (saturated). In general, cased-hole geophysics includes gamma-gamma density, natural gamma, and thermal neutron.	In stable, open-borehole environments, geophysics measurements will include caliper, electromagnetic induction, natural gamma, magnetic susceptibility, color camera, borehole digital camera, gamma-gamma, and thermal/epithermal neutron logs. In the cased borehole, geophysics measurements will include gamma-gamma density, natural gamma, and thermal neutron logs.	Same as field implementation plan
Water-level measurements			Water levels will be determined for each saturated zone by water-level meter or by pressure transducer.	Water levels were determined for each saturated zone by water-level meter or by pressure transducer.
Field hydraulic tests			Slug tests planned for all zones of saturation encountered.	Slug tests were not appropriate for the perched zones as they possibly spanned confined and unconfined conditions. Injection and pumping tests were conducted for the regional zone of saturation but neither sufficiently stressed the aquifer.
Air permeability/ borehole anemometry		Conducted in Bandelier Tuff at 10-ft intervals after removing the hollow-stem auger and/or Odex/Stratex casing	In unsaturated environments, borehole anemometry and straddle packer air-permeability measurements will be made in stable, open-borehole environments at locations determined in the field.	Air permeability was measured in two borehole regions in the Cerros del Rio basalt. Four measurements were made in the upper region, and three measurements were made in the lower region.
Surface casing		Approximately 20-in. O.D.; extends from land surface to 10-ft depth in underlying competent layer and grouted in place	10-in.-diameter low carbon steel casing set to a minimum depth of 20 ft with a 3-ft stickup	16-in. surface casing extends from surface to 7.5-ft depth.
Minimum well casing size	4 in.	6-5/8-in. O.D.	5-in. I.D.	5.56 in. O.D.

Table 10.0-1 (continued)

	Work Plan for Los Alamos Canyon and Pueblo Canyon	Hydrogeologic Workplan and Core Document for Canyons Investigations	R-9 Field Implementation Plan	R-9 Actual Work
Well screen	10-ft stainless steel with top at top of SWL	Machine-slotted (0.01-in.) stainless-steel screen(s) with flush-jointed threads; number and length of screens to be determined on a site-specific basis and proposed to NMED	60 ft of prepacked, 6.68-in.-diameter, machine-slotted (0.01-in.) stainless-steel screen with flush-jointed threads 5 ft of the screen to extend above SWL; screen specifications based on well life expectancy of 50 yr and on discussions with NMED	65 ft of wire-wrapped 304 stainless-steel screen, 0.01-in. slots
Filter material		>90% silica sand, properly sized for the 0.010-in. slot size of the well screen; extends 2 ft above and below the well screen	>98% silica sand, properly sized for the 0.010-in. slot size of the well screen; extends 2 ft above and below the well screen	>98% 20/40 silica sand from 7.5 ft above the screen to the bottom of the screen
Conductor casing		Carbon-steel casing from land surface to top of stainless-steel casing	Carbon-steel casing 5.56 in. in diameter extending from land surface to dielectric coupling at top of stainless-steel casing; 10 ft of 5.56-in.-diameter stainless-steel casing below dielectric coupling	Carbon-steel casing from land surface to top of stainless-steel casing
Backfill materials (exclusive of filter materials)		Uncontaminated drill cuttings below sump and bentonite above sump	Bentonite in borehole below well; fine sand in transition zone 10 ft above and 3 ft below filter pack; bentonite above transition zone to bottom of surface casing; cement grout between surface casing and borehole wall and between surface casing and well casing	Bentonite and coarse sand in borehole below well screen; fine sand in transition zone above filter pack; bentonite above transition; cement grout between surface and abandoned well casings and borehole wall and between surface casing and well casing
Sump		Stainless-steel casing	5.56-in.-diameter stainless-steel casing 10 ft long	5.56-in.-diameter stainless-steel casing 10 ft long
Bottom seal		Bentonite	Bentonite	Bentonite

Other modifications to R-9 were relatively minor. In some cases, molybdenum, uranium-236, and nitrogen-15/nitrogen-14 were added to the analytical suite for water samples because of groundwater issues that were identified during the drilling program. Also, the percentage of core collected was increased from 10% as planned in the "Hydrogeologic Workplan" and the core document to 34.4% that was actually collected. The additional core was needed to adequately characterize the geologic conditions and perched zones encountered during drilling.

11.0 SUMMARY OF SIGNIFICANT RESULTS

In descending order, geologic units penetrated in R-9 included alluvium, basaltic rocks of the Cerros del Rio volcanic field, old alluvium, the Puye Formation, and basaltic rocks of the Santa Fe Group. The following geologic conditions were unexpected.

- Overall, the Puye Formation was found to be finer grained than expected based on lithologic logs of existing wells in the area. The upper Puye Formation consists primarily of siltstone and sandstone.
- The lower part of the Puye Formation is composed of a thick sequence of diagenetically altered, reworked tuffaceous sandstone and conglomerate. Pervasive diagenesis of the tuffaceous sedimentary deposits resulted from the alteration of volcanic glass to clay minerals. Similar "tuffs" were assigned to the top of the Santa Fe Group in well PM-1, but the dacitic nature of these deposits indicates they are part of the Puye Formation.
- The axial facies of the Puye Formation (Totavi Lentil) was expected in R-9 based on lithologic logs of existing wells in the area; however, these deposits were not present.
- The top of the Santa Fe Group in R-9 is represented by a basalt flow with a minimum eruption age of 8.45 to 8.63 Ma. This basalt may correlate with basalts in the upper part of the Santa Fe Group penetrated by wells Otowi-4 and PM-1.

Four saturated zones were encountered during R-9 drilling operations. Three of the four saturated zones are believed to be perched groundwater zones, and the fourth is believed to be associated with the regional aquifer.

The upper perched zone occurs in the middle of basaltic rocks of the Cerros del Rio volcanic field. After the water was encountered at 180 ft, it rose quickly in the borehole before it stabilized at a depth of 137 ft. Fractures probably provide the permeability in this perched zone. This groundwater body is perched on massive basalt. Groundwater from this zone has a sodium-calcium-chloride-bicarbonate ionic composition with a pH value of 8.30. This zone is characterized by above-background activities/concentrations of tritium (347 pCi/L) and chloride (29.2 ppm).

The second perched zone occurs at the base of the Cerros del Rio basalt. A clay-rich basaltic breccia provides permeability, and the perching layer is a fine-grained basaltic tephra. Groundwater in this zone is characterized by a sodium-sulfate-bicarbonate ionic composition with a pH value of 8.79. This zone, which is approximately 7 ft thick, is characterized by 106 pCi/L tritium and 48.4 ppb dissolved uranium. The lower zone in the Cerros del Rio basalt has a higher TDS content (330 ppm) than the upper zone (200 ppm), possibly reflecting a longer groundwater residence time. In addition to tritium and possibly dissolved uranium, other possible anthropogenic constituents include chloride, nitrate, and oxalate.

A third saturated zone with three thin intervals of permeability was encountered in the Puye Formation. These transmissive intervals are intercalated in clay-rich tuffaceous sedimentary deposits. They are

hydraulically connected, with a head of 524 ft. Groundwater within the Puye Formation varies from calcium-sodium-bicarbonate to sodium-chloride-bicarbonate compositions. Tritium concentrations in groundwater of the Puye Formation range from 2.71 to 30.3 pCi/L. Concentrations of chloride, nitrate, and oxalate appear to be elevated relative to background values in all three intervals.

The deepest groundwater system was encountered at a depth of 688 ft near the top of basalt in the Santa Fe Group. This deep system is unconfined, and it is almost certainly associated with the regional aquifer. The depth of the regional water table is 29 to 85 ft lower than what was predicted based on water levels in nearby water supply wells and water-level maps for the regional aquifer. Groundwater from this zone is characterized by a calcium-sodium-bicarbonate ionic composition with a TDS content of 275 ppm. This groundwater is chemically similar to regional aquifer water in wells PM-1 and PM-3; it has a tritium concentration of 14.43 pCi/L.

12.0 ACKNOWLEDGMENTS

Tonto Environmental Drilling Company provided drilling services under the direction of John Eddy, the drilling supervisor. The drilling crew consisted of Larry Thoren, Casy Howe, Gray Rich, Frank Hight, Kelly Dixon, and Glenn Woodward.

Darril Stafford and Ray Wright were the site safety officers and the radiological control technicians for drilling activities. Trung Nguyen provided Laboratory oversight for health and safety; Marty Peifer provided Laboratory oversight for radiological controls.

Steve Bolivar, Joe Skalski, and Willanne Winchester provided contract oversight for drilling activities, field support, sample management and curation, and analytical support. Felicia Aguilar, Candi Chroninger, and Robert Trujillo provided data management support. Jenny Harris and Andy Adams supported water sampling activities.

Dale Counce was the analyst for water chemistry analyses used for screening groundwaters collected from saturated zones. Emily Kluk was the analyst for x-ray fluorescence of rock samples and for moisture and matric-potential determinations. Margaret Snow performed some of the moisture and matric-potential determinations. Steve Chipera was the analyst for x-ray diffraction of core and cuttings. Andy Adams prepared thin sections.

The Groundwater Integration Team, led by Charles Nylander, participated in the planning and evaluation of data collected during this investigation. Steve McLin provided equipment and field support for water-level measurements.

Bruce Gallaher and Lars Soholt provided technical reviews of this document.

COLOG, Inc., provided borehole geophysics services. Joe Beveridge helped to reduce the geophysical data.

Bonnie Koch and Gene Turner provided DOE oversight during the investigation. They were assisted by Bob Enz.

John Young of NMED provided regulatory oversight during drilling operations. Michael Dale and Chris Hanlon-Meyer from NMED's DOE Oversight Bureau collected sample splits from groundwater zones and acted as liaisons with the regulators.

The geodetic survey was performed by Bill Kopp of ESH-19.

Maureen Oakes and Jan Torline served as editors for this report, Christy Fläming was the illustrator, and Pam Maestas was the compositor.

Allyn Pratt supported all phases of this investigation as leader of the Canyons Focus Area. Deba Daymon supported the completion of this activity as leader of the Groundwater Investigations Focus Area.

13.0 REFERENCES

Adams, A. I., F. Goff, and D. Counce, February 1995. "Chemical and Isotopic Variations of Precipitation in the Los Alamos Region, New Mexico," Los Alamos National Laboratory Report LA-12895-MS, Los Alamos, New Mexico. (Adams et al. 1995, 47192)

Allison, J. D., D. S. Brown, and K. J. Novo-Gradac, March 1991. "MINTEQA2/PRODEFA2, A Geochemical Assessment Model for Environmental Systems: Version 3.0 User's Manual," EPA/600/3-91/021, Office of Research and Development, Athens, Georgia. (Allison et al. 1991, 49930)

Blake, W. D., F. Goff, A. I. Adams, and D. Counce, May 1995. "Environmental Geochemistry for Surface and Subsurface Waters in the Pajarito Plateau and Outlying Areas, New Mexico," Los Alamos National Laboratory Report LA-12912-MS, Los Alamos, New Mexico. (Blake et al. 1995, 49931)

Brookins, D. G., 1984. *Geochemical Aspects of Radioactive Waste Disposal,* Springer-Verlag, New York, New York. (Brookins 1984, 12453)

Broxton, D. E., and S. L. Reneau, August 1995. "Stratigraphic Nomenclature of the Bandelier Tuff for the Environmental Restoration Project at Los Alamos National Laboratory," Los Alamos National Laboratory Report LA-13010-MS, Los Alamos, New Mexico. (Broxton and Reneau 1995, 49726)

Broxton, D. E., G. H. Heiken, S. J. Chipera, and F. M. Byers, Jr., June 1995. "Stratigraphy, Petrography, and Mineralogy of Bandelier Tuff and Cerro Toledo Deposits," in Earth Science Investigation for Environmental Restoration—Los Alamos National Laboratory Technical Area 21, Los Alamos National Laboratory Report LA-12934-MS, Los Alamos, New Mexico, pp. 33–63. (Broxton et al. 1995, 50121)

Cooper, J. B., W. D. Purtymun, and E. C. John, July 1965. "Records of water-supply wells Guaje Canyon 6, Pajarito Mesa 1, and Pajarito Mesa 2, Los Alamos, New Mexico, Basic Data Report," US Geological Survey, Albuquerque, New Mexico. (Cooper et al. 1965, 8582)

Dethier, D. P., 1997. "Geology of the White Rock Quadrangle, Santa Fe and Los Alamos Counties, New Mexico," New Mexico Bureau of Mines and Mineral Resources, Geological Map 73, Socorro, New Mexico. (Dethier 1997, 49843)

Duff, M. C., D. B. Hunter, I. R. Triay, P. M. Bertsch, D. T. Reed, S. R. Sutton, G. Shea-McCarthy, J. Kitten, P. Eng, S. J. Chipera, and D. T. Vaniman, 1999. "Mineral Associations and Average Oxidation States of Sorbed Pu on Tuff," *Environmental Science and Technology*, Volume 33, Number 13, pp. 2163–2169. (Duff et al. 1999, 65654)

Environmental Protection Group, December 1990. "Environmental Surveillance at Los Alamos During 1989," Los Alamos National Laboratory Report LA-12000-ENV, Los Alamos, New Mexico. (Environmental Protection Group 1990, 6995)

Environmental Protection Group, March 1992. "Environmental Surveillance at Los Alamos During 1990," Los Alamos National Laboratory Report LA-12271-MS, Los Alamos, New Mexico. (Environmental Protection Group 1992, 7004)

Environmental Protection Group, August 1993. "Environmental Surveillance at Los Alamos During 1991," Los Alamos National Laboratory Report LA-12572-ENV, Los Alamos, New Mexico. (Environmental Protection Group 1993, 23249)

Environmental Protection Group, July 1994. "Environmental Surveillance at Los Alamos during 1992," Los Alamos National Laboratory Report LA-12764-ENV, Los Alamos, New Mexico. (Environmental Protection Group 1994, 45363)

Environmental Protection Group, October 1995. "Environmental Surveillance at Los Alamos during 1993," Los Alamos National Laboratory Report LA-12973-ENV, Los Alamos, New Mexico. (Environmental Protection Group 1995, 50285)

Environmental Protection Group, July 1996. "Environmental Surveillance at Los Alamos during 1994," Los Alamos National Laboratory Report LA-13047-ENV, Los Alamos, New Mexico. (Environmental Protection Group 1996, 54769)

Environmental Surveillance and Compliance Programs, September 1997. "Environmental Surveillance and Compliance at Los Alamos during 1996," Los Alamos National Laboratory Report LA-13343-ENV, Los Alamos, New Mexico. (Environmental Surveillance and Compliance Programs 1997, 56684)

Environmental Surveillance Program, 1996. "Environmental Surveillance at Los Alamos during 1995," Los Alamos National Laboratory Report LA-13210-ENV, Los Alamos, New Mexico. (Environmental Surveillance Program 1996, 55333)

EPA (US Environmental Protection Agency), May 1987. "Test Methods for Evaluating Solid Waste, Laboratory Manual, Physical/Chemical Methods," SW-846, Third Edition, Update III, Washington, DC. (EPA 1997, 57589)

Gee, G. W., M. D. Campbell, G. S. Campbell, and J. H. Campbell, 1992. "Rapid Measurement of Low Soil Water Potentials Using a Water Activity Meter," in *Soil Science Society of America Journal*, Vol. 56, pp. 1068–1070. (Gee et al. 1992, 58717)

Griggs, R. L., 1964. "Geology and Ground-Water Resources of the Los Alamos Area New Mexico," with a section on Quality of Water by John D. Hem, US Geological Survey Water-Supply Paper 1753, Washington, DC. (Griggs 1964, 8795)

Keller, C., D. Engstrom, and F. West, November 1973. "In Situ Permeability Measurements for the Event in U1-C," Los Alamos Scientific Laboratory Report LA-5425-MS, Los Alamos, New Mexico. (Keller et al. 1973, 59119)

Langmuir, D., 1997. *Aqueous Environmental Geochemistry,* Prentice-Hall, Inc., Upper Saddle River, New Jersey. (Langmuir 1997, 56037)

LANL (Los Alamos National Laboratory), May 1981. "Formerly Utilized MED/AEC Sites Remedial Action Program, Radiological Survey of the Site of a Former Radioactive Liquid Waste Treatment Plant (TA-45) and Effluent-Receiving Areas of Acid, Pueblo, and Los Alamos Canyons, Los Alamos, New Mexico," Los Alamos National Laboratory Report LA-8890-ENV (DOE/EV-0005/30), Los Alamos, New Mexico. (LANL 1981, 6059)

LANL (Los Alamos National Laboratory), October 25, 1995. “Groundwater Protection Management Program Plan” (draft), Revision 2.0, Los Alamos, New Mexico. (LANL 1995, 50124)

LANL (Los Alamos National Laboratory), November 1995. “Task/Site Work Plan for Operable Unit 1049: Los Alamos Canyon and Pueblo Canyon,” Los Alamos National Laboratory Report LA-UR-95-2053, Los Alamos, New Mexico. (LANL 1995, 50290)

LANL (Los Alamos National Laboratory), February 13, 1996. “Decontamination Water Discharge Procedure: Containerized Decon Water,” ESH-18 Policy, Revision 1, Los Alamos, New Mexico. (LANL 1996, 58716)

LANL (Los Alamos National Laboratory), April 1997. “Core Document for Canyons Investigations,” Los Alamos National Laboratory Report LA-UR-96-2083, Los Alamos, New Mexico. (LANL 1997, 55622)

LANL (Los Alamos National Laboratory), September 1997. “Field Implementation Plan for the Drilling and Testing of LANL Regional Characterization Well R-9,” Revision 2, Los Alamos, New Mexico. (LANL 1997, 59163)

LANL (Los Alamos National Laboratory), May 22, 1998. “Hydrogeologic Workplan”, Revision 1.0, Los Alamos, New Mexico. (LANL 1998, 59599)

LANL (Los Alamos National Laboratory), September 1998. “Evaluation of Sediment Contamination in Upper Los Alamos Canyon Reaches LA-1, LA-2, and LA-3,” Los Alamos National Laboratory Report LA-UR-98-3974, Los Alamos, New Mexico. (LANL 1998, ER ID 59160)

Longmire, P. A., S. Kung, J. M. Boak, A. I. Adams, F. Caporuscio, and R. N. Gray, 1996. “Aqueous Geochemistry of Upper Los Alamos Canyon, Los Alamos, New Mexico,” in *New Mexico Geological Society Guidebook*, 47th Field Conference, Jemez Mountains Region, New Mexico, pp. 473–480. (Longmire et al. 1996, 54168)

Lowry, W. E., and S. M. Narbutovskih, 1991. “High Resolution Gas Permeability Measurements with the SEAMIST System,” in *Proceedings of the Fifth National Outdoor Action Conference in Aquifer Restoration, Ground Water Monitoring, and Geophysical Methods*, Las Vegas, Nevada, pp. 685–698. (Lowry and Narbutovskih 1991, 59120)

McDowell, F. D., May 22, 1987. "K - Ar Results, Nevada Test Site," unpublished data. (McDowell 1987, 65418)

Newman, B. D., December 9, 1996. “Vadose Zone Water Movement at Area G, Los Alamos National Laboratory, TA-54: Interpretations Based on Chloride and Stable Isotope Profiles,” Los Alamos National Laboratory Report LA-UR-96-4682, Los Alamos, New Mexico. (Newman 1996, 59118)

Purtymun, W. D., January 1984. “Hydrologic Characteristics of the Main Aquifer in the Los Alamos Area: Development of Ground Water Supplies,” Los Alamos National Laboratory Report LA-9957-MS, Los Alamos, New Mexico. (Purtymun 1984, 6513)

Purtymun, W. D., S. G. McLin, A. K. Stoker, M. N. Maes, and B. G. Hammock, 1993. “Water Supply at Los Alamos During 1990,” Los Alamos National Laboratory Progress Report LA-12471-PR, Los Alamos, New Mexico. (Purtymun et al. 1993, 15371)

Rogers, D. B., A. K. Stoker, S. G. McLin, and B. M. Gallaher, 1996. "Recharge to the Pajarito Plateau Regional Aquifer System," Los Alamos National Laboratory Report LA-UR-96-486 in *New Mexico Geological Society Guidebook,* 47th Field Conference, Jemez Mountains Region, New Mexico, pp. 407–412. (Rogers et al. 1996, 54714)

Stoker, A. K., S. G. McLin, W. D. Purtymun, M. N. Maes, and B. G. Hammock, May 1992. "Water Supply at Los Alamos During 1989," Los Alamos National Laboratory Progress Report LA-12276-PR, Los Alamos, New Mexico. (Stoker et al. 1992, 58718)

Stone, W. J., August 2000. "Laboratory-Derived Hydraulic Properties of Selected Materials from Wells R-9, R-12, and R-25," Los Alamos National Laboratory Report LA-UR-00-3587, Los Alamos, New Mexico. (Stone 2000, 66781)

van Genuchten, M. Th., F. J. Leij, and S. R. Yates, December 1991. "The RETC Code for Quantifying the Hydraulic Functions of Unsaturated Soils," EPA/600/2-91/065, prepared by the US Salinity Laboratory, US Department of Agriculture, Agricultural Research Service, Riverside, California. (van Genuchten et al. 1991, 65419)

Vaniman, D., S. Chipera, and D. Bish, 1999. "Sources of Fe in eolian and soil detritus at Exile Hill, Nevada, USA," *in* "Clays for Our Future," H. Kodama, A. R. Mermut, and J. K. Torrance, Eds., *Proceedings of the 11th International Clay Conference*, 1997, Ottawa, Canada, pp. 661–670. (Vaniman et al. 1999, 65655)

Waresback, D. B., August 1986. "The Puye Formation, New Mexico: Analysis of a Continental, Rift-Filling, Volcaniclastic Alluvial-Fan Sequence," Master of Science in Geology thesis, The University of Texas, Arlington, Texas. (Waresback 1986, 58715)

Warren, R. G., E. V. McDonald, and R. T. Ryti, 1997. "Baseline Geochemistry of Soil and Bedrock Tshirege Member of the Bandelier Tuff at MDA-P," Los Alamos National Laboratory Report LA-13330-MS, Los Alamos, New Mexico. (Warren et al. 1997, 59180)

WoldeGabriel, G., June 22, 1998. "Ar/Ar Results of R9 basalts," personal communication from Giday WoldeGabriel (EES-1) to David E. Broxton (EES-1), Los Alamos National Laboratory, Los Alamos, New Mexico. (WoldeGabriel 1998, 58705)

WoldeGabriel, G., A. W. Laughlin, D. P. Dethier, and M. Heizler, 1996. "Temporal and Geochemical Trends of Lavas in White Rock Canyon and the Pajarito Plateau, Jemez Volcanic Field, New Mexico, USA," *New Mexico Geological Society Guidebook*, 47th Field Conference, p. 251–261. (WoldeGabriel et al. 1997, 54427)

Appendix A

Lithologic Log

This appendix contains the lithologic log prepared for characterization well R-9. With minor variations and additions, the log follows the format specified in the Los Alamos National Laboratory Environmental Restoration Project standard operating procedure LANL-ER-SOP-12.01, R2, "Field Logging, Handling, and Documentation of Borehole Samples," Attachment E, "Core Sample Log." The log depicts cored intervals and recovery; noncored intervals of cuttings production; locations and identity numbers of contract laboratory samples; locations, identity numbers, and type of samples for hydrologic testing; curation of borehole materials; lithologic interpretations; and interim well construction. All borehole materials (i.e., core, cuttings, and chips), except samples removed for analysis, are stored at the Laboratory's field support facility in accordance with LANL-ER-SOP-12.01, R2.

The column for field analytical sample number shows the intervals of the borehole material sampled for contract laboratory analysis and the associated sample identity number. The column for hydraulic property samples indicates samples collected for moisture and matric potential analysis and/or samples that were protected from moisture loss for subsequent hydraulic property and isotope analysis.

The legend on the following page shows abbreviations and symbols that were used in the log.

Lithologic Log Legend

Abbreviations and explanations

Bearing = direction of angled borehole

crse. = course

Orientation = borehole angle from horizontal

devit. = devitrified

dk. = dark

dkr. = darker

FeOx = iron oxidation

Fm = formation

lt. = light

mass. = massive

med. = medium

Mn02 = manganese oxide

mod. = moderate

modly. = moderately

ol. = olivine

plag. = plagioclase

PWZ = perched water zone

SAA = same as above

sat. = saturated

sltly. = slightly

strgly. = strongly

TD = total depth

w/ = with

wk. = weak

wkly. = weakly

Lithologic Symbols

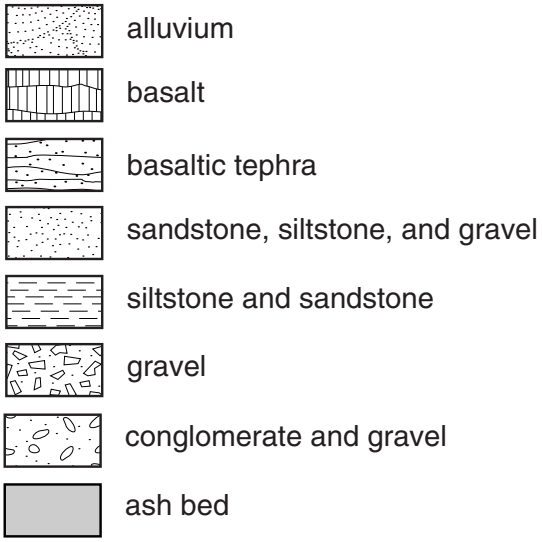

LOS ALAMOS NATIONAL LABORATORY
REGIONAL HYDROGEOLOGIC CHARACTERIZATION PROJECT
ENVIRONMENTAL RESTORATION, CANYONS FOCUS AREA
BOREHOLE LOG

BOREHOLE ID: R-9 TA/ OU: LA Canyon Aggregate: 1 Page: 1 of: 7

Drilling Co.: Tonto Environmental Drilling Inc. Core Box # (s) 29 Core 24 Cuttings Start Date: 9/25/97 Time: 0906 End Date: 10/18/99 Time: 1235

Drilling Equip./Method: Ingersoll-Rand T-4/ODEX casing/air core with total dust suppression Sampling Method: Wireline core barrel sampling

Driller: Larry Thoren Geologist: Jon Marin, Rick Warren Orientation: Vertical Bearing: NA TD: 771.0 ft

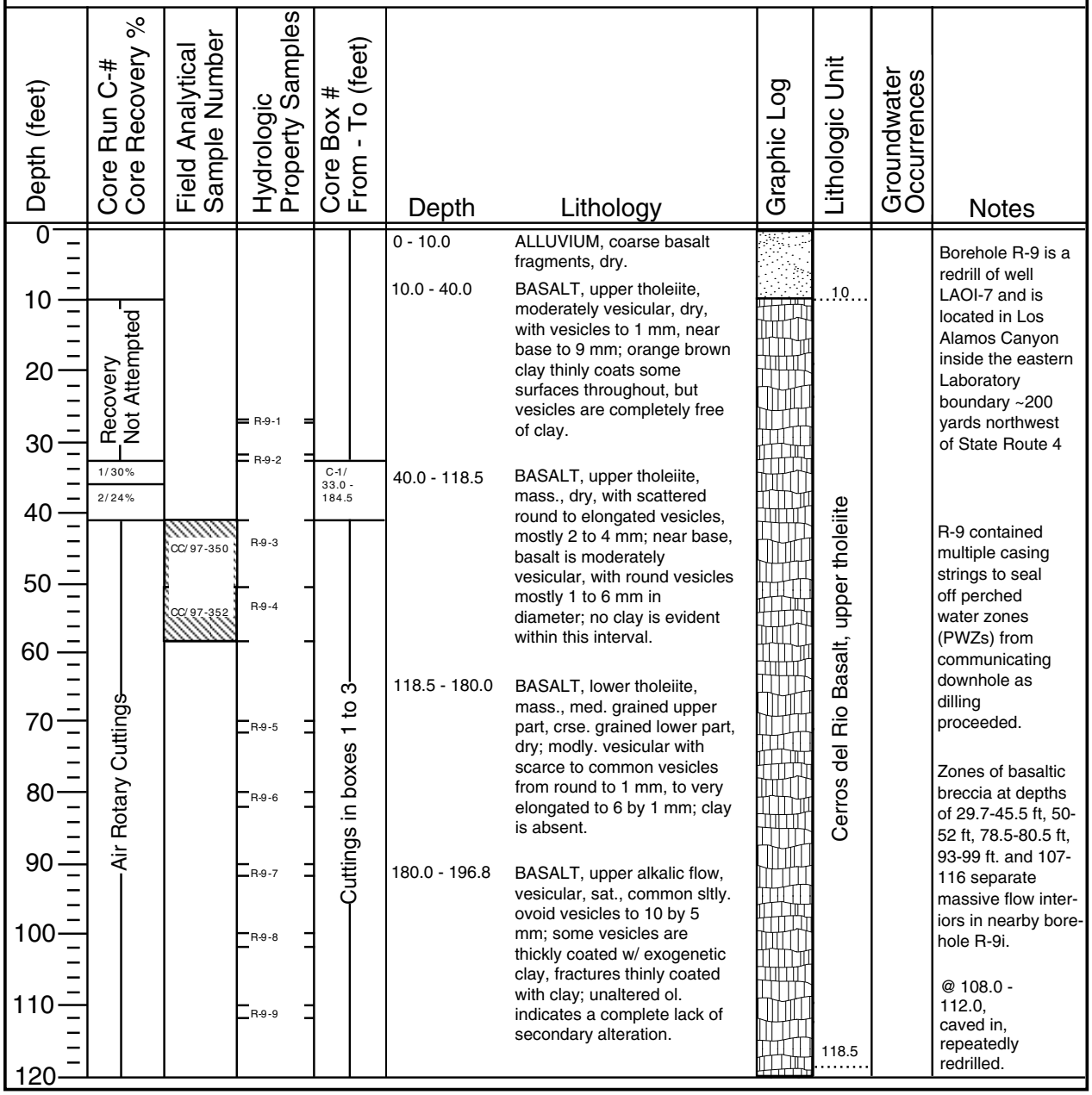

Depth	Lithology
0 - 10.0	ALLUVIUM, coarse basalt fragments, dry.
10.0 - 40.0	BASALT, upper tholeiite, moderately vesicular, dry, with vesicles to 1 mm, near base to 9 mm; orange brown clay thinly coats some surfaces throughout, but vesicles are completely free of clay.
40.0 - 118.5	BASALT, upper tholeiite, mass., dry, with scattered round to elongated vesicles, mostly 2 to 4 mm; near base, basalt is moderately vesicular, with round vesicles mostly 1 to 6 mm in diameter; no clay is evident within this interval.
118.5 - 180.0	BASALT, lower tholeiite, mass., med. grained upper part, crse. grained lower part, dry; modly. vesicular with scarce to common vesicles from round to 1 mm, to very elongated to 6 by 1 mm; clay is absent.
180.0 - 196.8	BASALT, upper alkalic flow, vesicular, sat., common sltly. ovoid vesicles to 10 by 5 mm; some vesicles are thickly coated w/ exogenetic clay, fractures thinly coated with clay; unaltered ol. indicates a complete lack of secondary alteration.

Notes

Borehole R-9 is a redrill of well LAOI-7 and is located in Los Alamos Canyon inside the eastern Laboratory boundary ~200 yards northwest of State Route 4

R-9 contained multiple casing strings to seal off perched water zones (PWZs) from communicating downhole as dilling proceeded.

Zones of basaltic breccia at depths of 29.7-45.5 ft, 50-52 ft, 78.5-80.5 ft, 93-99 ft. and 107-116 separate massive flow interiors in nearby borehole R-9i.

@ 108.0 - 112.0, caved in, repeatedly redrilled.

LOS ALAMOS NATIONAL LABORATORY
REGIONAL HYDROGEOLOGIC CHARACTERIZATION PROJECT
ENVIRONMENTAL RESTORATION, CANYONS FOCUS AREA
BOREHOLE LOG

BOREHOLE ID: R-9 TA/ OU LA Canyon Aggregate: 1 Page: 2 of: 7

Drilling Co.: Tonto Environmental Drilling Inc. Core Box # (s) 29 Core 24 Cuttings Start Date: 9/25/97 Time: 0906 End Date: 10/18/99 Time: 1235

Drilling Equip./Method: Ingersoll-Rand T-4/ODEX casing/air core with total dust suppression Sampling Method: Wireline core barrel sampling

Driller: Larry Thoren Geologist: Jon Marin, Rick Warren Orientation: Vertical Bearing: NA TD: 771.0 ft

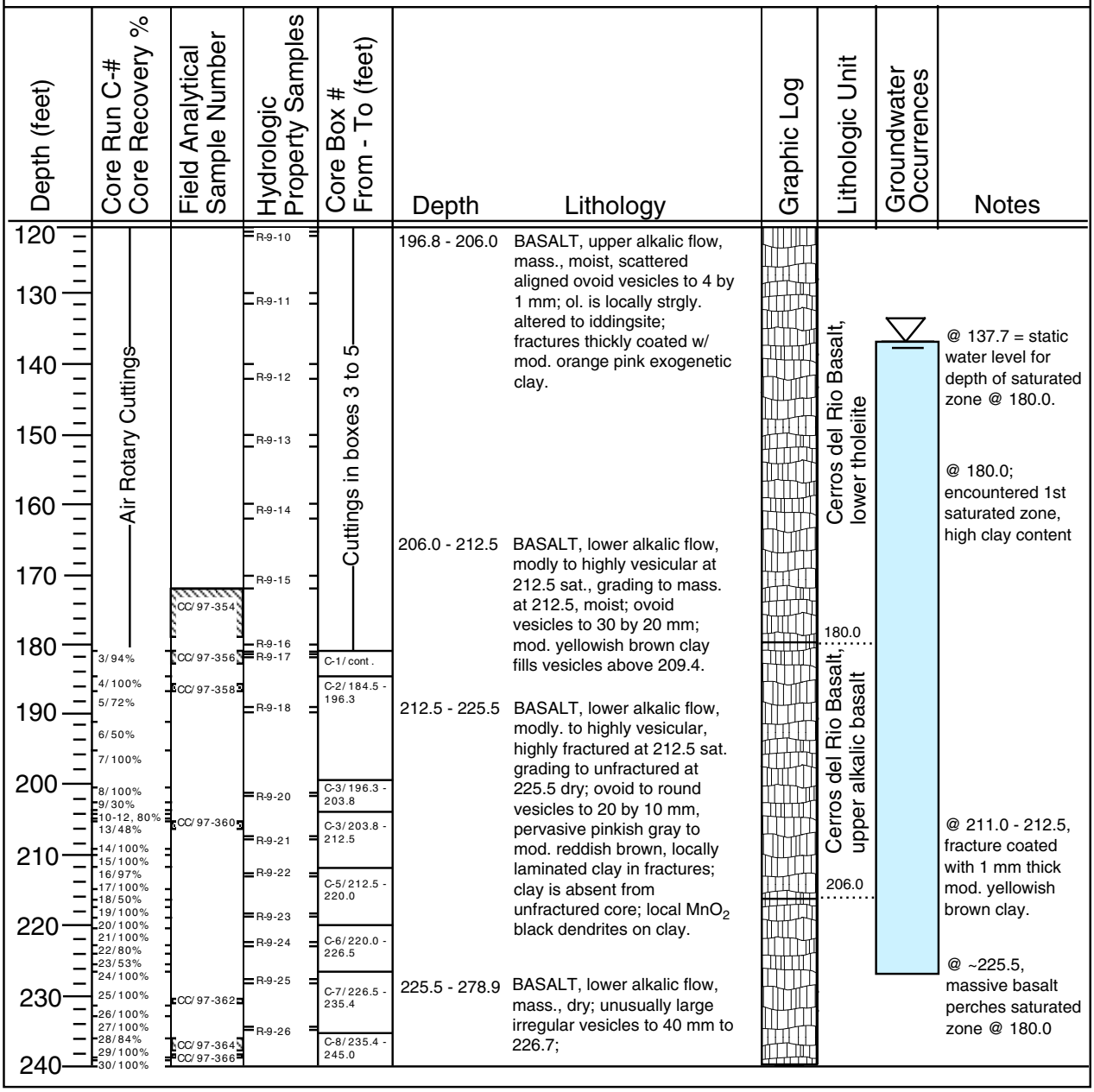

Depth	Lithology
196.8 - 206.0	BASALT, upper alkalic flow, mass., moist, scattered aligned ovoid vesicles to 4 by 1 mm; ol. is locally strgly. altered to iddingsite; fractures thickly coated w/ mod. orange pink exogenetic clay.
206.0 - 212.5	BASALT, lower alkalic flow, modly to highly vesicular at 212.5 sat., grading to mass. at 212.5, moist; ovoid vesicles to 30 by 20 mm; mod. yellowish brown clay fills vesicles above 209.4.
212.5 - 225.5	BASALT, lower alkalic flow, modly. to highly vesicular, highly fractured at 212.5 sat. grading to unfractured at 225.5 dry; ovoid to round vesicles to 20 by 10 mm, pervasive pinkish gray to mod. reddish brown, locally laminated clay in fractures; clay is absent from unfractured core; local MnO_2 black dendrites on clay.
225.5 - 278.9	BASALT, lower alkalic flow, mass., dry; unusually large irregular vesicles to 40 mm to 226.7;

LOS ALAMOS NATIONAL LABORATORY
REGIONAL HYDROGEOLOGIC CHARACTERIZATION PROJECT
ENVIRONMENTAL RESTORATION, CANYONS FOCUS AREA
BOREHOLE LOG

BOREHOLE ID: R-9 | TA/ OU LA Canyon | Aggregate: 1 | Page: 3 of: 7

Drilling Co.: Tonto Environmental Drilling Inc. | Core Box # (s) 29 Core 24 Cuttings | Start Date: 9/25/97 Time: 0906 | End Date: 10/18/99 Time: 1235

Drilling Equip./Method: Ingersoll-Rand T-4/ODEX casing/air core with total dust suppression | Sampling Method: Wireline core barrel sampling

Driller: Larry Thoren | Geologist: Jon Marin, Rick Warren | Orientation: Vertical | Bearing: NA | TD: 771.0 ft

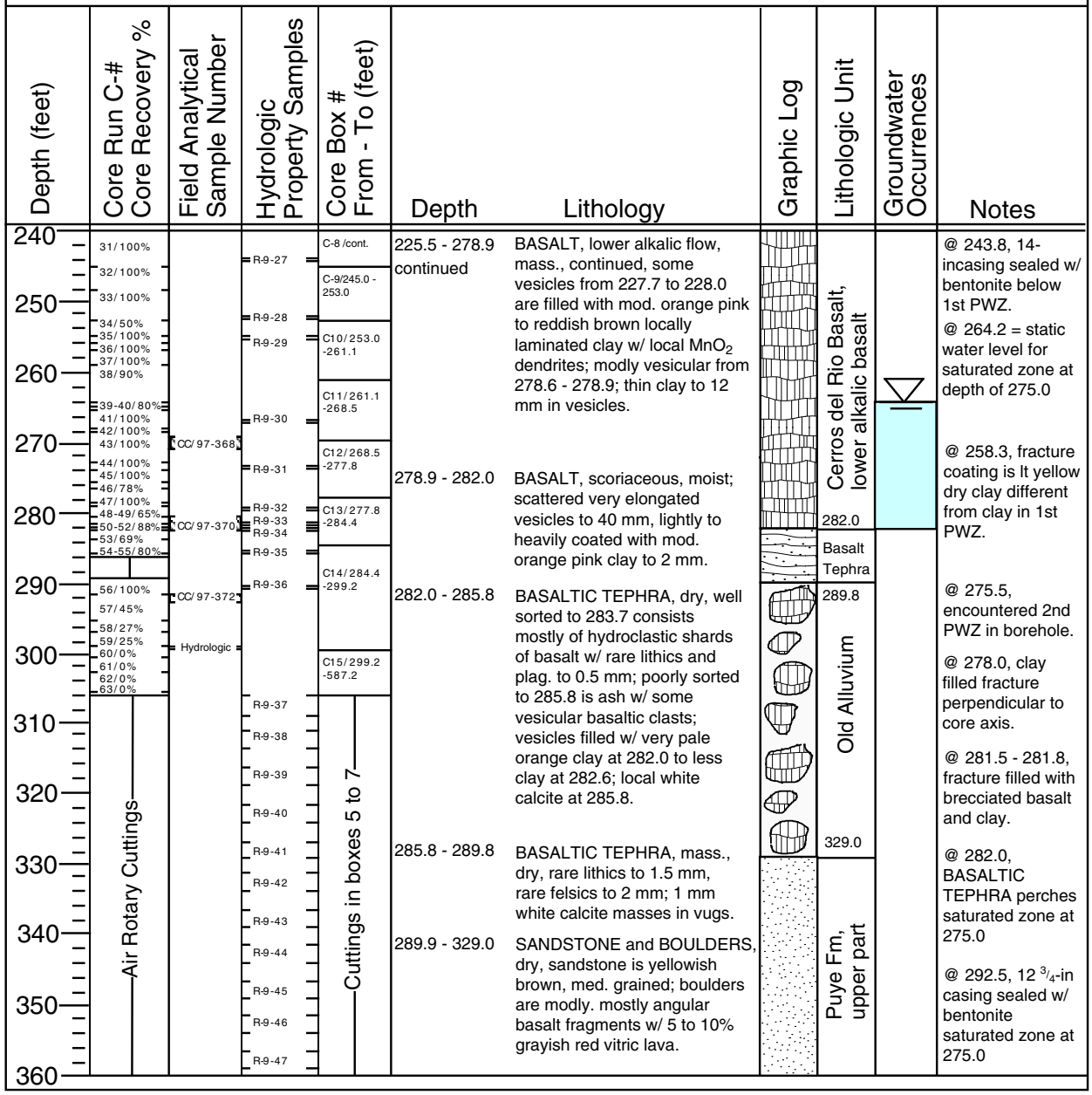

Depth	Lithology
225.5 - 278.9 continued	BASALT, lower alkalic flow, mass., continued, some vesicles from 227.7 to 228.0 are filled with mod. orange pink to reddish brown locally laminated clay w/ local MnO_2 dendrites; modly vesicular from 278.6 - 278.9; thin clay to 12 mm in vesicles.
278.9 - 282.0	BASALT, scoriaceous, moist; scattered very elongated vesicles to 40 mm, lightly to heavily coated with mod. orange pink clay to 2 mm.
282.0 - 285.8	BASALTIC TEPHRA, dry, well sorted to 283.7 consists mostly of hydroclastic shards of basalt w/ rare lithics and plag. to 0.5 mm; poorly sorted to 285.8 is ash w/ some vesicular basaltic clasts; vesicles filled w/ very pale orange clay at 282.0 to less clay at 282.6; local white calcite at 285.8.
285.8 - 289.8	BASALTIC TEPHRA, mass., dry, rare lithics to 1.5 mm, rare felsics to 2 mm; 1 mm white calcite masses in vugs.
289.9 - 329.0	SANDSTONE and BOULDERS, dry, sandstone is yellowish brown, med. grained; boulders are modly. mostly angular basalt fragments w/ 5 to 10% grayish red vitric lava.

Notes

@ 243.8, 14-incasing sealed w/ bentonite below 1st PWZ.

@ 264.2 = static water level for saturated zone at depth of 275.0

@ 258.3, fracture coating is lt yellow dry clay different from clay in 1st PWZ.

@ 275.5, encountered 2nd PWZ in borehole.

@ 278.0, clay filled fracture perpendicular to core axis.

@ 281.5 - 281.8, fracture filled with brecciated basalt and clay.

@ 282.0, BASALTIC TEPHRA perches saturated zone at 275.0

@ 292.5, 12 $^{3}/_{4}$-in casing sealed w/ bentonite saturated zone at 275.0

LOS ALAMOS NATIONAL LABORATORY
REGIONAL HYDROGEOLOGIC CHARACTERIZATION PROJECT
ENVIRONMENTAL RESTORATION, CANYONS FOCUS AREA
BOREHOLE LOG

BOREHOLE ID: R-9 TA/ OU LA Canyon Aggregate: 1 Page: 4 of: 7

Drilling Co.: Tonto Environmental Drilling Inc. Core Box # (s) 29 Core 24 Cuttings Start Date: 9/25/97 Time: 0906 End Date: 10/18/99 Time: 1235

Drilling Equip./Method: Ingersoll-Rand T-4/ODEX casing/air core with total dust suppression Sampling Method: Wireline core barrel sampling

Driller: Larry Thoren Geologist: Jon Marin, Rick Warren Orientation: Vertical Bearing: NA TD: 771.0 ft

Depth (feet)	Core Run C-# Core Recovery %	Field Analytical Sample Number	Hydrologic Property Samples	Core Box # From - To (feet)	Depth	Lithology	Graphic Log	Lithologic Unit	Groundwater Occurrences	Notes
360	Air Rotary Cuttings		R-9-48	Cuttings in boxes 7 to 11	329.0' - 349.0'	SAND, vitric, pebbly, dry.		Puye Fm,upper part		Air rotary cuttings collected while advancing the 10 3/4-in. and 8 5/8 in. casings.
370			R-9-49		349.0' - 365.0'	SAND, vitric, dry, fine-grained at 349', peblly at 365';				
			R-9-50		365.0' - 379.0'	SAND, vitric, fine-grained at 365'; medium-grained to peblly at 379'.				
380			R-9-51							
			R-9-52		379.0' - 399.0'	SAND, vitric, pumiceous, medium-grained; pumice to 1 mm, few to 6 mm, pumice abundant from 384' to 394'.				@ 365.5' - 359.0' and 409' - 414' pebbles are mostly subangular devit. dacitic lava similar to Rendija Canyon rhyodacite.
390			R-9-53							
			R-9-54							
			R-9-55		399.0' - 401.5'	SAND, vitric, fine-grained, w/ some pebbles to 7 mm.				
400			R-9-56		401.5' - 407.7'	GRAVEL, vitric, w/ pebbles from 5 to 10 mm.				
			R-9-57		407.7' - 436.5'	SAND, fine- to coarse-grained, sltly pebbly, vitric, pumiceous; some vitric lava pebbles.				
410			R-9-58							
			R-9-59		436.5' - 469.0'	GRAVEL, some sand, vitric, pumiceous, pebbles 5 to 10 mm; coarsest gravel occurs between 442' to 443', sand occurs from 455' to 458'.				@ 420', advancement of 10 3/4-in. casing halted; no bentonite seal installed.
420			R-9-60							
			R-9-61							
430			R-9-62							
			R-9-63		469.0' - 482.7'	SAND and GRAVEL, medium-grained, sand at 469' grades to gravel at 482.7'; vitric, pumiceous.				
440			R-9-64							
			R-9-65		482.7' - 496.5'	SAND and GRAVEL, medium-grained sand at 482.7' grades to gravel at 496.5'; vitric, pumiceous.				@ 496.5' - 539'; pebbles are subangular lithics of devit. to vitric phenocryst-poor Rendija Canyon rhyodacite.
450			R-9-66							
			R-9-67							
460			R-9-68		496.5' - 539.0'	GRAVEL, dry, vitric, pumiceous; 2 to 5 mm pebbles.				
			R-9-69							
470			R-9-70		539.0' - 544.4'	SANDSTONE, dry, argillic, pumiceous, fine-grained, w/ pebbles to 6 mm.				
480			R-9-71							

LOS ALAMOS NATIONAL LABORATORY
REGIONAL HYDROGEOLOGIC CHARACTERIZATION PROJECT
ENVIRONMENTAL RESTORATION, CANYONS FOCUS AREA
BOREHOLE LOG

BOREHOLE ID: R-9 TA/ OU LA Canyon Aggregate: 1 Page: 5 of: 7

Drilling Co.: Tonto Environmental Drilling Inc. Core Box # (s) 29 Core 24 Cuttings Start Date: 9/25/97 Time: 0906 End Date: 10/18/99 Time: 1235

Drilling Equip./Method: Ingersoll-Rand T-4/ODEX casing/air core with total dust suppression Sampling Method: Wireline core barrel sampling

Driller: Larry Thoren Geologist: Jon Marin, Rick Warren Orientation: Vertical Bearing: NA TD: 771.0 ft

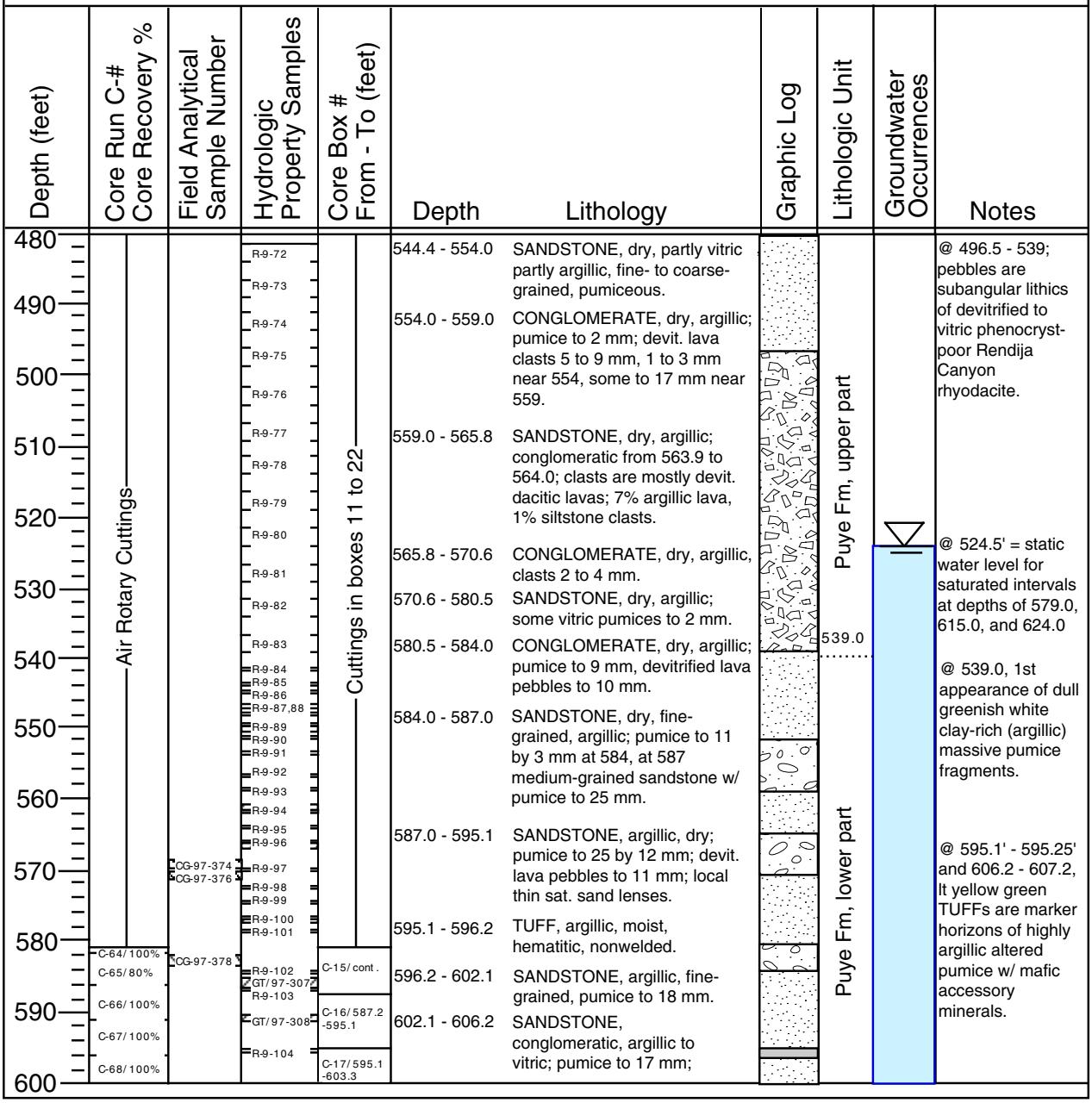

Depth	Lithology
544.4 - 554.0	SANDSTONE, dry, partly vitric partly argillic, fine- to coarse-grained, pumiceous.
554.0 - 559.0	CONGLOMERATE, dry, argillic; pumice to 2 mm; devit. lava clasts 5 to 9 mm, 1 to 3 mm near 554, some to 17 mm near 559.
559.0 - 565.8	SANDSTONE, dry, argillic; conglomeratic from 563.9 to 564.0; clasts are mostly devit. dacitic lavas; 7% argillic lava, 1% siltstone clasts.
565.8 - 570.6	CONGLOMERATE, dry, argillic, clasts 2 to 4 mm.
570.6 - 580.5	SANDSTONE, dry, argillic; some vitric pumices to 2 mm.
580.5 - 584.0	CONGLOMERATE, dry, argillic; pumice to 9 mm, devitrified lava pebbles to 10 mm.
584.0 - 587.0	SANDSTONE, dry, fine-grained, argillic; pumice to 11 by 3 mm at 584, at 587 medium-grained sandstone w/ pumice to 25 mm.
587.0 - 595.1	SANDSTONE, argillic, dry; pumice to 25 by 12 mm; devit. lava pebbles to 11 mm; local thin sat. sand lenses.
595.1 - 596.2	TUFF, argillic, moist, hematitic, nonwelded.
596.2 - 602.1	SANDSTONE, argillic, fine-grained, pumice to 18 mm.
602.1 - 606.2	SANDSTONE, conglomeratic, argillic to vitric; pumice to 17 mm;

Notes:
- @ 496.5 - 539; pebbles are subangular lithics of devitrified to vitric phenocryst-poor Rendija Canyon rhyodacite.
- @ 524.5' = static water level for saturated intervals at depths of 579.0, 615.0, and 624.0
- @ 539.0, 1st appearance of dull greenish white clay-rich (argillic) massive pumice fragments.
- @ 595.1' - 595.25' and 606.2 - 607.2, lt yellow green TUFFs are marker horizons of highly argillic altered pumice w/ mafic accessory minerals.

LOS ALAMOS NATIONAL LABORATORY
REGIONAL HYDROGEOLOGIC CHARACTERIZATION PROJECT
ENVIRONMENTAL RESTORATION, CANYONS FOCUS AREA
BOREHOLE LOG

BOREHOLE ID: R-9 TA/ OU LA Canyon Aggregate: 1 Page: 6 of: 7

Drilling Co.: Tonto Environmental Drilling Inc. Core Box # (s) 29 Core 24 Cuttings Start Date: 9/25/97 Time: 0906 End Date: 10/18/99 Time: 1235

Drilling Equip./Method: Ingersoll-Rand T-4/ODEX casing/air core with total dust suppression Sampling Method: Wireline core barrel sampling

Driller: Larry Thoren Geologist: Jon Marin, Rick Warren Orientation: Vertical Bearing: NA TD: 771.0 ft

Depth (feet)	Core Run C-# Core Recovery %	Field Analytical Sample Number	Hydrologic Property Samples	Core Box # From - To (feet)	Depth	Lithology	Graphic Log	Lithologic Unit	Groundwater Occurrences	Notes
600	C-68/ cont.		GT/ 97-310	C-17/ cont.	602.1 - 606.2	(continued) devit. lava pebbles to 7 mm.		Puye Fm, lower part		@ 606.2 - 607.2, TUFF, marker horizon.
	C-69/ 70%		GT/ 97-311 GT/ 97-312	C-18/ 603.3 -613.8	606.2 - 607.2	TUFF, argillic, non-welded; pumice to 10 by 1 mm.				
610	C-70/ 50%		GT/ 98-005		607.2 - 613.0	SILTSTONE and SANDSTONE, argillic, fine-grained w/ pumice at 611.				@ 607.2 - 612.0, siltstone is paleosol.
	C-71/ 85%			C-19/ 613.8 -626.8	613.0 - 626.8	CONGLOMERATE, argillic, clasts 1 to 8 mm, friable, sltly calcareous, zeolitic; abundant pumice near 626.8.				@ 626.8', base of lowest Puye saturated interval
620	C-72/ 100%		R-9-108 GT/ 98-006							
	C-73/ 50%		GT/ 98-007							
	C-74/ 50%			C-20/ 626.8 -634.5						
	C-75/ 33%		GT/ 98-008 GT/ 98-009							
630	C-76/ 50%									
	C-77/ 100%		GT/ 98-010 GT/ 98-011	C-21/ 634.5 -642.0						
	C-78/ 100%		R-9-109 GT/ 98-012		626.8 - 640.8	SANDSTONE, argillic, pebbly, white pumice to 13 mm.				
	C-79/ 100%									
	C-80/ 90%		GT/ 98-013 R-9-110	C-22/ 642.0 -653.1	640.8 - 652.2	SANDSTONE, argillic, sltly calcareous, zeolitic, fine-grained.				
640	C-81/ 90%									
	C-82/ 140%		GT/ 98-016 R-9-111							
	C-83/ 100%		GT/ 98-017 R-9-112	C-23/ 653.1 661.5	652.2 - 676.3	SANDSTONE, argillic, very friable, sltly zeolitic, pumice to 9 mm, 5/1 flattening ratio.				
650	C-84/ 100%		GT/ 98-018 R-9-113							
	C-85/ 100%		GT/ 98-019 R-9-114 R-9-115	C-24/ 661.5 -668.8						
	C-86/ 94%		GT/ 98-020 R-9-116 R-9-117 GT/ 98-021	C-25/ 668.8 -676.3						
	C-87/ 90%									
660	C-88/ 80%		GT/ 98-022 R-9-118	C-26/ 676.3 -684.5	676.3 - 686.4	SANDSTONE, pumiceous, coarse-grained, modly well sorted, w/ abundant lithics to 2 mm; thin sat. sandstone lenses.				
	C-89/ 60%		R-9-119 GT/ 98-023							
	C-90/ 100%		R-9-120 GT/ 98-024	C-27/ 684.5 -691.7						
	C-91/ 100%		GT/ 98-025 R-9-121		686.4 - 689.0	BASALT, weathered, argillic, calcareous; mass. exogenetic clay and sand in fractures to 12 mm wide.		686.4 Santa Fe Group Basalt		688.0 = static water level regional aquifer
670	C-92/ 80%			C-28/ 691.7 -699.1						
	C-93/ 73%									
	C-94/ 100%									
	C-95/ 53%			C-29/ 699.1 -703.0						
	C-96/ 50%									
680	C-97/ 40%				689.0 - 771.0	BASALT, mass. to vesicular, fine-grained, Miocene age. Weathering and alteration at 722' - 727', 737' - 747'. Saturated.				Well screen = 683 - 748 ft
690										
700										
710										
720										

LOS ALAMOS NATIONAL LABORATORY
REGIONAL HYDROGEOLOGIC CHARACTERIZATION PROJECT
ENVIRONMENTAL RESTORATION, CANYONS FOCUS AREA
BOREHOLE LOG

BOREHOLE ID: R-9 TA/ OU LA Canyon Aggregate: 1 Page: 7 of: 7

Drilling Co.: Tonto Environmental Drilling Inc. Core Box # (s) 29 Core 24 Cuttings Start Date: 9/25/97 Time: 0906 End Date: 10/18/99 Time: 1235

Drilling Equip./Method: Ingersoll-Rand T-4/ODEX casing/air core with total dust suppression Sampling Method: Wireline core barrel sampling

Driller: Larry Thoren Geologist: Jon Marin, Rick Warren Orientation: Vertical Bearing: NA TD: 771.0 ft

Depth (feet)	Core Run C-# Core Recovery %	Field Analytical Sample Number	Hydrologic Property Samples	Core Box # From - To (feet)	Depth	Lithology	Graphic Log	Lithologic Unit	Groundwater Occurrences	Notes
720					Continued					
730										
740	NA	NA	NA	NA				Santa Fe Group Basalt		675.5' - 748.5' Filter Pack (20/40)
750										Bentonite Pellets (748.5' - 755') Sump (748.5' - 758')
760										755' - 771' Coarse Sand (8/12 size)
770										
780					TD = 771.0'					

Appendix B

Descriptions of Geologic Samples

Sample No.	Description*	Discussion
R9-50.5D	B	Unwashed cuttings from 41 to 50.5 ft depths in drill hole R9 are fragments of generally massive dark gray basalt to 15 mm, and occasionally to 40 mm. The basalt contains scattered vesicles to 1 mm, scarce to common pale olive olivine to 1.4 mm, and scarce to rare prismatic feldspar to 1.5 mm.
R9-92D	B	Ultrasonically cleaned cuttings from 90 to 92 ft depths in drill hole R9 are dark gray, fine-grained basalt with common ovoid vesicles to 11 mm, scarce to common olive olivine to 2.5 mm, and scarce feldspar laths to 1 mm.
R9-92D	T	This polished thin section consists of four large fragments of cuttings, all medium-grained hypocrystalline, pilotaxitic basalt with phenocrysts of common olivine and scarce plagioclase. Olivine and pyroxene in groundmass, presumed all to be clinopyroxene, are distinguishable by a slightly higher reflectance and generally slight alteration to iddingsite for olivine. Scarce Fe-Ti oxides all occur as groundmass phases, including tiny ilmenite prisms and much more abundant, highly skeletal magnetite. Granular spinel inclusions within olivine phenocrysts are relatively large. Intergranular brown glass is partly devitrified along grain boundaries to a cryptocrystalline assemblage of basaltic minerals. Smectite completely fills smaller vesicles, those with diameters of about 0.1 mm, but large vesicles, with diameters >1 mm, are thinly lined with smectite. Olivine rims are thinly altered to iddingsite, and large voids within olivine are usually completely filled with smectite, clearly associating the slight alteration with smectite.
R9-122D	B	This sample of washed and ultrasonically cleaned cuttings to 25 mm, from 121 to 122 ft depths in drill hole R9, is medium dark gray, medium-grained, moderately vesicular basalt with scarce to common vesicles that range from round to 1 mm to very elongate (6/1 mm). Mafics are scarce pale olive olivine to 1.5 mm and pale brownish black pyroxene rhombs that might be pigeonite. Feldspar, to 0.6 mm, is very rare.
R9-122D	T	This polished thin section consists of three large fragments of cuttings, all medium-grained hypocrystalline, ophitic basalt with common phenocrysts of olivine and rare microphenocrysts of plagioclase. Olivine and clinopyroxene in groundmass are distinguishable by the generally dusky brown color of clinopyroxene and slightly higher reflectance and generally slight alteration to iddingsite for olivine. Scarce Fe-Ti oxides all occur as groundmass phases, including tiny ilmenite prisms and more abundant magnetite. Intergranular brown glass is partly devitrified along grain boundaries to a cryptocrystalline assemblage of basaltic minerals. Minor smectite partly fills some vesicles.
R9-162D	B	Ultrasonically cleaned cuttings from 160 to 162 ft depths in drill hole R9 are medium dark gray, massive, coarse-grained basalt with common olive-green olivine to 3 mm. A few surfaces, which probably represent fractures, are thinly coated with moderate orange pink clay.
R9-162D	T	This polished thin section consists of four fragments of cuttings, all medium grained ophitic basalt with common phenocrysts of olivine. Rare microphenocrysts of plagioclase could also be classified as the largest groundmass plagioclase. Smectite mostly fills vesicles and slightly replaces some olivine.
R9-181.3	B	Core from 181.2 to 181.3 ft depths in drill hole R9 is light brownish gray vesicular basalt with common, generally slightly ovoid vesicles to 10/5 mm diameters. Near vertical fracture surface that has split off about 10% of core piece is heavily coated with light brown authigenic clay. Common, completely unaltered olivine indicates a complete lack of secondary alteration of basalt. Feldspar is scarce to common as prisms to 1 mm.
R9-201.5	B	Core from 201.2 to 201.5 ft depths in drill hole R9 is medium dark gray massive basalt with scattered, aligned ovoid vesicles to 4/1 mm. Scarce to rare feldspar occurs to 1 mm, and scarce to common pale olive-green to dark olive-green olivine to 3 mm, strongly locally altered to iddingsite, probably in association with fractures that are thickly coated with moderate orange pink authigenic clay.

Sample No.	Description*	Discussion
R9-219	B	Core from 218.8 to 219.0 ft depths in drill hole R9 is brownish gray vesicular basalt, pervasively coated with pinkish gray to moderate reddish brown clay. In thick accumulations, the clay is laminated, with the darker color towards the interior of the clay deposit. Black dendrites of manganese oxides thinly and spottily coat some clay.
R9-219CY1	X	Clay subsample was scraped from host basalt and then processed in deionized water. This sample is a residue from settling for 1 hour. Approximate grain sizes in this separate are 5 to 18 microns.
R9-219CY2	X	Clay subsample was scraped from host basalt and then processed in deionized water. This sample is a residue from settling overnight, following settling for 1 hour. Approximate grain sizes in this separate are 1.5 to 5 microns.
R9-219CY3	X	Clay subsample was scraped from host basalt and then processed in deionized water. This sample is a residue from a 5 minute centrifuge at 5000 rpm, following settling overnight. Approximate grain sizes in this separate are 0.25 to 1.5 microns.
R9-219CY4	X	Clay subsample was scraped from host basalt and then processed in deionized water. This sample is a residue from a 1 hour centrifuge at 8000 rpm, following a 5 minute centrifuge at 5000 rpm. Approximate grain sizes in this separate are 0.1 to 0.25 microns.
R9-219CY5	X	Clay subsample was scraped from host basalt and then processed in deionized water. This sample is a residue after evaporating the supernatant fluid from a 1 hour centrifuge at 8000 rpm. Approximate grain sizes in this separate are <0.1 microns.
R9-228	B	Core from 227.7 to 228.0 ft depths in drill hole R9 is medium dark gray basalt with rare, somewhat ovoid vesicles to 6/3.5 mm. Olive-green olivine to 1.5 mm is common; no feldspar was observed. Some fractures and vesicles are thickly coated with very pale orange pink authigenic clay.
R9-228.2	B	Core from 228.0 to 228.2 ft depths in drill hole R9 is mostly massive medium gray basalt with scarce unaltered pale olive-green olivine to 1.5 mm. The few irregular, elongate vesicles to 16 mm that occur are filled with moderate orange pink and much lesser moderate reddish brown clay. These clays are laminated in part; the darker color always occurs at the top of the deposit. Dendrites of manganese oxides spottily coat interior surfaces of clay.
R9-228.2CY1	X	Clay subsample was scraped from host basalt and then processed in deionized water. This sample is a residue from settling for 1 hour. Approximate grain sizes in this separate are 5 to 18 microns.
R9-228.2CY2	X	Clay subsample was scraped from host basalt and then processed in deionized water. This sample is a residue from settling overnight, following settling for 1 hour. Approximate grain sizes in this separate are 1.5 to 5 microns.
R9-228.2CY3	X	Clay subsample was scraped from host basalt and then processed in deionized water. This sample is a residue from a 5 minute centrifuge at 5000 rpm, following settling overnight. Approximate grain sizes in this separate are 0.25 to 1.5 microns.
R9-228.2CY4	X	Clay subsample was scraped from host basalt and then processed in deionized water. This sample is a residue from a 1 hour centrifuge at 8000 rpm, following a 5 minute centrifuge at 5000 rpm. Approximate grain sizes in this separate are 0.1 to 0.25 microns.
R9-228.2CY5	X	Clay subsample was scraped from host basalt and then processed in deionized water. This sample is a residue after evaporating the supernatant fluid from a 1 hour centrifuge at 8000 rpm. Approximate grain sizes in this separate are <0.1 microns.
R9-257.6	B	Core from 257.2 to 257.6 ft depths in drill hole R9 is medium light gray basalt with rare round vesicles to 3.5 mm, and common light green olivine to 3 mm. No feldspar was observed. A 40/17 mm clast of very light gray quartzite at 257.3 ft depth is equigranular, with grains mostly 1 to 3 mm diameter.

Sample No.	Description*	Discussion
R9-273.7	B	Core from 273.3 to 273.7 ft depths in drill hole R9 is massive medium gray basalt with scarce to common pale olive-green olivine to 2 mm. No feldspar phenocrysts were observed.
R9-281.8	B	Core from 281.5 to 281.8 ft depths in drill hole R9 is dark gray basalt with common very light green olivine to 5 mm. Irregular fracture 2 to 6 mm wide is partly filled with brecciated basalt, but mostly with moderate orange pink authigenic clay. This fracture dips 68 degrees, and is terminated by another irregular fracture that dips 15 degrees.
R9-281.8CY	X	Clay subsample was scraped from host basalt and then processed in deionized water. This sample is a residue from settling for 1 minute.
R9-281.8CY0	X	Clay subsample was scraped from host basalt and then processed in deionized water. This sample is a residue from settling for 5 minutes, following settling for 1 minute. Approximate grain sizes in this separate are 18 to 40 microns.
R9-281.8CY1	X	Clay subsample was scraped from host basalt and then processed in deionized water. This sample is a residue from settling for 1 hour, following settling for 5 minutes. Approximate grain sizes in this separate are 5 to 18 microns.
R9-281.8CY2	X	Clay subsample was scraped from host basalt and then processed in deionized water. This sample is a residue from settling overnight, following settling for 1 hour. Approximate grain sizes in this separate are 1.5 to 5 microns.
R9-281.8CY3	X	Clay subsample was scraped from host basalt and then processed in deionized water. This sample is a residue from a 5 minute centrifuge at 5000 rpm, following settling overnight. Approximate grain sizes in this separate are 0.25 to 1.5 microns.
R9-281.8CY4	X	Clay subsample was scraped from host basalt and then processed in deionized water. This sample is a residue from a 1 hour centrifuge at 8000 rpm, following a 5 minute centrifuge at 5000 rpm. Approximate grain sizes in this separate are 0.1 to 0.25 microns.
R9-281.8CY5	X	Clay subsample was scraped from host basalt and then processed in deionized water. This sample is a residue after evaporating the supernatant fluid from a 1 hour centrifuge at 8000 rpm. Approximate grain sizes in this separate are <0.1 microns.
R9-282.2	B	Core from 282.0 to 282.2 ft depths in drill hole R9 is dark gray, well sorted basaltic ash, mostly subangular hydroclastic shards of basalt, scarce felsics, and rare lithics, all mostly 0.1 to 0.5 mm diameter.
R9-282.6	B	Core from 282.4 to 282.6 ft depths in drill hole R9 is very dark yellowish brown, poorly sorted basaltic tephra, mostly ash but with scarce to common black basaltic shards, many in elongate pumiceous forms to 8/2 mm diameters. Generally very irregular vesicles are completely filled with clay; common to abundant clay fillings to 12/2 mm diameters are very pale orange at top of interval, grading down to scarce to common clay fillings to 3/2 mm diameters at base. Lowermost several mm of core piece are basaltic ash as described for sample R9-282.2; contact between the two layers is approximately horizontal, with undulations of 2 mm.
R9-285.5	B	Core from 285.3 to 285.5 ft depths in drill hole R9 is light olive-green gray well sorted basaltic ash, mostly 0.1 to 0.3 mm, mostly subangular black hydroclastic shards of basalt, and common felsics. Scarce to rare white globules of white secondary mineral are probably calcite.
R9-292.7	B	Core from 292.6 to 292.7 ft depths in drill hole R9 is yellowish brown siltstone that probably represents a paleosol, with scarce lithics to 4 mm, mostly devitrified dacitic lava. Generally tiny mafics to 0.7 mm are black, vitreous, and include orthopyroxene and biotite. Round aggregates of white calcite to 1 mm diameter sparsely fill some voids. Felsic fragments >0.1 mm are absent.
R9-292.7CY1	X	Sample R9-292.7 was disaggregated and then processed in deionized water. This sample is a residue from settling for 1 hour. Approximate grain sizes in this separate are 5 to 18 microns.

Sample No.	Description*	Discussion
R9-292.7CY2	X	Sample R9-292.7 was disaggregated and then processed in deionized water. This sample is a residue from settling overnight, following settling for 1 hour. Approximate grain sizes in this separate are 1.5 to 5 microns.
R9-292.7CY3	X	Sample R9-292.7 was disaggregated and then processed in deionized water. This sample is a residue from a 5 minute centrifuge at 5000 rpm, following settling overnight. Approximate grain sizes in this separate are 0.25 to 1.5 microns.
R9-292.7CY4	X	Sample R9-292.7 was disaggregated and then processed in deionized water. This sample is a residue from a 1 hour centrifuge at 8000 rpm, following a 5 minute centrifuge at 5000 rpm. Approximate grain sizes in this separate are 0.1 to 0.25 microns.
R9-292.7CY5	X	Sample R9-292.7 was disaggregated and then processed in deionized water. This sample is a residue after evaporating the supernatant fluid from a 1 hour centrifuge at 8000 rpm. Approximate grain sizes in this separate are <0.1 microns.
R9-297A	B	Sample is 38 mm fragment of dark gray basalt from rubble zone in core of drill hole R9 from 296.8 to 297 ft depths. Basalt has common feldspar to 2 mm and common mafics, mostly black pyroxene and lesser green olivine to 1 mm.
R9-297B	B	Sample is 43 by 10 by 20 mm fragment of dark gray basalt from rubble zone in core of drill hole R9 from 296.8 to 297 ft depths. Basalt has rare, irregular vesicles to 2 mm, rare feldspar to 0.5 mm, and scarce light to dark green olivine to 1 mm. Several lithic fragments occur in the fragment; the largest is an 8 mm long light gray, devitrified, crystal-poor lava with quartz phenocrysts to 2 mm, possibly Rendija Canyon rhyolite.
R9-297C	B	Sample is 40 by 20 by 20 mm fragment of medium gray vitric lava from rubble zone in core of drill hole R9 from 296.8 to 297 ft depths. The fragment has scarce to common feldspar to 3.5 mm, and to 5 mm in glomerocrysts. Mafics include common black to brown, equant to prismatic orthopyroxene to 1 mm, and scarce green prismatic clinopyroxene to 2 mm.
R9-359D	B	Cuttings from 356.5 to 359 ft depths in drill hole R9 are pale yellowish brown sandy gravel with subangular lithic fragments to 10 mm.
R9-359D1	B	Cuttings from 356.5 to 359 ft depths in drill hole R9 were originally collected on a 0.5-mm screen during wet sieving, and later wet sieved to remove the fraction coarser than 2 mm.
R9-359D2	B	Cuttings from 356.5 to 359 ft depths in drill hole R9 were collected on a 2-mm screen during wet sieving. Most of the matrix that probably is the dominant constituent is much finer than this size fraction, and these cuttings are all subangular lithics of devitrified lava, with thin spots of adhering grayish orange-pink matrix. About half of the lithics are grayish red to pale grayish red devitrified lava with conspicuous felsics to 1.5 mm and conspicuous black, vitreous mafics that include orthopyroxene prisms to 1.2 mm length. Most of the remaining lithics are medium gray devitrified lava with conspicuous prisms of black orthopyroxene to 1.5 mm, and lesser hornblende to 1.5 mm. A few fragments appear to represent white, hydrothermally altered lava. Some lithics are mottled black vitric lava.
R9-414D	B	Cuttings from 409 to 414 ft depths in drill hole R9 are very light brownish gray sandy gravel with mostly subangular and some subrounded lithic fragments to 13 mm.
R9-414D1	B	Cuttings from 409 to 414 ft depths in drill hole R9 were originally collected on a 0.5-mm screen during wet sieving, and later wet sieved to remove the fraction coarser than 2 mm.

Sample No.	Description*	Discussion
R9-414D2	B	Cuttings from 409 to 414 ft depths in drill hole R9 were collected on a 2-mm screen during wet sieving. Sample R9-414D1 (above) passed the 2-mm screen and was collected on a 0.5-mm screen. Most of the matrix that probably is the dominant constituent is much finer than either the D1 or D2 size fractions; these coarser fractions are almost entirely subangular lithics of devitrified lava, discontinuously covered with adhering grayish orange pink matrix. About two-thirds of the lithics are light gray devitrified lava with conspicuous felsics to 1.5 mm that include quartz. Very pale red devitrified lava with bronze biotite comprises most of the remaining lithics. About 5% of the fragments are very light brown siltstone.
R9-454D	B	Cuttings from 453 to 454 ft depths in drill hole R9 are pale yellowish brown conglomerate with subangular and subrounded lithic fragments to 12 mm.
R9-454D1	B	Cuttings from 453 to 454 ft depths in drill hole R9 were collected on a 2-mm screen during wet sieving. Most of the matrix that probably is the dominant constituent is much finer than this size fraction, and these cuttings are all subangular lithics of devitrified lava, discontinuously covered with adhering grayish orange pink matrix. About half of the lithics are light gray to medium dark gray. Biotite was observed in one light gray lithic and a 1-mm black orthopyroxene prism was observed in a medium gray fragment. The remaining lithics are reddish, and include pale red devitrified lava with feldspar to 1.5 mm and orthopyroxene to 0.7 mm.
R9-509D	B	Cuttings from 506.5 to 509 ft depths in drill hole R9 are yellowish brown sandy gravel with subangular and subrounded lithic fragments to 15 mm.
R9-509D1	B	Cuttings from 506.5 to 509 ft depths in drill hole R9 were collected on a 2-mm screen during wet sieving. Most of the matrix that probably is the dominant constituent is much finer than this size fraction, and these cuttings are all subangular lithics of devitrified lava, well coated with adhering grayish orange pink matrix. Lithics are mostly grayish and lesser reddish, uniformly mafic-poor with black to bronze biotite the only mafic observed (within three fragments), and with feldspar to 2.5 mm and some quartz. One very light gray fragment is pumiceous and aphyric.
R9-564D	B	Cuttings from 563.9 to 564.0 ft depths in drill hole R9 are dark yellowish brown pebbly sand with subangular and subrounded lithic fragments to 8 mm.
R9-564D1	B	Cuttings from 563.9 to 564.0 ft depths in drill hole R9 were collected on a 2-mm screen during wet sieving. Most of the matrix that probably is the dominant constituent is much finer than this size fraction, and these cuttings are mostly subangular lithics of devitrified lava, sparsely and discontinuously coated with adhering grayish orange pink matrix. Devitrified lavas are mostly medium dark gray to medium gray with feldspar to 1.5 mm and with conspicuous mafics, mostly black orthopyroxene, mostly equant but with some prisms to 1.7 mm, and some very dark green clinopyroxene. Lesser pale red devitrified lava is more mafic-poor; some fragments contain biotite and others contain quartz. About 5% of the fragments are white to very light gray pumice, one of which contains conspicuous biotite.
R9-587.4	B	Core from 587.2 to 587.4 ft depths in drill hole R9 is very light brown argillic tuffaceous sandstone. Abundant clasts are dominantly pumice; the largest are conspicuous grayish pink argillic pumice to 25/12 mm, with common feldspar to 2 mm and common, subequal black hornblende to 1.5 mm and biotite to 1 mm. Also conspicuous are light gray, highly elongate pumices to 22/5 mm, which may owe their high aspect ratios to a primary habit as long tube pumice or to epigenetic load compaction of this highly argillic rock; these pumices contain common small equant dark green clinopyroxene and orthopyroxene to 0.5 mm. The volumetrically dominant white pumices are 1 to 3 mm, and these are foliated perpendicular to the core axis. Scarce to rare lithics to 11 mm in long dimension are moderately angular, and are mostly devitrified lavas, but also include conspicuous pale reddish brown sandstone to 10 mm. The groundmass of reworked tuff contains abundant black mafics, mostly hornblende to 1.5 mm with lesser biotite.

Sample No.	Description*	Discussion
R9-596	B	Core from 595.8 to 596.0 ft depths in drill hole R9 is light greenish white argillic nonwelded tuff. The relatively coarse size of mafic minerals suggests that this sample consists mostly of pumice fragments that are individually indistinguishable due to the pervasive argillic alteration. Several large, irregular, very light brownish gray argillic pumices or rip-up clasts to 30 mm in long dimension are common; these clasts contain very abundant white clay pseudomorphs of feldspar and tiny black mafics, mostly hornblende occasionally to 1 mm, with lesser biotite. Scarce light gray pumices to 18/4 mm contain only scarce equant pyroxene pseudomorphs to 0.8 mm, but have abundant unaltered tiny groundmass mafics. One 9 mm light gray pumice is intermingled with a 4 mm very light brownish gray pumice. The groundmass of the tuff contains abundant black mafics, mostly hornblende to 1.5 mm and lesser biotite.
R9-606.4	B	Core from 606.2 to 606.4 ft depths in drill hole R9 is light greenish gray argillic nonwelded tuff. The relatively coarse size of mafic minerals suggests that this sample consists mostly of pumice fragments that are individually indistinguishable due to the pervasive argillic alteration. Scarce to common, small light brownish gray argillic pumices to 10/1 mm define prominent compaction foliation that gives a vague appearance of low-angle cross bedding. Some light gray pumices to 5 mm are present. The groundmass of tuff contains common mafics that include light to dark green clinopyroxene and partly altered black orthopyroxene prisms, both to 1.5 mm.
R9-616.5	B	Core from 615.5 to 616.5 ft depths in drill hole R9 is pale yellowish brown, completely disaggregated tuffaceous sandstone with abundant lithic fragments, mostly 1 to 8 mm in diameter, along with scarce white vitric pumice.
R9-616.5LI	B	Separate of largest individual clasts within core from 615.5 to 616.5 ft depths in drill hole R9 consists of 6 to 12 mm diameter lithics, white pumice, and aggregates of cemented matrix, all coated with pale yellowish brown matrix. All lithics are devitrified. Most pumice clasts are vitric, but others are argillic. Pumices contain scarce to common mafics that include conspicuous biotite, some bronzy, and one 1.4 mm long orthopyroxene.
R9-621.3	B	Core from 621.0 to 621.3 ft depths in drill hole R9 is pinkish gray tuffaceous sandstone with abundant vitric pumices, with colors that include very light gray in pumices to 11 mm, white pumices to 8 mm, and pale yellowish orange pumices to 3 mm. Common mafics to 1.2 mm include black to bronze biotite and black hornblende. Lithics to 4 mm are common, and feldspar to 1.5 mm is evident.
R9-639.8	B	Core from 639.6 to 639.8 ft depths in drill hole R9 is pale orange tuffaceous sandstone with common white argillic pumice to 13 mm. Both matrix and pumices contain common black mafics to 1 mm, including biotite and strongly subordinate hornblende. Lithics, to 1.5 mm, are scarce and albite-twinned plagioclase to 2 mm is evident.
R9-645.3	B	Core from 645.3ft depth in drill hole R9 is mostly dark yellowish brown argillaceous fine sandstone with scarce white argillic pumice to 11 mm. The sample is very crumbly along desiccation cracks. Abundant black mafics to 1 mm include biotite and hornblende. Light brown lithics of tuffaceous sandstone to 7 mm are scarce to common, and have conspicuous black mafics that include biotite.
R9-661	B	Core from 660.8 to 661.0 ft depths in drill hole R9 is very friable pale red tuffaceous sandstone with abundant white partly argillic pumice to 9 mm that contains abundant biotite and hornblende to 3 mm. Fine- to coarse-grained sandstone with abundant tiny black mafics form lenses >20 mm in length.

Sample No.	Description*	Discussion
R9-679	B	Core from 678.8 to 679.0 ft depths in drill hole R9 is medium light gray, moderately well sorted, coarse tuffaceous sandstone with abundant medium gray lithics to 2 mm that give rock a salt and pepper appearance. White to very light gray vitric pumice to 3 mm is scarce to common, and concentrated in one lens >30 mm in length. Common mafics are mostly tiny black biotite, with one 1.2 mm dark green prism of clinopyroxene observed. Several feldspar grains were observed to 2.5 mm, mostly albite-twinned plagioclase.
R9-688.6CY	B	Separate from 688.4 to 688.6 ft depths in drill hole R9 is massive very light brown clay and sand-sized grains accumulated in thicknesses to 12 mm. The clay fills vesicles within dusky yellowish brown basalt that has yellowish green olivine pseudomorphs to 1.5 mm and conspicuous plagioclase. The clay filling is partly calcareous. One vesicle in basalt is filled with a 13 mm thick aggregate of coarse drusy quartz grains to 3 mm, together with coarse white calcite grains to 1.2 mm.
R9-690.4	B	Core from 690.2 to 690.4 ft depths in drill hole R9 is dark gray, massive fine-grained basalt with common feldspar to 2.5 mm and common olivine to 1.5 mm, which ranges from light green unaltered to red iddingsite pseudomorphs. The sample is moderately veined with a white secondary mineral, probably calcite, filling hairline fractures.
R9-690.4	T	This polished thin section is microporphyritic basalt with phenocrysts of common to abundant olivine and scarce plagioclase. Large vesicles are completely filled with calcite, and smaller vesicles are completely filled with smectite. Plagioclase is slightly altered to smectite where adjacent to smectite-filled vesicles. Thick iddingsite rims of approximately constant thickness surround all olivine grains, so that the groundmass is mostly altered, but the largest phenocrysts have relatively little alteration. Clinopyroxene, all present as equant grains and grain aggregates in groundmass, is entirely unaltered.
R9-699.1	B	Core from 698.9 to 699.1 ft depths in drill hole R9 is medium gray, fine-grained, moderately vesicular basalt with round vesicles to 4 mm and ovoid vesicles to 14/4 mm. Vesicle surfaces are uniformly covered with an ultrathin coating of a secondary mineral that gives the vesicles a bluish appearance. Feldspar to 1 mm and olivine to 3 mm, mostly altered to iddingsite, are both common.

* B = description under binocular microscope, T = thin section narratives, and X = XRD processing information.

Appendix C

Moisture and Matric-Potential Results

Sample ID[a]	Matrix Type	Upper Depth (ft)	Lower Depth (ft)	Gravimetric Moisture (%)	Activity (H_20)	Num. of A(H_20) Meas.	Temp. (°C)	Matric Potential (cm)
R9-1	Cuttings	26.5	27	1.34	0.947	7	25.36	-7.69E+04
R9-2	Cuttings	32	33	0.82	0.917	3	26.56	-1.23E+05
R9-3	Cuttings	41	50.5	3.59	0.999	3	24.48	-1.40E+03
R9-4	Cuttings	50.5	58	1.94	0.995	3	24.84	-7.02E+03
R9-5	Cuttings	70	72	1.17	0.986	3	24.89	-2.02E+04
R9-6	Cuttings	80	82	1.65	0.997	3	25.06	-3.74E+03
R9-7	Cuttings	90	92	1.54	0.994	3	24.97	-7.97E+03
R9-8	Cuttings	100	102	1.41	0.996	3	25.21	-5.62E+03
R9-9	Cuttings	110	112	ND[b]	0.583	3	25.98	-7.58E+05
R9-10	Cuttings	121	122	1.32	0.989	7	24.81	-1.55E+04
R9-11	Cuttings	130	132	0.73	0.984	7	24.90	-2.21E+04
R9-12	Cuttings	140	142	0.73	0.981	7	25.03	-2.64E+04
R9-13	Cuttings	149	152	0.56	0.840	7	25.53	-2.44E+05
R9-14	Cuttings	160	162	1.46	0.983	3	25.34	-2.36E+04
R9-15	Cuttings	170	172	0.49	0.909	3	25.80	-1.35E+05
R9-16	Cuttings	180	182	6.87	1.000	3	25.85	-4.69E+02
R9-17	Core	181.3	181.5	19.84	1.004	3	26.06	6.08E+03
R9-18	Core	184.5	184.8	8.70	1.001	3	26.38	1.41E+03
R9-19	Core	189	189.3	9.61	1.003	3	25.97	4.21E+03
R9-20	Core	201.2	201.5	10.73	1.001	3	26.08	1.41E+03
R9-21	Core	206.5	206.8	13.34	1.002	3	26.03	3.28E+03
R9-22	Core	213	213.3	22.23	1.002	3	26.06	3.28E+03
R9-23	Core	218.5	218.8	17.43	1.007	3	25.35	9.33E+03
R9-24	Core	222.5	223	25.63	1.004	3	25.88	6.08E+03
R9-25	Core	227.7	228	3.63	1.001	3	25.93	9.37E+02
R9-26	Core	234.3	234.5	3.13	1.000	3	25.84	0.00E+00
R9-27	Core	243.85	244.1	2.31	0.997	3	24.83	-4.21E+03
R9-28	Core	252.4	252.6	2.14	0.998	3	24.87	-3.27E+03
R9-29	Core	255	255.5	1.83	ND	ND	ND	ND
R9-30	Core	266.35	266.6	1.59	0.958	3	24.84	-6.06E+04
R9-31	Core	273.3	273.7	2.07	0.987	3	25.19	-1.88E+04
R9-32	Core	279.2	279.5	11.55	1.001	3	25.52	1.40E+03
R9-36	Core	290.5	290.7	25.58	1.002	4	22.67	3.24E+03
R9-37	Cuttings	306	309	7.35	1.000	4	22.83	-4.64E+02
R9-38	Cuttings	311.5	314	7.81	0.999	3	22.79	-1.39E+03
R9-39	Cuttings	316.5	319	8.14	1.002	3	22.86	2.32E+03
R9-40	Cuttings	321.5	324	7.93	1.001	3	22.89	1.39E+03
R9-41	Cuttings	326.5	329	8.13	0.997	3	22.95	-3.72E+03
R9-42	Cuttings	331.5	334	7.35	0.992	3	23.02	-1.12E+04
R9-43	Cuttings	336.5	339	5.68	0.992	3	21.70	-1.16E+04
R9-44	Cuttings	341.5	344	5.71	0.993	3	21.86	-9.74E+03
R9-45	Cuttings	346.5	349	4.46	0.991	3	21.92	-1.25E+04

Sample ID[a]	Matrix Type	Upper Depth (ft)	Lower Depth (ft)	Gravimetric Moisture (%)	Activity (H_20)	Num. of A(H_20) Meas.	Temp. (°C)	Matric Potential (cm)
R9-46	Cuttings	351.5	354	6.23	0.997	3	22.00	-4.63E+03
R9-47	Cuttings	356.5	359	5.13	0.999	3	22.14	-1.39E+03
R9-48	Cuttings	361.5	364	4.48	0.993	3	22.08	-9.29E+03
R9-49	Cuttings	366.5	369	4.95	0.999	3	21.30	-1.85E+03
R9-50	Cuttings	371.5	374	3.22	0.993	3	21.50	-1.02E+04
R9-51	Cuttings	376.5	379	4.01	0.997	3	21.61	-4.16E+03
R9-52	Cuttings	381.5	384	4.74	0.996	3	21.76	-5.09E+03
R9-53	Cuttings	386.5	389	5.75	1.002	3	21.84	2.31E+03
R9-54	Cuttings	391.5	394	6.42	1.002	3	21.93	2.77E+03
R9-55	Cuttings	396.5	399	5.57	1.000	3	21.97	-6.16E-10
R9-56	Cuttings	401.5	404	7.54	0.999	3	22.00	-1.39E+03
R9-57	Cuttings	406.5	409	4.98	0.996	3	22.08	-5.56E+03
R9-58	Cuttings	411.5	414	4.10	0.998	5	21.12	-2.77E+03
R9-59	Cuttings	416.5	419	5.00	0.996	5	21.32	-5.09E+03
R9-60	Cuttings	421.5	424	3.57	0.988	3	21.51	-1.72E+04
R9-61	Cuttings	426.5	429	3.66	0.998	3	21.66	-3.24E+03
R9-62	Cuttings	431.5	434	5.20	1.000	3	21.70	4.62E+02
R9-63	Cuttings	436.5	439	7.38	1.000	3	22.11	-4.63E+02
R9-64	Cuttings	443	444	4.79	0.999	3	22.09	-1.85E+03
R9-65	Cuttings	448	449	4.99	0.998	3	22.19	-2.78E+03
R9-66	Cuttings	453	454	5.60	0.998	3	22.22	-2.32E+03
R9-67	Cuttings	458	459	6.19	0.998	3	22.35	-2.32E+03
R9-68	Cuttings	463	464	5.01	0.999	3	22.02	-1.39E+03
R9-69	Cuttings	468	469	4.67	0.998	3	22.20	-2.32E+03
R9-70	Cuttings	471.5	474	5.06	0.998	3	22.24	-2.32E+03
R9-71	Cuttings	476.5	479	4.88	0.996	3	22.30	-5.57E+03
R9-72	Cuttings	481.5	484	6.64	0.998	3	22.24	-3.24E+03
R9-73	Cuttings	486.5	489	6.93	0.997	3	22.29	-4.17E+03
R9-74	Cuttings	491.5	494	6.35	0.997	3	22.44	-3.71E+03
R9-75	Cuttings	496.5	499	5.98	0.996	3	22.54	-5.57E+03
R9-76	Cuttings	501.5	504	6.88	0.998	3	22.41	-2.32E+03
R9-77	Cuttings	506.5	509	5.49	0.994	3	22.42	-7.90E+03
R9-78	Cuttings	511.5	514	5.93	0.996	3	22.44	-5.11E+03
R9-79	Cuttings	516.5	519	12.47	1.001	3	22.47	1.39E+03
R9-80	Cuttings	521.5	524	5.42	0.995	3	22.36	-6.97E+03
R9-81	Cuttings	526.5	529	4.02	0.993	3	22.44	-9.76E+03
R9-82	Cuttings	531.5	534	2.85	0.976	3	22.47	-3.38E+04
R9-83	Cuttings	536.5	539	3.65	0.981	3	22.43	-2.62E+04
R9-84	Cuttings	541.5	542	11.44	0.892	3	22.15	-1.58E+05
R9-85	Cuttings	543.5	544	12.17	0.959	3	22.24	-5.86E+04
R9-86	Cuttings	544.8	545	11.28	0.980	3	22.41	-2.81E+04
R9-87	Cuttings	546.6	547	12.78	0.995	3	22.27	-7.43E+03

Sample ID[a]	Matrix Type	Upper Depth (ft)	Lower Depth (ft)	Gravimetric Moisture (%)	Activity (H_20)	Num. of A(H_20) Meas.	Temp. (°C)	Matric Potential (cm)
R9-88	Cuttings	547.8	548	9.63	0.926	3	22.53	-1.07E+05
R9-89	Cuttings	549.4	549.8	12.88	0.986	3	22.36	-1.96E+04
R9-90	Cuttings	551.8	552	8.51	0.945	3	22.50	-7.86E+04
R9-91	Cuttings	553.9	554	8.17	0.927	3	22.59	-1.05E+05
R9-92	Cuttings	556.9	557	9.88	0.988	3	22.51	-1.63E+04
R9-93	Cuttings	558.9	559	11.31	0.976	3	22.69	-3.33E+04
R9-94	Cuttings	561.5	562	8.43	0.969	3	22.66	-4.43E+04
R9-95	Cuttings	563.9	564	7.55	0.937	3	22.78	-9.01E+04
R9-96	Cuttings	565.9	566	7.31	0.954	3	22.78	-6.50E+04
R9-97	Cuttings	569.7	570	4.47	0.807	3	22.95	-2.98E+05
R9-98	Cuttings	572.9	573	3.53	0.756	3	23.10	-3.90E+05
R9-99	Cuttings	574.8	575	3.58	0.815	3	23.14	-2.84E+05
R9-100	Cuttings	576.9	577	4.56	0.901	3	23.14	-1.45E+05
R9-101	Cuttings	578.9	579	4.19	0.706	3	23.16	-4.86E+05
R9-102	Core	584	584.3	17.83	0.996	3	22.98	-5.58E+03
R9-103	Core	586.4	586.7	21.12	0.999	3	22.88	-9.28E+02
R9-104	Core	595.2	595.8	20.88	1.001	3	22.85	1.85E+03
R9-105	Core	614.5	615.5	7.99	0.875	3	23.22	-1.87E+05
R9-106	Core	615.5	616.5	7.22	0.897	3	23.41	-1.52E+05
R9-107	Core	616.5	617.5	11.74	0.917	3	23.27	-1.21E+05
R9-108	Core	621	621.3	17.40	1.001	3	21.43	1.38E+03
R9-109	Core	639.6	639.8	23.82	0.997	3	21.89	-3.70E+03
R9-110	Core	645.25	645.35	44.78	1.005	3	21.44	7.37E+03
R9-111	Core	651.5	651.7	27.51	1.000	3	21.90	-6.16E-10
R9-112	Core	655.1	655.3	27.08	0.999	3	21.85	-1.39E+03
R9-113	Core	660.8	661	27.31	0.998	3	22.00	-2.32E+03
R9-114	Core	665.5	665.7	18.74	1.001	3	22.14	9.25E+02
R9-116	Core	669	669.2	25.56	0.998	3	22.27	-3.25E+03
R9-115	Core	669.8	669.9	25.30	1.000	3	22.06	0.00E+00
R9-117	Core	672.9	673.1	22.09	1.002	3	22.26	2.31E+03
R9-118	Core	678.8	679	15.31	1.001	3	22.42	9.26E+02
R9-119	Core	684.9	685.1	15.10	1.001	3	22.51	1.39E+03
R9-120	Core	688.4	688.6	9.25	1.001	3	22.61	9.27E+02
R9-121	Core	692.2	692.4	4.34	1.001	3	22.60	1.39E+03

[a] See Appendix A.

[b] ND = not determined.

Appendix D

Results of Unsaturated Hydraulic-Property Testing

This appendix consists of the actual laboratory sheets provided by Daniel B. Stephens & Associates, Inc., for analysis of a sample of Puye Formation from a depth of 642.3 to 642.8 ft.

Daniel B. Stephens & Associates, Inc.

Data for Initial Moisture Content, Bulk Density, Porosity, and Percent Saturation

Job Name:	LANL
Job Number:	9958.01
Sample Number:	8814
Ring Number:	8814
Depth:	642.3-642.8
Test Date:	13-Oct-99
Field weight of sample* (g):	249.06
Tare weight, ring (g):	122.88
Tare weight, cap/plate/epoxy (g):	0.00
Dry weight of sample (g):	110.29
Sample volume (cm^3):	70.31
Assumed particle density:	2.65

Initial Volumetric Moisture Content (% vol):	22.6
Initial Gravimetric Moisture Content (% g/g):	14.4
Dry bulk density (g/cm^3):	1.57
Wet bulk density (g/cm^3):	1.79
Calculated Porosity (% vol):	40.8
Percent Saturation:	55.4

Comments:

* Weight including tares

Laboratory analysis by: E. Koenig
Data entered by: M. Devine
Checked by: R. Smith

Daniel B. Stephens & Associates, Inc.

Saturated Hydraulic Conductivity
Falling Head Method

Job name:	LANL	*Type of water used:*	TAP
Job number:	9958.01	*Backpressure* (psi)*:*	0.0
Sample number:	8814	*Offset* (cm)*:*	0.0
Ring number:	8814	*Sample length* (cm)*:*	2.58
Depth:	642.3-642.8	*Sample x-sectional area* (cm^2)*:*	27.29
		Reservoir x-sectional area (cm^2)*:*	0.70

Date	Time	Temp (°C)	Reservoir head (cm)	Corrected head (cm)	Elapsed time (sec)	Ksat (cm/sec)	Ksat @ 20°C (cm/sec)
Test # 1:							
20-Oct-99	09:04:42	17.0	18.9	18.9	16116	5.3E-07	5.5E-07
20-Oct-99	13:33:18	19.0	16.6	16.6			
Test # 2:							
20-Oct-99	13:33:18	19.0	16.6	16.6	12947	5.9E-07	6.0E-07
20-Oct-99	17:09:05	18.5	14.8	14.8			
Test # 3:							
20-Oct-99	17:09:05	18.5	14.8	14.8	56865	5.9E-07	6.0E-07
21-Oct-99	08:56:50	19.5	8.9	8.9			

Average Ksat* (cm/sec)*: **5.8E-07**

Comments:

Laboratory analysis by: D. O'Dowd
Data entered by: M. Devine
Checked by: R. Smith

Daniel B. Stephens & Associates, Inc.

Moisture Retention Data

Hanging Column/Pressure Plate/Thermocouple

(Main Drainage Curve)

Job Name: LANL
Job Number: 9958.01
Sample Number: 8814
Ring Number: 8814
Depth: 642.3-642.8

Dry wt. of sample (g): 110.29
Tare wt., screen & clamp (g): 2.10
Tare wt., ring (g): 122.88
Tare wt., epoxy (g): 0.00
Sample volume (cm^3): 70.31

Saturated weight at 0 cm tension* (g): 286.44
Volume of water † in saturated sample (cm^3): 51.17
Saturated moisture content (% vol): 72.78
Sample bulk density (g/cm^3): 1.57

	Date/Time	Weight* (g)	Matric Potential (-cm water)	Moisture Content† (% vol)	
Hanging column:	20-Oct-99 / 10:00	286.44	0.00	72.78	
	23-Oct-99 / 14:55	287.70	6.00	74.57	
	26-Oct-99 / 09:45	287.12	29.70	73.75	
	28-Oct-99 / 13:30	285.43	125.60	71.34	
Pressure plate:	01-Nov-99 / 09:35	282.42	499.70	67.06	
	28-Nov-99 / 20:00	135.98	8158.40	65.24	SS1
	22-Nov-99 / 17:45	126.21	15297.00	60.01	SS2

Comments:

* Weight including tares
† Assumed density of water is 1.0 g/cm^3

SS1 = Analysis using subsample #1: Dry wt* = 129.43 g, Tare wt = 113.68 g.
SS2 = Analysis using subsample #2: Dry wt* = 123.36 g, Tare wt = 115.91 g.

Laboratory analysis by: E. Koenig
Data entered by: R. Smith
Checked by: R. Smith

Daniel B. Stephens & Associates, Inc.

Moisture Retention Data

Relative Humidity Box

(Main Drainage Curve)

Job Name: LANL
Job Number: 9958.01
Sample Number: 8814
Ring Number: 8814
Depth: 642.3-642.8

Dry weight of relative humidity box sample* (g)*:* 77.33
Tare weight (g)*:* 40.97
Sample bulk density (g/cm^3)*:* 1.57

	Date/Time	Weight* (g)	Matric Potential (-cm water)	Moisture Content† (% vol)
Relative humidity box:	17-Dec-99 / 08:30	82.82	848426	23.70

Comments:

* Weight including tares

† Assumed density of water is 1.0 g/cm^3

Laboratory analysis by: B. Baum
Data entered by: R. Smith
Checked by: R. Smith

Water Retention Data Points

Sample Number: 8814

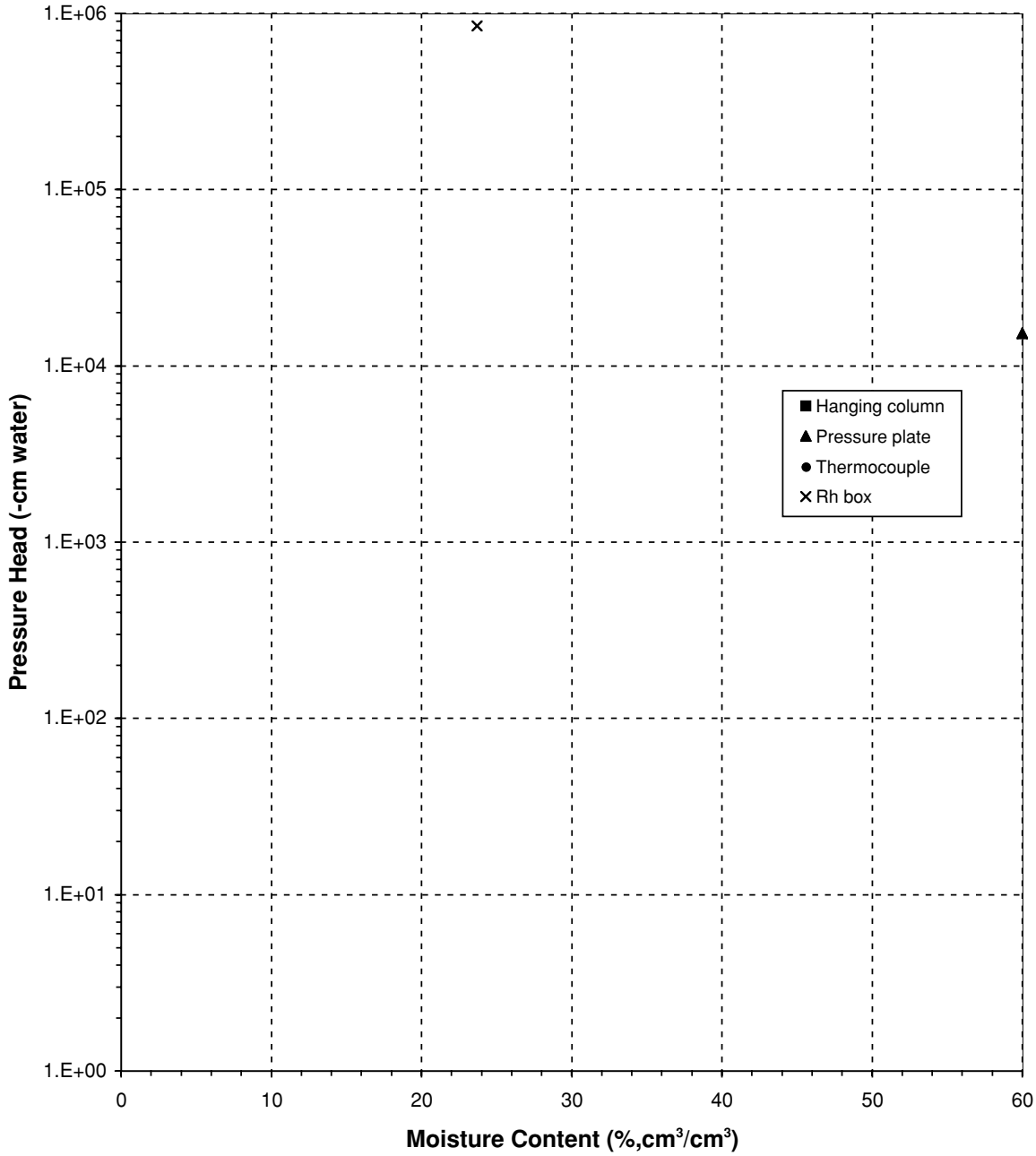

Predicted Water Retention Curve and Data Points

Sample Number: 8814

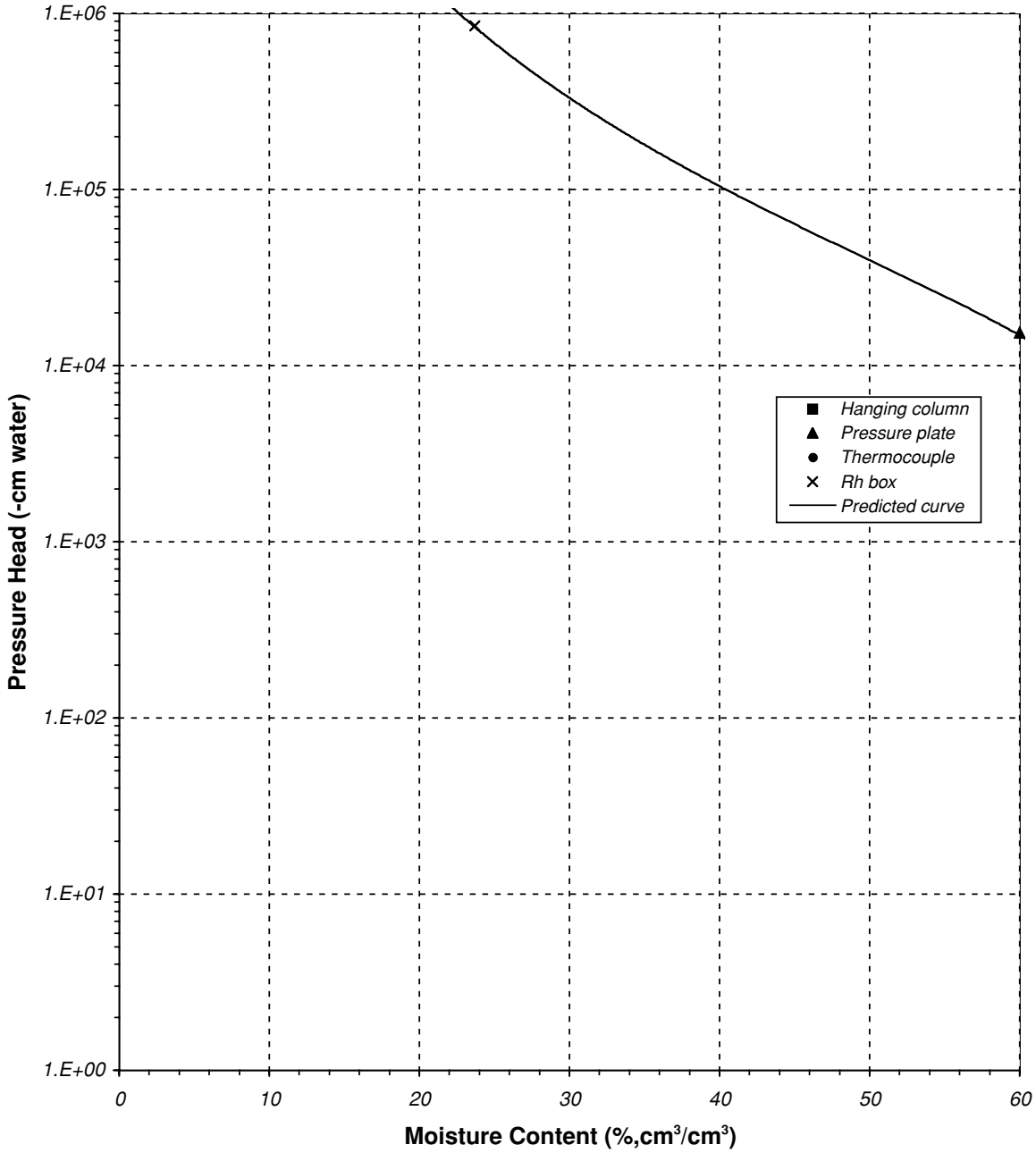

Plot of Relative Hydraulic Conductivity vs Moisture Content

Sample Number: 8814

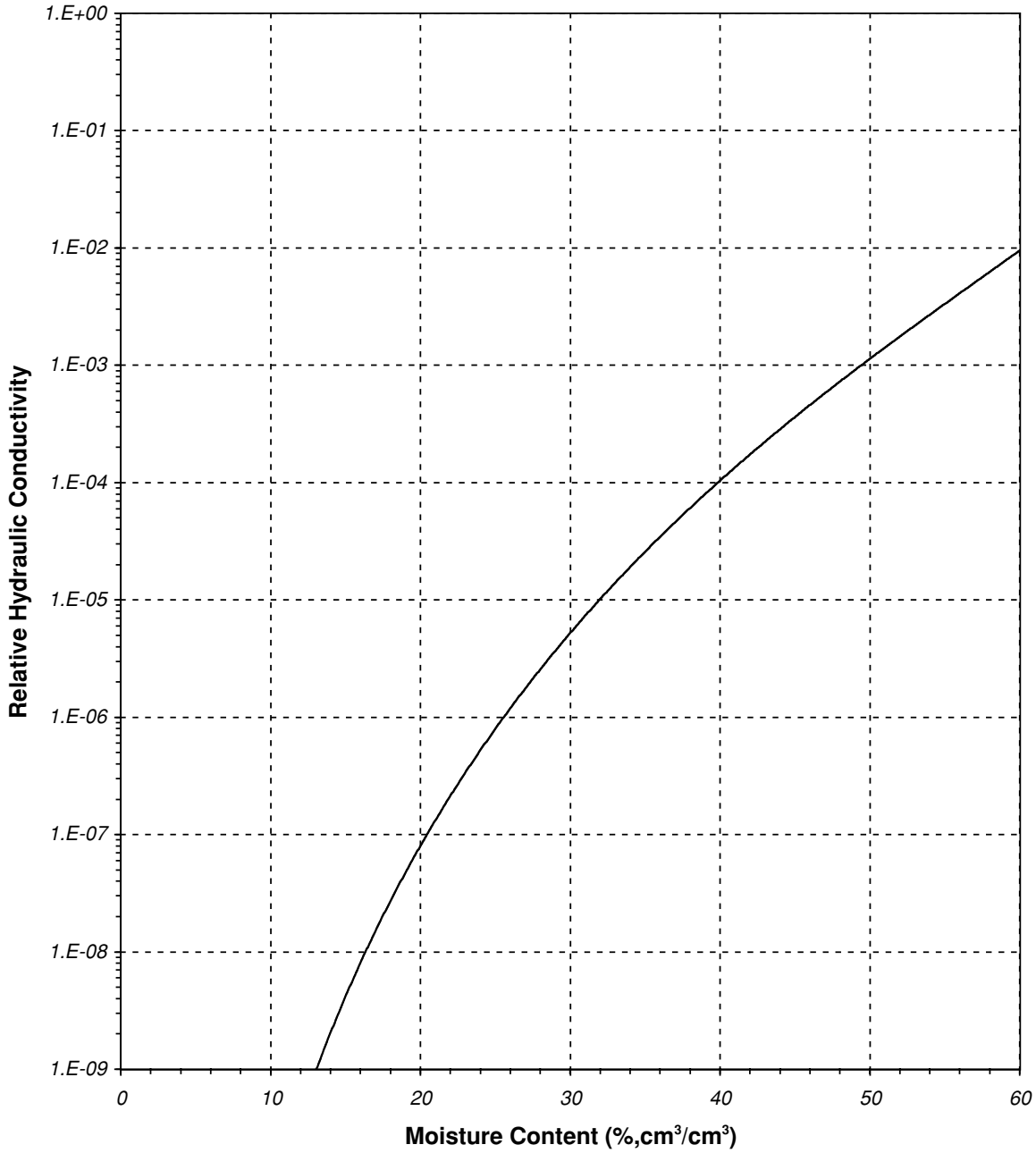

Plot of Hydraulic Conductivity vs Moisture Content

Sample Number: 8814

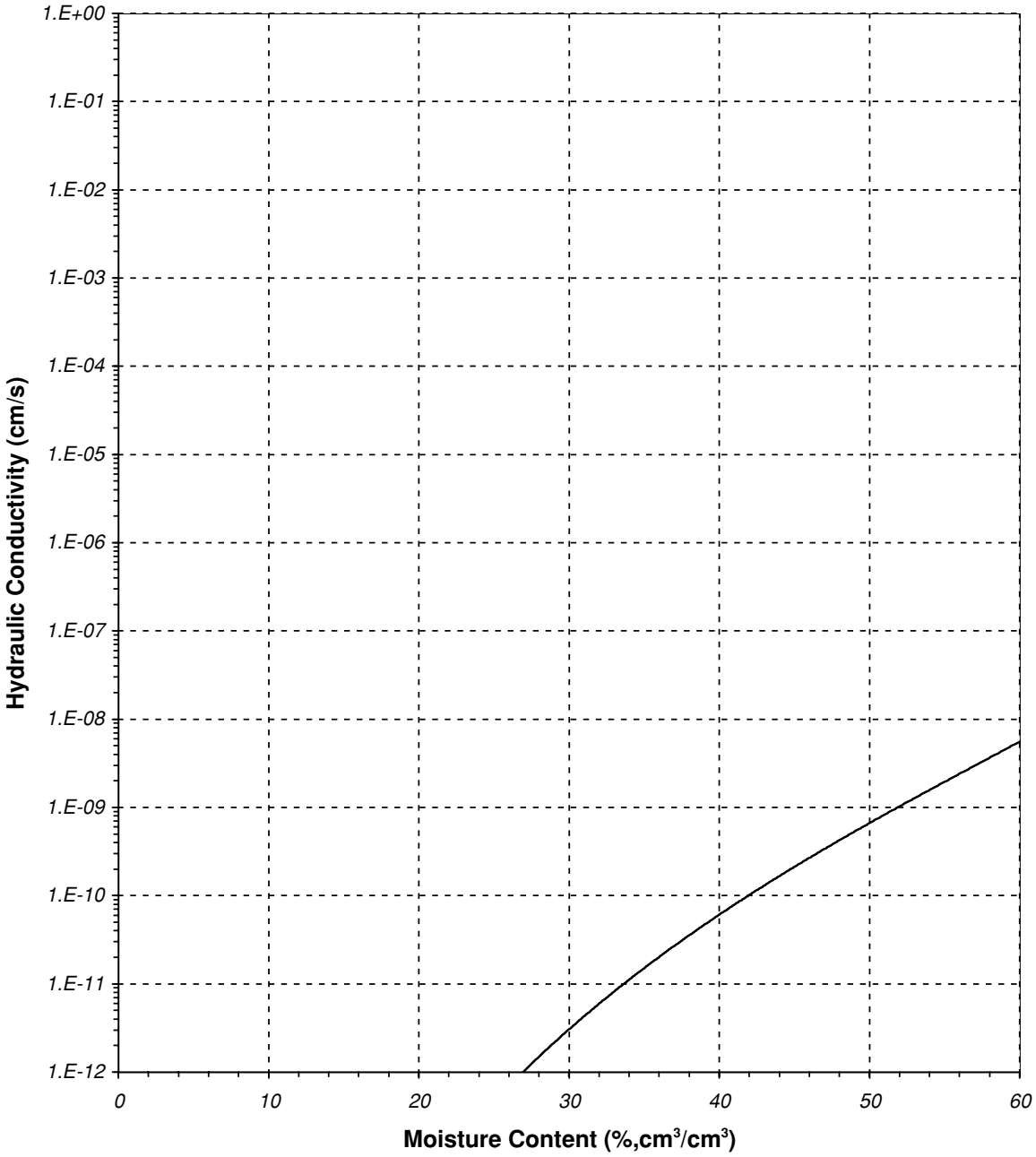

Plot of Relative Hydraulic Conductivity vs Pressure Head

Sample Number: 8814

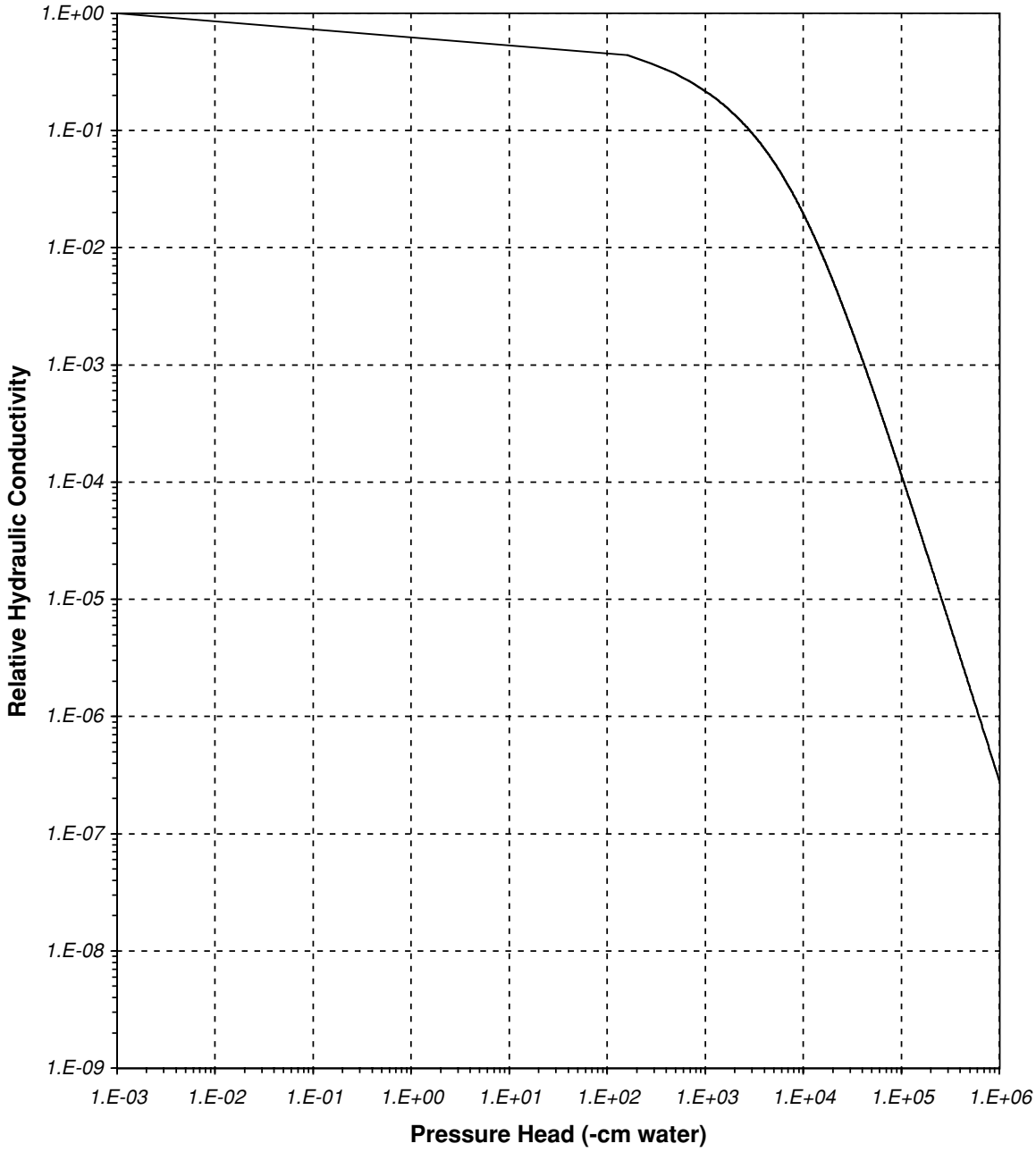

Plot of Hydraulic Conductivity vs Pressure Head

Sample Number: 8814

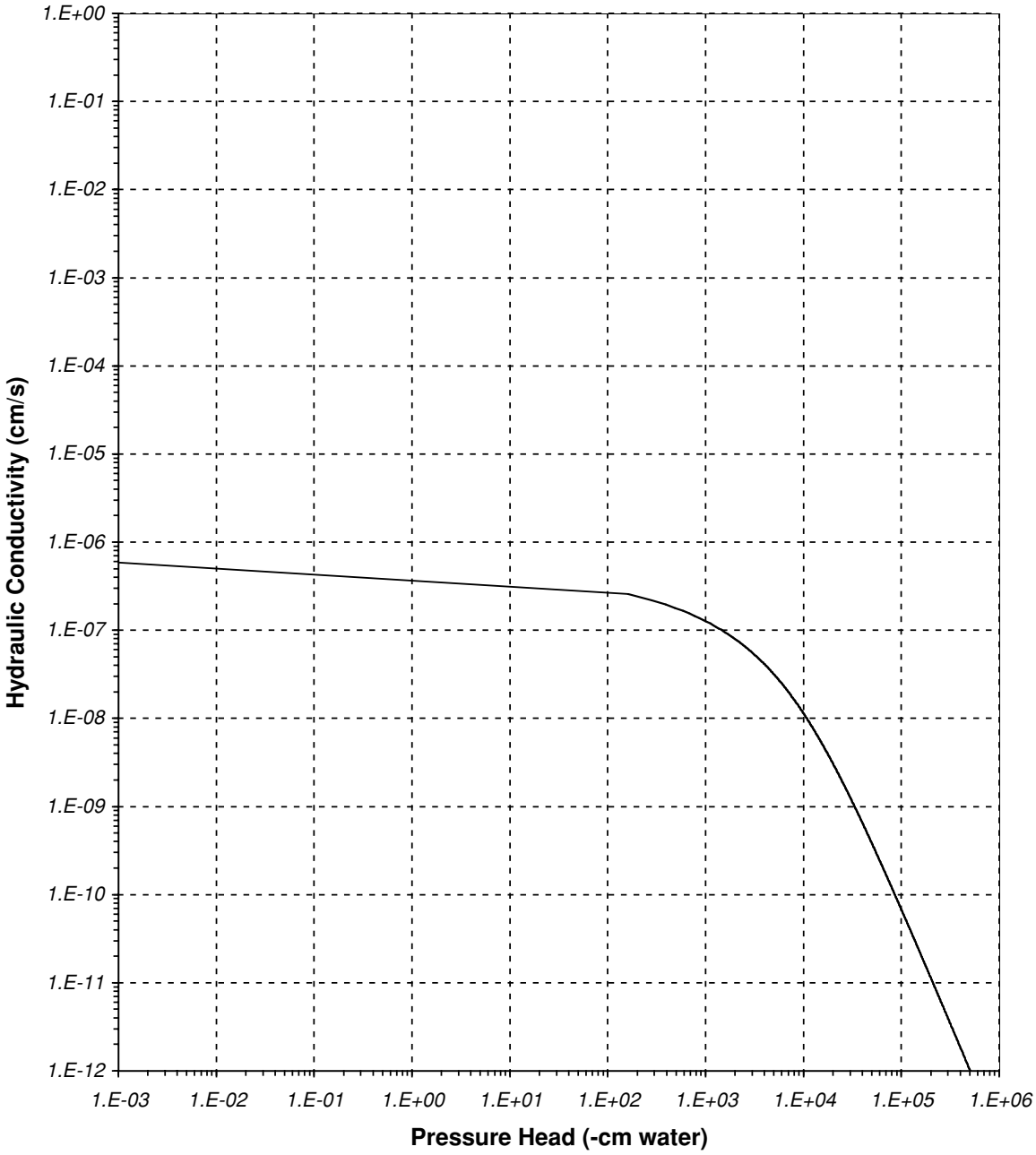

Los Alamos
NATIONAL LABORATORY
Los Alamos, New Mexico 87545